Optical In-Process Monitoring Tools for Laser Powder Bed Fusion: Verifying Powder Area Coverage of a Layer Setup

by

Jane Ellen Modes

Bachelor of Science in Engineering, Mechanical Engineering
University of Michigan -- Ann Arbor, 2017

Submitted to the Department of Mechanical Engineering
In partial fulfillment of the requirements for the degree of

MASTER OF ENGINEERING IN ADVANCED MANUFACTURING AND DESIGN

at the

MASSACHUSETTS INSTITUTE OF TECHNOLOGY

February 2022

Author_____
Jane Ellen Modes
Department of Mechanical Engineering
September 19, 2022

Certified by_____
David E. Hardt
Ralph E. & Eloise F. Cross Professor of Mechanical Engineering
Thesis Supervisor

Accepted by_____
Nicolas Hadjiconstantinou
Chairman, Department Committee on Graduate Theses

This page intentionally left blank

OPTICAL IN-PROCESS MONITORING TOOLS FOR LASER POWDER BED
FUSION: VERIFYING POWDER AREA COVERAGE OF A LAYER SETUP

by

Jane Ellen Modes

Submitted to the Department of Mechanical Engineering on September 19, 2022, in partial
fulfillment of the requirements for the degree of Master of Engineering in Advanced
Manufacturing and Design

Abstract

Additive manufacturing (AM) allows for the creation of complex geometries that cannot be created with traditional manufacturing methods and is widely used in many industries. With any additive manufacturing process, achieving a successful Flayer is critical to the quality of the final part. Currently, no machine can provide objective evidence of a proper layer setup with in-process monitoring equipment. The strategy of this project was to utilize various sensors in tandem with the camera available within the machine to distinguish between passing and failing layers in a quantifiable manner. This thesis aimed to test the 3D printer's on-machine camera and several other off the shelf cameras, (Spectral Instruments RVT100, GoPro HERO7 Black, STPCTOU Wireless Digital Microscope, and iPhone 12 camera,), to determine which if any of them were suitable for quantifying a layer setup through powder area coverage. Several tests were performed to look at the camera repeatability across one or several locations by analyzing image intensity values in ImageJ. Another test was performed to determine if there was a linear correlation between layer thickness and image intensity. The cumulative results from all tests indicate that the on-machine camera is the best option of all cameras tested for this application.

Thesis Supervisor: David E. Hardt

Title: Ralph E. & Eloise F. Cross Professor of Mechanical Engineering

This page intentionally left blank

About the Author

Jane Ellen Modes currently has a passion for additive manufacturing and medical device design. She aims to support projects focused on scaling up additive manufacturing for new product introductions.

Jane is pursuing her Master's degree at the Massachusetts Institute of Technology, (MIT). At MIT, she is enrolled in the Master of Engineering (MEng) program focused on Advanced Manufacturing and Design. The project outlined in the thesis was completed in partial fulfillment of the requirements for the MEng Degree.

Jane holds a Bachelor's in Science and Engineering in Mechanical Engineering from the University of Michigan -- Ann Arbor. Jane discovered her passion for additive manufacturing and medical device design while attending the University of Michigan -- Ann Arbor. While there, Jane worked as an Undergraduate Research Assistant in the Scaffold Tissue Engineering Group (STEG) Lab under the advisement of Dr. Scott Hollister. She worked on several projects in the STEG lab developing methods to grow bone and cartilage tissue with 3D printed bioscaffolds.

After completing her Bachelor's degree, Jane continued her career working in the additive manufacturing industry as an Application Engineer at Materialise in Plymouth, MI. In this role, she was exposed to numerous projects in a vast array of industries taking advantage of additive manufacturing. After a short time in the Application Engineer role, Jane was promoted to a Technical Consultant for Partnership Business Development role where she was able to work closely with machine manufacturers in the additive manufacturing industry.

This page intentionally left blank

Dedication

This research is lovingly dedicated to my grandfather, Gerald Thomas Shaughnessy, and my grandmother, Mary Ellen Shaughnessy. My grandparents instilled the importance of education, discipline, and ambition in me. They held me accountable and encouraged me to always strive for more: "Don't they give out A+ at this school?" Without their love, encouragement, and occasional nagging, I would not have decided to further my education with a Master's from MIT.

Sláinte.

This page intentionally left blank

Acknowledgements

I would like to acknowledge and give my warmest thanks to those who made this work possible. Thank you to the co-directors of the MEng program: Jose Pacheco and Professor David Hardt who also served as my thesis advisor.

I would like to express my gratitude to my thesis project teammates, Maya Kota, Satvik Sabarad, and Jayna Wittenbrink along with the rest of the 2021-2022 MEng Cohort for their support throughout the program. Maya, Satvik, Jayna, thank you for all the hard work. It was a pleasure to work alongside you even when the project was very challenging.

I would like to thank Aditi Joshi for her patience and support throughout the MITx Principles of Manufacturing MicroMasters Program.

Last but certainly not least, I would like to thank my parents, siblings, grandparents, and friends for their endless support, encouragement, and counsel. Mom, Dad, Michael, Grace, and Molly: I would not be where I am today without you. I find comfort in knowing you will be there supporting me no matter the hour of the day or the length of the journey ahead. Thank you from the bottom of my heart.

This page intentionally left blank

Contents

List of Figures

This page intentionally left blank

List of Tables

This page intentionally left blank

Chapter 1: Introduction

The broad objective of this thesis is to improve data acquisition during a machine setup for additive manufacturing. The specific aim is to improve the in-process monitoring methods using various sensors.

1.1.   Additive Manufacturing

Additive manufacturing (AM) allows for the creation of complex geometries which cannot be created with traditional manufacturing methods. This is appealing to industries looking to improve service performance [1]. This process also allows parts to be manufactured with a high level of customization and reliability. Additive manufacturing, also known as 3D printing, creates parts by fusing or depositing layer by layer of material to form a complete part. Numerous technologies fall under the umbrella of additive manufacturing, and parts can be produced from various materials.

1.2. The Importance of Characterization in Additive Manufacturing

With any additive manufacturing process, achieving a successful characterization of certain powder layer properties is critical to the quality of the final part. Often, many parts are built at the same time within the build platform. If powder is deposited unevenly, this will produce inconsistencies in parts across the batch which could lead to performance issues. If the powder is too thick, for example, the laser beam may not fully penetrate through the layer of powder, resulting in a part that fails process verification tests such as tensile testing. If too thin, it is possible that the part being printed on could warp from the heat stress introduced by the print laser.

1.3. The Manufacturing Process

Layer thickness will be defined in generic units to protect the intellectual property (IP) of the project. This project aimed to investigate a powder layer of 1 to 3 units. This specification was treated as part of a defined parameter set meaning it could not be changed.

In typical additive manufacturing, important powder layer properties can be verified by unquantifiable means that fit within two categories of failure. The first is gross powder defects across the build plate. The second is uniformity in the powder layer. There are a number of different gross powder failure conditions that can occur within powder layers. Several failures that can occur during the printing and that require adjustment of a setup can be identified. One common failure mode in additive manufacturing is caused by short feeding. Short feeding occurs when there is not enough powder being spread across the build plate. Other failures can include an inconsistent powder layer and powder clumping.

1.4. Problem Statement

As additive manufacturing processes begin to mature for use in industry, the tools to monitor parts need to develop as well. The use of existing approaches prompts the need for more specified monitoring equipment to ensure the manufacturing of safe, high-performing parts. This project aims to create a tool that could be used to objectively quantify a setup on an AM machine. This project investigates the possible sensor technologies and strategies that can provide in-process data to objectively quantify the layer condition, along with the varying advantages and shortcomings of each. The manufacturing process requires a powder layer thickness on each part to be between 1 and 3 units.

Identifying and analyzing gross powder defects are not part of the project scope. We assumed that all powder anomalies which were discussed previously were not occurring or would be fixed before our tool performed an analysis of the pertinent layer. If such powder anomalies were actually occurring, then our analysis would not be useful since the consideration of powder layer thickness would be a secondary concern to gross powder defects in the powder bed.

The ideal solution would take advantage of the existing hardware, software, and space available in an AM machine without interfering with the working space available. The most effective approach would be built out as an add-on module that can be used on any AM machine. Implementing in-process monitoring technologies for layer setups will provide the objective evidence to set up an AM machine for a build. While quantitatively measuring the layer could assist during set-up, identifying and fixing the cause for a poor layer set-up is not the main objective of this project. The scope of this project is to deliver a proof of concept functional prototype which could be installed and tested on one 3D printer.

For this project, it is important to come up with a quick and cost-effective method of verifying a proper layer setup. The final tool should not cost more than the benefits of using the tool are worth.

1.5. Prior Work

Prior to the start of this project, other related work was completed. The prior work involved a Keyence CL 3000 Series confocal laser displacement sensor. The sensor can be used to detect the distance from to the object at which it is pointed.

1.6.   Collaboration with MIT

This project was completed as part of the Master of Engineering in Advanced

Manufacturing and Design at the Massachusetts Institute of Technology (MIT). All four team

members worked collaboratively, especially at the beginning stages of the process. After a broad

evaluation of possible powder characterization techniques, which are outlined in Chapter 3, the

team devised a solution strategy and split the work. More information on this is contained within

the shared Introduction section of the Methodologies. The author of this thesis (Jane Modes) is

presenting the details of various optical in-process monitoring tools which contributed to the

overall solution of quantitatively characterizing the layer and providing a verification tool to

check an AM layer setup. Much of the content in Chapters 1 through 5 are common among the

individual theses. The related work is documented in the MEng theses of Jayna Wittenbrink[1]

with a focus on using displacement sensors to quantify the thickness of a layer, Maya Kota[2] with

a focus on characterizing the on-machine camera performance, and Satvik Sabarad[3] with a focus

on compiling the work from all theses to create a verification tool.

Chapter 2: Overview of Existing AM Monitoring Tools

While additive manufacturing is growing in popularity, few companies are scaling to

large volume production using additive manufacturing. As such, there are not yet defined process

and component certification methodologies for additive manufacturing [2]. The American

---

[1] J. Wittenbrink, "Using Displacement Sensors to Characterize Critical Powder Layers in Laser Powder Bed Fusion" thesis, 2022.

[2] M. Kota, "Using Optical Imaging and Image Processing to Verify Initial Layer Setup in a Laser Powder Bed Fusion Process," thesis, 2022.

[3] S. Sabarad, "Comparing Various Methods for Validation of the Initial Layer in an LPBF process using Optical and Displacement Sensors," thesis, 2022.

Society for Testing and Materials (ASTM) and the International Organization for Standardization (ISO) have released some guidelines for additive manufacturing which are very broad and allow for much flexibility in the manufacturing process. With no defined standards, companies turn to trial and error manufacturing and testing using in situ process monitoring methodologies [2]. The following section describes the most commonly used methods in AM to monitor the quality of parts during manufacturing.

2.1. Traditional Quality Controls for AM

Current manufacturing tools are capable of monitoring many potential sources of variation in additive manufacturing. While some real-time, closed-loop control systems exist, most collect data during a 3D print that is analyzed afterward. The most commonly used monitoring tools utilize optical and thermal techniques to track spatial variations and defects across the build surface over time [2] - [4]. Optical imaging tools are advantageous since they provide a large amount of data, do not require contact with the parts, are non-hazardous, and have relatively large working distances [4] - [5]. Thermal sensors are usually used to measure features of the melt pool, while optical sensors can capture a large variety of data [4]. For example, 3D printing companies Velo3D, Aconity3D, and Concept Laser all have optical systems for powder bed monitoring, and thermal sensors to monitor the melt pool [3]. Similarly, the AM machine used for this project is equipped with a camera. Acoustic monitoring tools are also increasing in use [4]. For example, Renishaw's InfiniAM Sonic system determines the location of defects within the build using four ultrasonic sensors located under the build plate. Many companies also monitor the scanning laser itself such as SLM Solutions' Laser Power Monitoring system and Renishaw's LaserView module [3].

Several companies are working on software monitoring tools specifically geared towards additive manufacturing. Tools have been developed to simulate the processes of AM which are highly dynamic [6]. Such simulation software packages are typically used to identify issues in an AM build due to the high strain and cooling rates that a part undergoes during the AM building process [6]. Other software tools, such as PrintRite3D from SigmaLabs use thermal imaging and machine learning to detect defects in real-time for AM [7]. SigmaLabs has been able to validate the results of PrintRite3D against results from X-Ray tomography [8]. None of the above systems are able to directly measure a 1 to 3 units powder thickness. The optical solutions are generally built to detect defects and can only visualize surface features [4].

A few companies have focused systems aimed at powder layer verification. SigmaLabs has performed multiple case studies to show that their PrintRite3D system can use thermal measurements to show the proper layer setup in a 3D printer after scanning with the laser [9]. However, this validation will not be acceptable with the quality applicable for this project. Concept Laser's QM Coating system varies the amount of powder spread for each layer by using feedback from high-resolution cameras [3]. "An intelligent algorithm" makes a decision based on the subtraction of before and after powder images [10]. Open Additive's Panda system also offers a high-resolution recoating imaging solution that they offer as an add-on for integration into other machines [3]. To find a new sensor to fulfill our requirements, we completed a thorough exploration of many different sensing methods. The overview of these explorations is discussed in the next section.

2.2.   Non-Destructive Powder Bed Monitoring Tools for AM

Research on sensors that can more closely monitor powder bed conditions is available for a much broader range of sensor types than the more popular thermal and optical techniques

described above. The preliminary review of sensor types is described here and is categorized into devices of optical, thermal, or acoustic nature. There are numerous types of sensors with unique operating principles, and this exploration is not exhaustive. However, we were able to disregard certain categories of tools given our project constraints. From there, we determined the most likely candidates for a deeper literature review, which is included in Chapter 4.

2.2.1.   Optical Imaging and Radiography

Optical sensors detect wavelengths of light between 100 nanometers of the UV range and 20,000 nanometers of the near-infrared (NIR) portion of the electromagnetic spectrum (EMS) [11]. Sensors operating in the X-ray portion of the EMS were also explored. Preliminary explorations removed UV, radiography (x-ray imaging), and time of flight sensors like Lidar from our considerations owing to insufficient accuracy [4], [12], [13].

In ultraviolet (UV) photography, only radiation from the ultraviolet (UV) spectrum is used to capture images and the wavelength of this spectrum ranges roughly from 10 nm to 400 nm. In reflected UV photography, the subject is directly lit by UV emitting lamps (radiation sources) or by bright sunshine. The lens has a UV transmitting filter on it that lets only ultraviolet light through while absorbing or blocking all visible light and infrared light [12].

X-ray imaging is commonly used in additive manufacturing to check the quality, more specifically the internal porosity, of parts after they have been built and post-processed [14] - [15]. X-rays have been used to take measurements with accuracy down to hundreds of microns, which is not sufficient for this project [16]. In addition to the lack of accuracy, exposure to X-rays introduces a health and safety concern for the operators of the equipment [17].

Lidar, or Light Detection and Ranging, emits pulsed light waves to the surrounding environment that bounce off surrounding objects and return to the sensors [18]. The distance to

an object is calculated by the time it takes each pulse to return to the sensor [18]. Lidar is ideal for sensing non-stationary objects, such as a pedestrian on a sidewalk being sensed by an autonomous vehicle [18]. Lidar has many uses but does not have the micron accuracy necessary for this project [19].

While NIR and Infrared optical cameras improved the accuracy of melt pool data, especially in combination with visible light cameras, we concluded that their accuracy on pre-scanned powder would be insufficient [3]. In NIR spectroscopy, light is cast onto the target substance with a broad spectrum of near-infrared light. This broad spectrum refers to light of many frequencies and wavelengths. The near-infrared light could be absorbed, reflected, or scattered by the target substance. Because of this, NIR posed an issue in our application. Reflective materials could reflect the NIR light. This would increase glare in images and make image processing difficult. This is why NIR was not further considered [20].

The use of a digital camera would be ideal for reasons described earlier, so we did a more thorough review of their use on powder monitoring. Digital cameras record the amount of reflected visible light received at the sensor. Variations in lighting and the reflectivity behavior of the material will vary the resulting intensity values received by a camera. On the other hand, laser triangulation responds to the physical geometry of the subject by detecting the angular displacement of reflected light [21]. Laser scanners use the same principle, but disperse the laser into a line that can produce a 3D dataset when moved across a sample [22]. Both of these were chosen for further study in this application.

Topography, or profilometry, are techniques that characterize the features of a surface including shape and roughness, and different methods of optical nature can be employed [23]. Laser confocal microscopy is a popular method for high-resolution surface topography

measurements [24]. The Keyence sensor used for previous tests is a white light confocal displacement sensor which works by splitting white light into different colors and detecting the most prominent wavelengths through a spectrometer [25].

Other methods of optical topography include shape-from-focus and structured light [23]. Some of the more accurate sensors including microscopes that use shape-from-focus principles are machines too large to be used within an AM chamber or have a field of view that is too small. On the other hand, structured light has been used directly within the AM environment, and showed promise for our application. For example, Li et al. utilized a variety of structured light called enhanced phase measuring profilometry (EPMP) to offset the bad lighting and other challenges of the environment and saw improved processing speed and accuracy [26].

We also considered the 3D optical technique, stereovision, which mimics the human eye by calculating depth from two images [27]. In their study of the formation and behavior of thin dust layers on bag filters, Saleem and Kramer built a custom in-process stereovision system [5]. This required the use of markers for calibration and alignment across the surface being studied, which determines the achievable accuracy of the setup. It has also been mentioned that there is difficulty in designing and implementing markers within the AM build area [26].

Tomography is a technique that involves producing 3D output from layers of 2D data that are generally collected with optical or x-ray sensors. It is distinct from topography since it provides a full 3D depiction including internal features instead of only capturing surface details. Optical tomography generally requires at least a partially translucent subject, but for AM, it is achieved by capturing images at each layer of the build. X-ray tomography techniques are used for very high-resolution post-production quality analysis. However, its integration into an AM manufacturing process itself is not yet feasible [3]. The most promising technology for AM in

situ measurement with these techniques is optical coherence tomography (OCT) [28]. OCT operates through the principle of coherence scanning interferometry that operates similarly to ultrasound [3]. Several studies use an OCT setup that places the tool in-line with the scanning laser. The melt pool can be monitored during printing, and the powder bed can also be analyzed before printing. In all of these studies, the researchers had full control over the system including the design of the scanning laser, optics, controllers, etc. [29] - [31].

2.2.2. Thermal Monitoring

Numerous types of thermal sensors from applications such as surveillance, search and rescue, and defense could be used [32]. Thermal sensors are easy to use and are becoming lower cost as they grow in popularity [32]. For this project, thermal sensors that require contact with the part such as thermocouples, thermistors, resistance temperature detectors, and temperature integrated circuits, were not considered [33]. However, non-contact thermal sensors, such as infrared thermometers, were considered for this project as we did not expect that the thermal map would change in a detectable way with the sub-millimeter scale of powder that would be deposited on the parts [34].

One thermal monitoring tool which was explored in more detail is flash thermography. Flash thermography is an active thermography method that uses a heat source to induce heat into a part and a thermal camera to inspect the part [35]. This allows for a high contrast thermal image to be created for a part at ambient temperature [35]. It is unclear if flash thermography would lend the resolution and accuracy needed for the measurements we are aiming to take [35].

Other thermal monitoring tools may involve thermography and thermal cameras. Thermography can detect the variance in thermal behavior between a defect and the part [4]. High-speed infrared imaging can be used along with optical imaging to track deposition and

28

predict the surface temperature during powder deposition, temperature gradients, and liquid-solid interface velocity. These can be used to understand the quality and microstructure of additively manufactured parts [2]. Conventional charge-coupled devices and near-infrared cameras have been used to detect porosity in additively manufactured parts [2]. These techniques have been shown to correlate with the results seen from 3D X-Ray tomography [2]. Like optical methods, post-processing of data is required for correlating measurement values to part features, though the emissivity of the powder bed will be highly variable depending on surface morphology, oxygen content, and how often the powder has been recycled, etc. [3] - [4].

2.2.3. Acoustic

One newer method for defect detection in additive manufacturing is acoustic monitoring. The two main acoustic monitoring techniques are ultrasonic testing and acoustic emission spectroscopy. Acoustic emission spectroscopy detects the acoustic emissions from the process laser, so it is not relevant for our purposes. Ultrasonic testing measures induced waves that are conducted and reflected through a part as it's being built [3]. An ultrasonic probe mounted underneath the build plate measures reflected acoustic signals that occur with sudden changes in density in the material [36]. This technique can be used to detect defects such as cracks and porosity [4]. We concluded that this would not be the right approach to measure loose powder to our desired accuracy.

2.3. Summary of Selected Technologies

After looking into a broad range of possible sensors, we narrowed down the list of sensors to further research. Table 1 displays an overview of all technologies considered, which were selected for further evaluation, and the reasoning behind that consideration. We decided to

29

do a deeper literature review on digital cameras, laser triangulation sensors, confocal chromatic sensors, and structured light sensors.

Table 1. Below is a summary of various measurement principles and sensor types that were evaluated for our application.

Categories of Measurement Principles	Considered for further evaluation?	Reason
Optical + Radiography Methods		
X-ray	No	Safety concerns
Pulse Based (Time of flight)	No	Not accurate, not many articles are available on this technology
NIR	No	Not enough accuracy
Visible Light (Digital Cameras)	**Yes**	Provides a lot of information, large working distances, already integrated in the machine
Laser Triangulation	**Yes**	High accuracy and ease of use
Confocal Microscopy	No	Can't find a modular or portable one
UV Photography	No	Lacking evidence of use in AM; Primarily used in the medical field
Chromatic Confocal Sensor	**Yes**	Already available for testing on-site, high accuracy and precision
Structured Light	**Yes**	Previous use in AM
Stereoscopic Vision	No	Requires use of precise markers in the measurement area for high accuracy readings
Optical Coherence Tomography	No	In-line assembly with scanning laser difficult as an add-on module
Thermal Methods		
Flash Thermography	No	Expensive, not enough accuracy
IR Imaging	No	Hard to use, not enough accuracy
Acoustic Methods		
Ultrasonic	No	Not enough accuracy
Acoustic Emission Spectroscopy	No	Requires use of the acoustic emissions from the scanning laser

Chapter 3: Background Principles

3.1.   Powder Spreadability

Powder spreadability over the build surface and the corresponding powder density greatly

affect the mechanical properties of a 3D printed part [37] - [38]. In characterizing the important

powder layer properties, it is helpful to study the parameters that influence how the powder

spreads across the parts. Features of the powder, the surface across which powder is being

spread, and the recoating system, all affect the resulting powder coverage.

3.1.1. Contributing Powder Characteristics

Particle size distribution (PSD) and shape are some of the important powder qualities that

affect powder density [37] - [38]. To improve spreadability, the particle distribution should be

narrow to reduce the interparticle friction that prevents flow [39] - [40]. For a homogenous

powder layer coating, increasing the sphericity of the powder particles increases powder

coverage [41]. While powder flowability is often equated to spreadability, Phua et al. and

Mitterlehner et al. demonstrate that powders with worse flowability can have superior

spreadability when a realistic surface is considered instead of the perfectly flat surfaces used in

simulations [38], [41].

In addition to powder characteristics, features of the recoater system including recoater

speed and the recoater gap will affect the powder layer. Generally, increasing the speed of the

recoater results in less powder coverage and reduces uniformity [38], [39]. The recoater gap is

the distance from the bottom of the recoater blade to the surface over which powder is being

spread. Ideally, when the recoater blade moves over the build plate, it spreads powder uniformly

over the surface to the thickness of that gap. However, in reality, this does not happen because of a phenomenon called jamming.

3.1.2. Jamming

Jamming describes a state of disordered particle systems when they behave as a solid, meaning that the system is mechanically stable when exposed to perturbation, rather than flowing like a fluid [42]. In the powder recoating processes, transient jamming occurs when the recoater gap gets too small. Regions of particles begin to stick together and reduce powder spreadability, essentially creating large bald spots by dragging the jammed clumps and larger particles across the build area [37]. This can cause serious complications to the final quality of the product because the patchy area coverage leads to weak bonding during the sintering process [29]. Jamming is important for us to consider. Powder spreadability greatly influences pixel intensity values; it can cause an increase in intensity if there is an accumulation of powder or a decrease in intensity due to the previously mentioned bald spots. This was an important phenomenon for us to understand.

3.2. Lighting

Lighting plays an important role in optical in-situ monitoring techniques. The quality of videos taken for monitoring the process depends heavily on the lighting conditions inside the machine including brightness, contrast, reflection, and diffusion. The single most crucial choice in lighting an image is the effective size of the light source. It controls how shadows are cast and could have an impact on the kind of reflection. [43].

3.2.1. Family of Angles

Direct reflection is produced when the reflected light from the part is incident to the camera, as demonstrated in Figure 1 [43]. If the light source lies in the "Family of Angles" as

shown in Figure 1A, the surface becomes highly reflective. We want to avoid this from happening. Hence, the idea is to place the light source anywhere except in the zone of the "Family of Angles." A diffusion sheet can be used to capture the reflected light and this can help estimate the envelope.

(A)   (B)
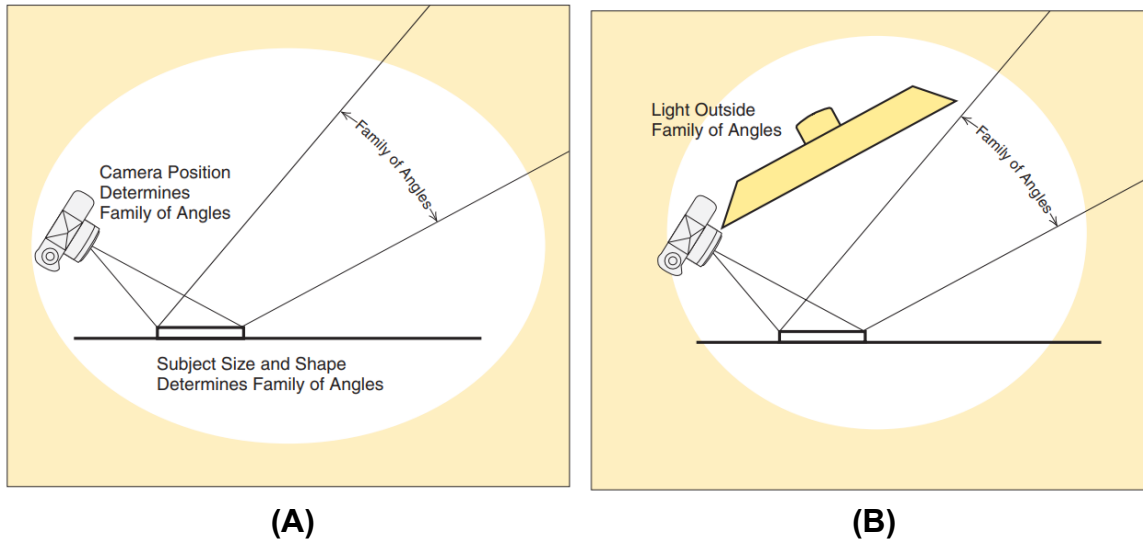
Figure 1. The "Family of Angles" that produces direct reflection depends on the position of the camera relative to the subject (**A**) Keeping the light source in the "Family of Angles" directly illuminates the object and the light is reflected into the camera. (**B**) Keeping light outside the Family of Angles to keep the object dark [43].

3.2.2.   Diffusion and Reflector Cards

One of the approaches to avoid reflection is to put the light near the camera; this is shown in Figure 1B [43]. Sometimes it is difficult to place the source of light outside of the "Family of Angles" zone and in this situation, several other methods can be tried as shown in Figure 2. One of the ways to avoid direct illumination is by adding a diffusion material in front of the light source. Diffusion ensures that the illuminated light is not too strong. It is also necessary to consider the distance of diffusion material from the light source because if it is too close, the illumination will increase, leading to high reflection and vice-versa [43].

Another method is to use a reflector card, shown in Figure 2B, which reflects the light from the light source onto the subject. However, a gobo (an opaque object) has to be used to avoid direct illumination. The gobo is placed such that only region B receives the direct light from the light source and this does not reflect the light onto the subject directly. Region A represents the "Family of Angles" and the gobo ensures that the light does not fall on this region. Furthermore, the distance between the light source and the subject only affects the brightness of the background and not of the object [43]. Also, using polarizing filters will not block the reflection from the surface as the reflected light is already often polarized.

(A)   **(B)**
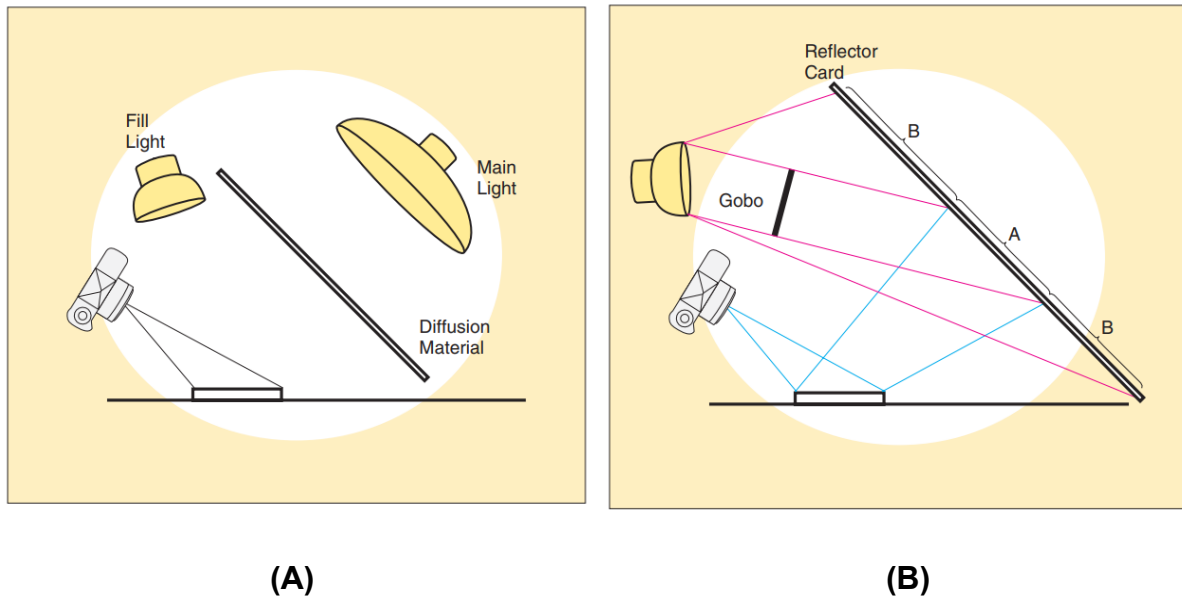
Figure 2. (A) A diffusion material is added in front of the light source to avoid direct illumination of the object **(B)** Using a reflector card to illuminate the subject but ensuring that a gobo is used to avoid direct illumination [43].

Chapter 4: Sensor Evaluation

After the preliminary study, we conducted a literature review for digital imaging, laser triangulation, structured light, and confocal chromatic sensors. The capability of measuring the proper scale of particles without contact and the ability to deploy within our time frame were the main characteristics considered to determine the feasibility of use.

4.1. Digital Cameras

Optical-based technologies are widely used to monitor the AM process. They are heavily used to identify defects and help in taking corrective action to avoid the part getting rejected in later stages. The more common application of external cameras is to monitor larger defects. Recoating defects perpendicular to the recoater blade movement were identified by Craeghs et al. by using an external camera system [45]. Scime et al. automated the detection and classification of anomalies in the powder bed using the EOS M290's stock illumination by using a 1.3 megapixel (MP) camera [45]. Caltanissetta et al. integrated a 10.5 MP camera into the build chamber laterally and combined it with ideal lighting conditions to get clear images of the build process. They also observed that diffused lighting helped them capture good images as compared to the direct reflection of light into the camera [46]. Furumoto et al. placed a Photron FASTCAM SA5 model 1300K C2 high-speed camera onto a custom machine to test a simpler, off-line method. They monitored the consolidation of powder during irradiation by placing a camera vertically above the powder bed to study the effect of altering powder layer thickness [47].

There is also research that studies the powder bed with higher resolution to identify smaller defects during the build process. Abdelrahman et al. identified different types of defects during the build process by focusing a 36 MP camera on a 250 by 250 mm build area (resolution of 45-88 microns per mm) [48]. They used optical imaging to study anomalies in the powder

layer before laser scanning and in the solidified material after scanning. Correlating numerous pictures under various lighting conditions and from multiple layers allowed the identification of lack-of-fusion flaws using optical data [48]. There was only one study where authors were able to achieve even higher resolution. F. G. Fischer et al. could identify features as small as 12 to14 micrometers over a 98 mm width by deploying their own optical process monitoring system which can be mounted on the recoater blade [49]. Since this study showed promising results, more optical sensors with higher resolution for the study were considered. These sensors were mounted closer as compared to the existing in-machine camera to reduce the field of view and thereby increase the resolution. This is the focus of this thesis, which specifically considers the results from a digital microscope, a vacuum compatible CMOS camera, and other digital cameras.

We explored deeply the approach of using optical imaging for this project's application. A common method for evaluating powder layers with a camera is to evaluate the percent area coverage over the build area [38], [41]. For example, Wei Lin et al.'s work analyzed the quality of powder layers through image processing by just this method [50]. They captured many images from an optical camera and they further processed the images in MATLAB to convert those images into binary images (only white and black pixels). Two tests were performed on the samples that were acquired during the studies. The pictures were first digitized and visually analyzed. The percentage of black or white pixels in the picture was examined next to check the quality of powder spread [50].

Furthermore, they studied how the powder spreadability is affected by the layer height and used binary images to evaluate the percentage area covered by the powder over the part [51]. For example, in Figure 3, a 24 by 16-pixel image is displayed along with the intensity values. We

37

can see that the value of a pixel is 0 when the pixel is completely black and 255 when the pixel is completely white.
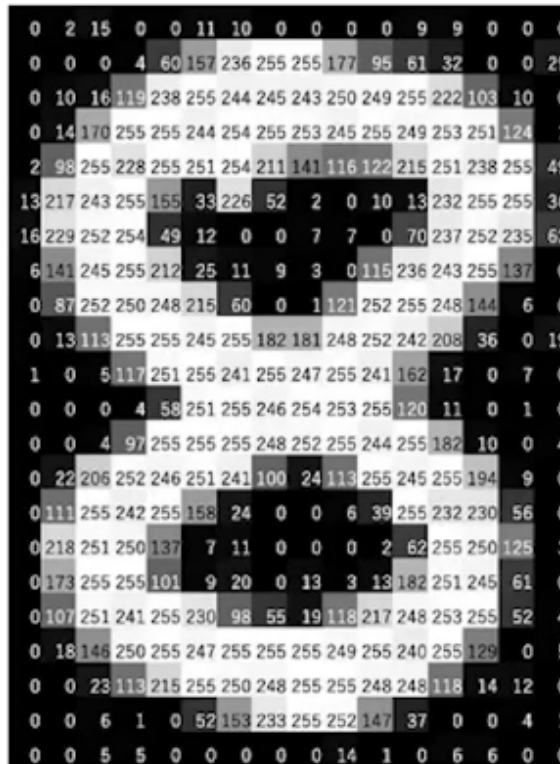
Figure 3. A 24 by 16 image with intensity values (ranging from 0 to 255) is displayed on each pixel [52].

Pixel intensity values can be used to characterize the powder deposition quality. As we discussed previously in the lighting section, the position of the lighting inside the machine is such that the light source is not in the 'Family of Angles' [44]. If we take a picture at this point, we will observe that the image is dark and the pixel values are in the lower range. However, when a layer of powder is spread, the pixel values change because the powder is light in color and reflects more light into the camera. Since the powder particles are light in color, the intensity values increase and this helps us in distinguishing. This method has been discussed by Lin et al., where they have demonstrated that the powder can be distinguished using an optical technique

[50]. As discussed earlier, a 12MP camera is already pre-installed in the machine for in-situ monitoring. We will discuss in detail how we used the images captured by this camera to characterize the process in the later sections.

4.2. Laser triangulation

Laser triangulation sensors are compact, non-contact 2D sensors that perform distance measurements by angle calculation as shown in Figure 4. They are commonly used to measure thickness with high accuracy [53].
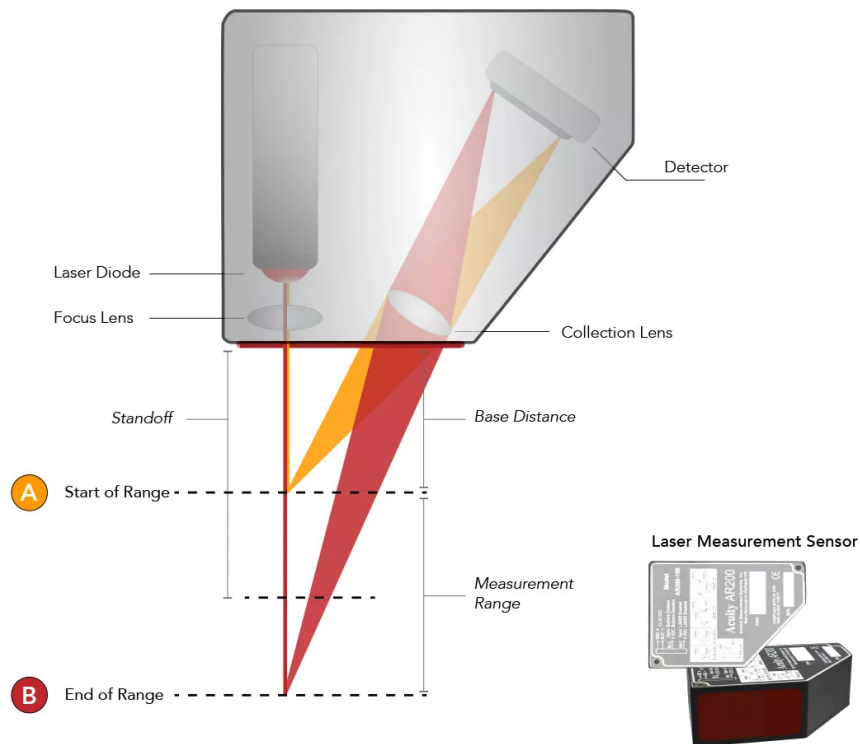
Figure 4. The principle of measurement in laser triangulation is demonstrated above [53]. In laser triangulation, a laser beam is projected from the sensor to the target and reflected in the collection lens. The laser emitter and collection lens are beside one another in the sensor enclosure.

There are two configurations of laser triangulation sensors: the point sensor and the line sensor. In a laser triangulation point sensor, the collection lens focuses on an image of the laser

spot on a linear array detector. The detector views the measurement range shown in the image above from an angle usually between 45 and 65 degrees, though this varies by sensor model. The location of the laser spot image on the detector's pixels is processed through digital or analog signals to measure the distance to the target [53].

In a laser triangulation line sensor, the laser projects a continuous line of light across the target. While the projected line does appear distorted, a detailed analysis of the distorted image allows for a highly accurate reconstruction of the object's shape. From this type of sensor, a 2D profile can be created [54]. Laser triangulation sensors can measure many different measurement ranges depending on the instrument model. These sensors can be used for any scale of measurement, but accuracy decreases as the measurement range increases. Both exposure and power levels of the laser can be controlled to improve accuracy based on outside factors like lighting [53].

To assess the applicability of laser triangulation sensors in the thesis project, various pieces of literature were reviewed. Donadello demonstrated the use of a laser triangulation sensor for process control of laser deposition [55]. This paper described laser triangulation for height monitoring for a type of additive manufacturing; it provided important insights about using laser triangulation sensors in the printing process. The system described in the article uses optical triangulation, in a coaxial and non-intrusive configuration, for height monitoring on an AM setup. A laser beam from the sensor enclosure is projected onto the melt pool and a coaxial camera, which is located adjacent to the laser beam in the sensor enclosure, obtains the laser spot and converts its position to relative height. In this paper, the laser triangulation device is being used for process monitoring of the deposition of a stainless steel cylinder. The ultimate output of the sensor is a spatial map displaying height variation in the melt pool [55].

Some of the main issues posed by the triangulation system utilized in the paper are that: (1) the system is used to monitor the height of a melt pool and (2) laser spot detection quality could deteriorate because of the target's reflectivity. As mentioned in the paper, "spot detection might partially suffer from … target reflectivity," and this is another major issue that could come about from using laser triangulation for the thesis' objective [55]. This article provided valuable insights and context into how laser triangulation can be used in process control of additive manufacturing as well as some issues that could arise through its usage.

Another reading that provided useful information on the use of laser triangulation for in-process monitoring for additive manufacturing was "Novel machine and measurement concept for micro machining by selective laser sintering," [56]. In this paper, a Keyence 2D laser displacement sensor operating according to the principle of optical triangulation was used to verify the thickness of deposited powder layers as well as the resulting sintered parts. For this paper, the main objective was to find inhomogeneities and surface defects in the deposited powder layer. The tools and approach produced useful results for the researchers [56].

Laser triangulation sensors are not often used on reflective surfaces because the laser light "would bounce directly back onto itself" [57]. The accuracy of a laser from a laser triangulation sensor on a reflective surface is challenged because the surfaces produce a distortion of the reflected beam called the speckle effect. The speckle effect is caused when the laser light is intermittently coherent and is scattered from a random, non-homogenous surface. This surface would cause small waves to overlap in the air after leaving the surface, leading to the speckle effect [58].

However, the accuracy of a red laser from a laser triangulation sensor on a reflective surface is challenged because the surfaces produce a distortion of the reflected beam called the

speckle effect. The speckle effect is caused when the laser light is intermittently coherent and is scattered from a random, non-homogenous surface. This surface would cause small waves to overlap in the air after leaving the surface, leading to the speckle effect [58].

Along with the reviewed literature on laser triangulation, it was found through general research that one of the most popular applications for laser triangulation sensors is the characterization of powder spread. Particularly in contexts like inventory management or quality or process control, which relates to this project, laser triangulation sensors can provide precise measurements and have begun replacing tools like manual contact gauges and Linear Variable Differential Transformer (LVDT) sensors [57]. Another relevant aspect of these types of sensors is their ability to measure in the correct scale of units.

4.3. Structured Light

Another type of sensor considered during preliminary research was the structured light sensor. Structured light imaging has the "potential for micrometer-level 3D measurement" and is commonly used in machine vision applications due to its high-resolution capabilities [31]. Structured light imaging sensors are able to capture 3D topographies of surfaces using a particular pattern of light and a 2D imaging camera, as seen in Figure 5. The pattern is projected onto a target object and as the camera observes the pattern from various perspectives, the target object's surface features distort the projected pattern. This distortion is then used to reconstruct the 3D topography of the target object [59].
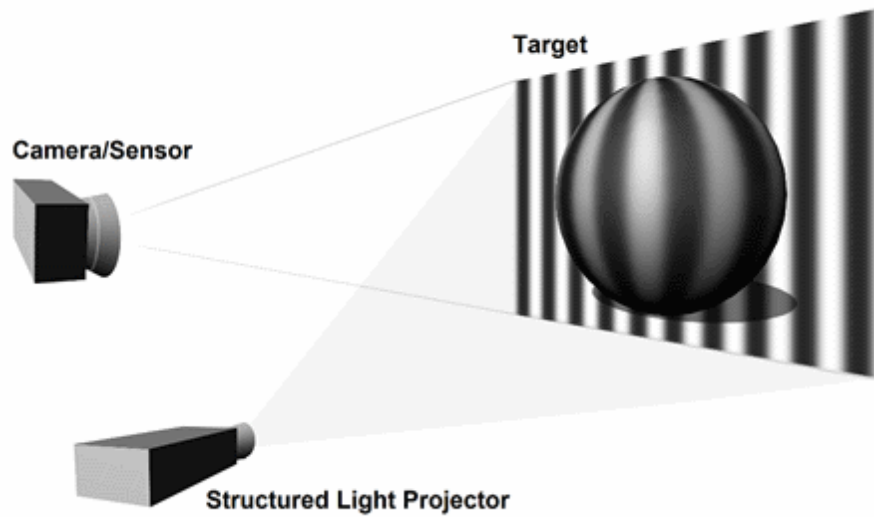
Figure 5. The principle of projecting a pattern on a target in structured light imaging is shown above [59].

One piece of literature that provided insight into the use of structured light imaging in additive manufacturing is "In situ Surface Topography of Laser Powder Bed Fusion Using Fringe Projection" [60]. As previously explained, the projected fringes will become deformed by the variations of the surface's features, and these deformed fringes are then used to get the surface topography [59]. The main components of a fringe projection system are a projector and a camera. The projector can produce structured light patterns (e.g. a sequence of sinusoidally varying intensity patterns) on the surface of the object, while the camera captures these patterns from a different viewing angle. The projected fringes appear deformed due to local height variations of the object surface. The deformed fringes captured by the camera are then reconstructed to obtain the 3D shape of the object [60].

One issue with structured light imaging that is also found with laser triangulation is that of the speckle effect, as previously discussed. The researchers in this paper were able to identify the saturated pixels and remove them from the data set before reconstructing the topography

43

[60]. By performing structured light imaging and adequately overcoming issues caused by the speckle effect, this paper presented a promising application for structured light imaging in the thesis project [60].

The main issue the researchers encountered is that the entire process of detecting and classifying defects is very manual. The system in place can take important measurements, such as the height profile, through manual selection, but would require machine learning techniques to be able to make the same detections in an automated way [31]. While this study does not specifically state the kind of powder used, there is no mention of reflectivity issues [31].

Other than the issue of the speckle effect, the literature reviewed provided strong evidence for the applicability of structured light sensors in the MIT thesis project. In particular, these sensors are able to capture a 3D topography of the target surface which provides a more complete view and therefore more comprehensive analysis of the surface under consideration. Additionally, the literature showed that structured light sensors were successful in an AM process, providing further credibility for its use. Because of this, the group decided to move forward with trying out a few different structured light sensors. The different scanners that we acquired for demonstration purposes will be explained in Chapter 5.

4.4. Confocal Chromatic Sensors

The confocal principle uses a single-point light source to measure only the reflected light from a surface that is in focus [61]. Confocal microscopy is a popular method for determining surface roughness including for AM produced parts, but the machines are large and bulky as they are meant to be used in a post-production quality analysis environment [29], [62]. Confocal chromatic sensors, also referred to as white light or multi-color confocal sensors, use a variation of the confocal principle that splits the point source light into different wavelengths, or different

colors through a series of lenses. The reflected light can then be analyzed for the wavelength that is most in focus through the use of a spectrometer. This eliminates the need for electronics within the sensor head which greatly reduces the size of the sensor and makes it usable in vacuum environments [63] - [64]. Sensor manufacturers laud the increased stability, precision, and accuracy of their confocal chromatic sensors even on difficult surfaces including transparent, high roughness, and tilted surfaces [65], [30], [63].

The use of confocal chromatic sensors within AM is not as common as other optical techniques. Their advantage in measuring through transparent media makes them more popular in the biological sciences. Scanning systems allow the point sensor to recreate 3D models of samples which can take about 2 hours to build for a window of 2.1 mm by 0.95 mm [61]. Yang developed an in-process confocal scanning imaging system with a fiber transceiver to characterize the powder and solid material within the print bed [66]. They reported successful imaging even with the high scattering of the loose powder surface, though they mentioned the need for further work on verifying these results in terms of surface roughnesses.

Chapter 5: Methodology for Evaluating Optical In-Process Monitoring Tools

5.1.   Overall Project Approach

As stated in the Problem Statement, this project investigates the possible sensor technologies and strategies that can provide in-process data to characterize the layer condition in a 3D printer, along with the varying advantages and shortcomings of each. This project aimed to investigate a powder layer of 1 to 3 units. The overall aim of the project is to create a verification tool that could be used to check the quality of a layer set up. Ideally, the tool would be created using existing sensors and cameras available on the project's machine to perform this check.

Before that could be done, the on-machine camera needs to be characterized and a source of truth for good and bad pertinent layer setups needs to be established. This was first approached by trying to find a laser sensor to characterize the powder on a part as covered in Wittenbrink's thesis. The measurement was performed and then converted to units for the sake of this project. Ultimately, no sensor was able to characterize the powder[4]. At the same time, alternative cameras giving a closer view of the part was explored as a comparison to the existing on-machine camera to determine if the on-machine camera is the best option for image analysis. This analysis is the focus of this thesis. An analysis of the on-machine camera was performed to characterize its performance as detailed in Kota's thesis[5]. Finally, a verification tool will be developed by correlating the laser sensor data and images from the on-camera machine which is

---

[4] J. Wittenbrink, "Using Displacement Sensors to Characterize Critical Powder Layers in Laser Powder Bed Fusion" thesis, 2022.

[5] M. Kota, "Using Optical Imaging and Image Processing to Verify Initial Layer Setup in a Laser Powder Bed Fusion Process," thesis, 2022.

outlined in Sabarad's thesis[6]. All images were analyzed by checking the average pixel intensity on each part using ImageJ image analysis software.

Ideally, these tasks would be performed in series as shown in the flowchart below in Figure 6. However, due to the timeline constraints of this project, all sensor analyses were performed in parallel. Input from all studies was considered when creating the verification tool. The colored blocks in Figure 6 show the aspects of the project which are covered in the four individual theses that were written for the project. The black blocks represent elements of the project covered in all theses.

---

[6] S. Sabarad, "Comparing Various Methods for Validation of the Initial Layer in an LPBF process using Optical and Displacement Sensors," thesis, 2022.
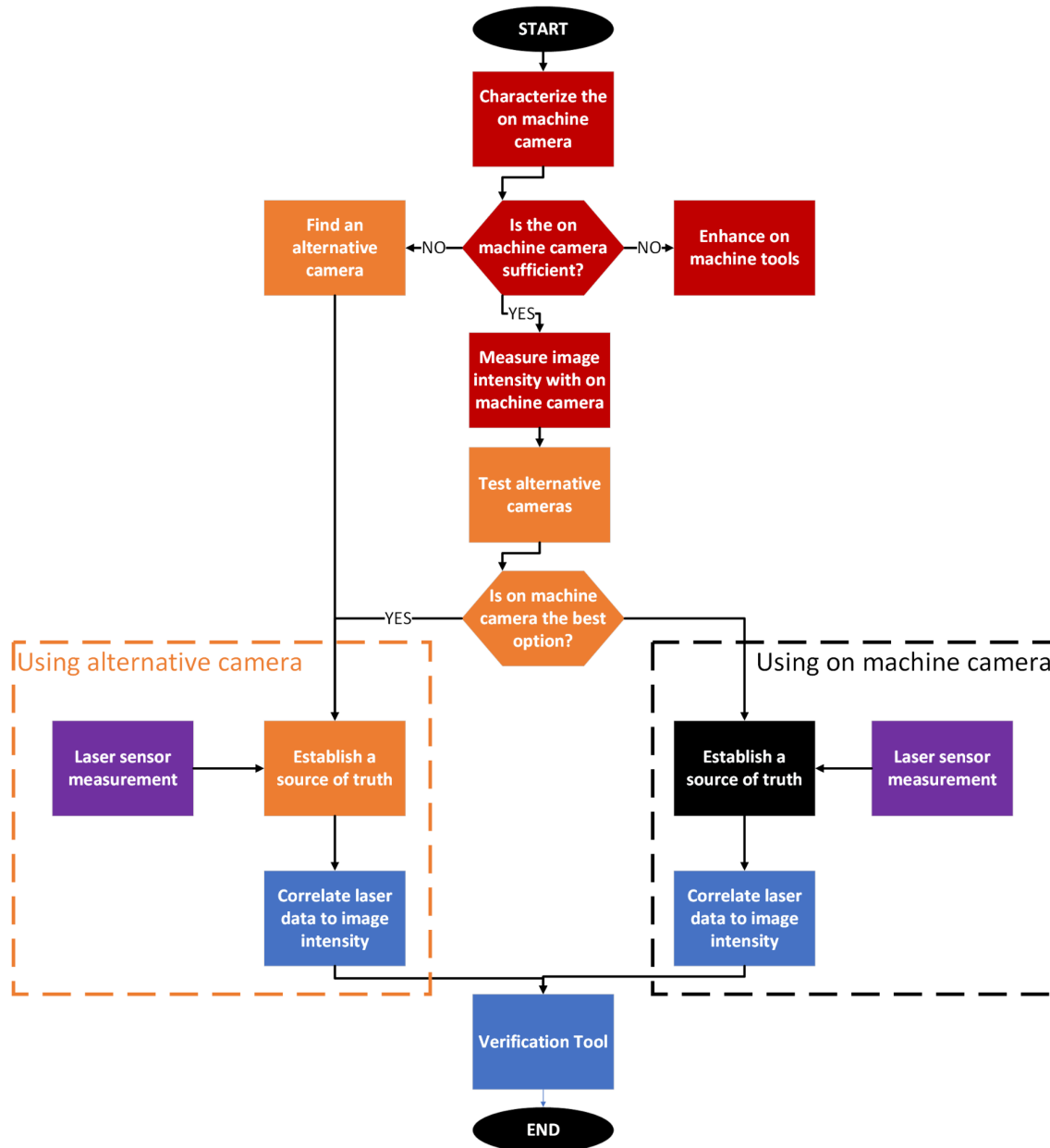
Figure 6. Flowchart describing the project approach for the full project. Items in orange are described in detail in this thesis. Items in red are the focus of Kota's thesis[7]. Items in purple are the focus of Wittenbrink's thesis[8]. Items in blue are the focus of Sabarad's thesis[9]. Items in black are covered in all project theses.

---

[7] M. Kota, "Using Optical Imaging and Image Processing to Verify Initial Layer Setup in a Laser Powder Bed Fusion Process," thesis, 2022.

[8] J. Wittenbrink, "Using Displacement Sensors to Characterize Critical Powder Layers in Laser Powder Bed Fusion" thesis, 2022.

[9] S. Sabarad, "Comparing Various Methods for Validation of the Initial Layer in an LPBF process using Optical and Displacement Sensors," thesis, 2022.

5.2.   Initial Tests of Optical In-Process Monitoring Tools

5.2.1.   The Goal of Testing

Early on in the project, proof of concept testing was performed with various sensors to determine if optical monitoring tools were a feasible solution to characrterize layer setup. These proof of concept tests were designed to quickly set up and gather data to test the higher-level technology powering the tool as a solution for the project. Literature reviews showed that optical monitoring tools presented promise, but it was unclear if the necessary resolution could be achieved given the space constraints in the machine.

Optical in-process monitoring tools were considered as tools that take readings from a stationary position as opposed to scanners which take readings while in motion as described in Wittenbrink's thesis[10]. Proof of concept testing for optical in-process monitoring tools in this project involved cameras, confocal microscopes, and 3D scanners including 3D snapshot sensors and a dual camera infrared structured light scanner.

5.2.2.   Keyence VHX 6000 Digital Microscope

Initial proof of concept testing was performed on a Keyence VHX 6000 Digital Microscope. The Keyence VHX 6000 Digital Microscope is a confocal digital microscope that was used to test the concept of detecting powder on a part from a close view. The digital microscope uses a confocal focus which allows for an adjustable focus over a Z height and provides a 3D map of the surface under inspection. A thin layer of powder was spread across the part to view under the microscope. The goal was only to determine if optical imaging was

---

[10] J. Wittenbrink, "Using Displacement Sensors to Characterize Critical Powder Layers in Laser Powder Bed Fusion" thesis, 2022.

possible to the resolution necessary. Images collected proved that it was possible to detect powder over a part.

5.2.3. Gocator 3D Smart Snapshot Sensor: 3210 series

A Gocator 3D Smart Snapshot Sensor: 3210 series was tested as a proof of concept for 3D scanning sensors. The Gocatro 3210 uses "blue-LED structured light technology and a wide field of view" to inspect large parts [67]. The sensor is commonly used to inspect automotive parts and assemblies [67]. This sensor was chosen to be evaluated for its large field of view. The sensor was mounted in the machine with a universal mount. Measurements were taken on a build platform with powder deposited over a part.

The results showed a clear topography of the powder and the part. In order to achieve these results, the build platform had to be dropped significantly. This would not be possible to do during a normal 3D printer setup. The working distance required to get a reading along with the size of the sensor itself did not meet the physical constraints of the project machine. Other 3D scanning systems were investigated, but the group was unable to find any sensor that would meet the physical constraints of the machine once the size of the sensor and working distance required were considered.

5.2.4. Revopoint POP 2 3D High Precision Scanner

Another 3D scanner that was tested for the project was the RevoPoint POP 2 3D High Precision Scanner. This scanner uses dual camera infrared structured light to scan objects. As mentioned in Chapter 3, the literature mentioned that a 3D optical scanner can require the use of markers for calibration and alignment across the surface being studied which can be difficult to implement within an AM production area [5], [31]. The RevoPoint POP 2 3D High Precision

Scanner ran into these issues. In order to scan a flat surface such as the build platform, markers would be required. Markers cwould present issues once powder was added to the build platfrom. Before placing the scanner in the machine, it was tested on a keyboard to check if it could scan a flat surface without markers. This test proved unsuccessful so the RevoPoint POP 2 3D High Precision Scanner was abandoned.

5.3.   Testing Optical In-Process Monitoring Tools

5.3.1. Introduction

Data for Optical In-Process Monitoring Tools testing was collected for two types of setups where the machine door could be opened and closed during testing. These will be referred to as the first configuration and the second configuration. For these tests data was collected with the on-machine camera, a Spectral Instruments RVT100 camera, a GoPro HERO7 Black, and a STPCTOU Wireless Digital Microscope, and an iPhone 12. These experiments are outlined in Chapters 5 and 6.

5.3.2. The On-Machine Camera

The camera which has been referred to as the on-machine camera is a monochrome camera paired with a lens. This camera lens combination was installed on the project's machine for testing. The camera is a CMOS (complementary metal oxide semiconductor) camera that can detect visible light. For documentation purposes, the on-machine camera was referred to with the acronym 3DP for 3D printer. The lens has an adjustable diaphragm ring and focus. The

diaphragm ring controls the amount of light that is allowed to pass to the image sensor. Further explanation of the lighting and camera setting experimentation can be found in Kota's thesis[11].

The camera captures photos and videos. For all testing with the on-machine camera, images were captured by taking a screenshot of the 4K video along with a captured image from the machine to test whether there was a difference in results. Captured images were saved as JPG files on the computer controlling the 3D printer. The 4K videos were saved as MP4 files on the computer controlling the 3D printer. JPG images were captured from the 4K videos by opening the video in the VLC media player and using the Video Capture Snapshot tool.

5.3.3.   Spectral Instruments 1700s RVT100 Camera with CMOS Camera HTTP Server

The Spectral Instruments RVT100 was chosen for testing [68]. The RVT100 camera is a 2-megapixel camera that requires a CMOS Camera HTTP Server to operate [68]. A CMOS sensor operates on semiconductor chips produced by photolithography. The chips feature light-capturing cells that "pick up the photons at their various wavelengths as focused by a lens, translating them into electrons" [69]. The charge of the electrons gathered by the cells is amplified by surrounding transistors and sent across the chip by tiny wires on the circuitry of the chip. The CMOS server converts the differing charges of the individual cells into pixels via a digital to analog converter [69].

The camera was connected to the CMOS server with a fiber optic cable and power cable. The CMOS server was connected to a power supply and a computer via an ethernet cable. The camera was controlled from the Spectral Instruments SI Image CMOS Software. Images from the software were saved as FITS files. The FITS native files could be opened natively in the

---

[11] M. Kota, "Using Optical Imaging and Image Processing to Verify Initial Layer Setup in a Laser Powder Bed Fusion Process," thesis, 2022.

Image Analysis Software for analysis, but for the sake of making a fair comparison to images from other cameras, pictures were converted to JPG for analysis.

The focus of the camera was adjustable by physically moving the camera closer or smaller to the part. As such, two camera mounts were printed on a fused deposition modeling machine before the optimal placement to get the picture in focus was achieved. Since the full part could not be captured in a single image, area sampling testing was performed. For documentation purposes, the Spectral Instruments RVT100 camera was referred to with the acronym SI.

5.3.4. GoPro HERO7 Black

A GoPro HERO7 Black was available for use on this project. The GoPro camera can take photos at 12 Megapixels as well as high dynamic range, (HDR), photos [70]. The fish eye lens on the GoPro camera allows for a large field of view to be taken from a close range. The GoPro was mounted in the machine with a universal mount that had to be removed each time the recoater was passed over the build platform. Images were captured with the camera via the GoPro Quik app. The images were saved as JPG files. For documentation purposes, the GoPro HERO7 Black camera was referred to with the acronym GP.

5.3.5. STPCTOU Wireless Digital Microscope

The STPCTOU Wireless Digital Microscope includes a 2 Megapixel camera that can operate with 50 to 1,000 times magnification zoom[71]. The microscope's LED light was not used during testing. Instead, the machine light was used to illuminate the part. The microscope has an adjustable focus which can be adjusted through an app which controls it [71]. For testing, 1920 by 1080 resolution, the largest resolution setting, was used to allow for the largest picture

of the part to be taken. Images were captured by controlling the microscope through a phone app. The pictures were saved to the phone. They were uploaded to a computer and renamed with their respective naming conventions as JPG files. Since the full part could not be captured in a single image, area sampling testing was performed. The acronym "UM" was used to name pictures captured with this USB Microscope.

5.3.6. iPhone 12

An iPhone 12 was available for use with this project. Pictures were taken with the Wide lens camera which is 12 megapixels, has an f/1.6 aperture, 100% focus pixels, and auto image stabilization [72]. Images were transferred to a computer and downloaded as JPG images. A mount was not used for the iPhone 12. Instead, the camera was held in an approximate location above the part and centered over the part for each picture. For documentation purposes, the iPhone 12 camera was referred to with the acronym PC for a phone camera.

5.4. Test Setup

5.4.1. Engineering Study Setup

An engineering study was documented prior to its execution. This ensured that the same setup and data collection procedures were followed for all replicates. All studies were performed with three replicates. In this case, a replicate represents a machine setup, (SU1, SU2, SU3). Some tests were performed to characterize the repeatability of cameras by taking the same image one after another for the same setup. Each of these images is called a repeat, (R1, R2, R3, etc.). Other tests were done to characterize the performance of a sensor for cameras that can only look at a small area by taking multiple images from different locations on the same part. Each of these images is referred to by the location, (L1, L2, L3, etc.), on the part. Additionally, some tests were

performed to characterize the variability of image intensity across several parts. Lastly, tests were performed with varying layer thicknesses. Each of these images is described by its layer height in units, (0, 0.25, 0.5, etc.).

5.4.2. Mounting Cameras in the Machine

The goal of the alternative camera testing was to verify whether the results from the on-machine camera were giving consistent and accurate results. Therefore, the alternative cameras needed to be mounted in the machine chamber. A custom recoater assembly piece, had already been machined for prior project work to support the line sensors analyzed in Wittenbrink's thesis[12].

A universal C-clamp mount was used to mount the USB Microscope and the GoPro HERO7 Black cameras. These mounts had to be removed and replaced in the machine every time the recoater was passed over the build platform during testing. This added some variability to the placement of the cameras.

Originally the iPhone 12 camera was just going to be used as a reference image. Due to limited space on the recoater and a limited number of clamps available, the iPhone was held by hand in approximately the same location for each image taken. Creating a mount for the iPhone may have improved the variability seen from the iPhone images. This could be taken into consideration for future work.

---

[12] J. Wittenbrink, "Using Displacement Sensors to Characterize Critical Powder Layers in Laser Powder Bed Fusion" thesis, 2022.

5.4.3. Lighting

As discussed in Chapter 4, lighting is one of the most important factors in getting a good image from a camera. The lighting was set up to be consistent for each sensor for all tests. For the on-machine camera, a light placed inside the 3D printer was turned on and light from outside the machine was blocked from getting in. This is true for both images and videos collected with the on-machine camera.

For the images captured with the USB Microscope and the iPhone 12, the light inside the 3D printer was turned on and the machine door was left open. The ambient lighting outside of the machine was always the same. The LED light on the USB microscope itself was turned off. The flash option on the iPhone was turned off. The iPhone images seemed to have a gradient from the LED light in some of them which is an indication that alternative lighting options should have been explored for the iPhone 12 pictures.

The machine light was turned off and the machine door was left open for pictures captured with the GoPro HERO7 Black and Spectral Instruments RVT100 cameras. This was chosen as the best option although it differed from the lighting for other cameras as it minimized the glare from lighting seen in the images.

5.5. Experimental Setup and Procedures

5.5.1. Introduction

As stated in the problem statement, this project aims to objectively characterize a layer in a 3D printer. Ideally, this would be done with existing equipment on the machine or additional equipment which is easy to install. Using cameras to capture images of the layer allows for an intensity value to be calculated for each part. This intensity value is a measure of the darkness of

the pixels which make up a grayscale image. The intensity of an image will vary depending on the camera, lighting, and camera placement which is why the setup for each camera was decided before testing began. The intensity values give a macro view of the powder on the part rather than looking at a percentage area covered with individual powder particles. The main goal of this testing was to characterize the repeatability and reproducibility of each camera. The hope was that this testing would serve as an interim step, as outlined in the flowchart in Figure 6, and that the on-machine camera could be used for a long-term solution.

5.5.2. Testing Order

Ideally, a Gage Repeatability & Reproducibility (Gage R&R) would be performed to assess the repeatability and reproducibility of each camera before moving on to further characterization testing. However, since there was a limited timeline and a timely data collection process, all data for all experiments was collected at one time. As such, the setup named for each setup configuration, (SU1, SU2, SU3), is the same setup across all tests.

Experiments took readings at different powder layer heights. The first readings were taken on the first configuration with no powder on it as a reference. Then the second configuration was set up and data was collected for a 3 unit layer. Once the build platform was at 3 units, data for all tests was collected before small increment drops for the Powder Layer Thickness Test continued. Readings for all tests were taken in the following order: iPhone 12, STPCTOU Wireless Digital Microscope, GoPro HERO7 Black, Spectral Instruments RVT100, and the on-machine camera. For tests where not all cameras were tested, the same order was followed with only the applicable cameras.

5.5.2. Camera Repeatability Test

Camera repeatability was tested for all cameras: the on-machine camera, Spectral Instruments RVT100, GoPro HERO7 Black, STPCTOU Wireless Digital Microscope, and an iPhone 12. This test aimed to determine which test would be the most repeatable. The hypothesis was that the on-machine cameras would not be as repeatable as closer mounted cameras. Out of the closer mounted cameras, the hypothesis was that the GoPro HERO7 Black would be the most repeatable since it had a standard mount to use, (unlike the iPhone 12), and could take photos in HDR.Data was gathered for both setup configurations. Three setups were performed for each configuration. Five repeats of each reading were taken one after another. Where applicable, the camera was placed in the build chamber with its removable mount.

For documentation purposes, the repeatability test for the first configuration was referred to as T0. The repeatability test for the second configuration was called T1. Images were saved with the following naming convention: "Setup#_Test#_Camera acronym_Layer height_Repeat #." For example, the measurement which was taken for the first repeat on the first setup on a first configuration with the Spectral Instruments RVT100 camera with no powder on it was named: SU1_T0_SI_0_R1. For setup 2, the reading taken from the alternative part followed the same naming convention with a designation appended.

5.5.3. Area Sampling Test within a Part

For cameras that could not capture the full part with one image, an area sampling test was performed. This test aimed to test the variability in intensity for a single part at different areas on the part. This test was performed for the Spectral Instruments RVT100 camera and the USB Microscope. The hypothesis was that there would be little variability for intensity values at different locations on the same part for both cameras in question. Data was gathered for both first

configurations and second configurations. Data was gathered with the on-machine camera as a reference. Three setups were performed for each configuration. Data was collected following the same process of the camera repeatability test (at 0 and 3 units for first and second configurations). For this test, only one image was captured in each position.

The Spectral Instruments RVT100 camera captured a very small portion of the part. For the Area Sampling Test, images were taken from five locations on the part. The location, L3, in the middle of the part is the location that was used for all other tests. For this test, images were also taken from the upper right, lower right, upper left, and lower left regions of the part. The location that the image was taken at is denoted with an alphanumeric code from L1 to L5 in its filename.

The STPCTOU Wireless Digital Microscope captured a larger area of the part compared to the Spectral Instruments RVT100 camera, but it still did not capture the entire part. For the Area Sampling Test, images were taken from three locations on the part. Images from each location could be stitched together to form an image of the entire part. For all other tests, images were taken over the center of the part. The location that the image was taken at is denoted with an alphanumeric code from L1 to L3 in its filename. The locations are unique to this test meaning images from other tests do not match the images taken for this test.

For documentation purposes, the area sampling test for the first configuration was referred to as T0.2. The area sampling test for the second configuration was called T1.2. Images were saved with the following naming convention: "Test#_Camera acronym_Layer height_Replicate #_Location #." Here, the replicate number refers to the setup number. For example, the measurement which was taken for location 1 on the first setup on a first configuration with the Spectral Instruments RVT100 camera with no powder on it was named:

T0.2_SI_0_R1_L1. Relocating the Spectral Instruments RVT100 camera along the X-axis of the machine could be done by manually pushing the recoater. Relocating the Spectral Instruments RVT100 camera along the Y-axis was completed by manually pushing the camera along the dovetail groove. This required the machine door to be opened.

5.5.4. Powder Layer Thickness Test

Variability in intensity value from one layer thickness to another was tested for all cameras. This test aimed to determine what change in intensity could be expected for increasing powder layer thicknesses as well as how small of a difference in powder layer thickness could be detected from each camera. The hypothesis was that image intensity would increase linearly with powder layer thickness until the jamming point was reached and intensity would reach an asymptote. The hope was that each camera would be able to detect differences in powder layer thickness with a granularity down to 0.25 units.

Data was gathered only for second configurations. Three setups were performed. Readings were taken at the following powder layer heights in units: 0 (datum), 0.50, 0.75, 1.00, 1.25, 2.00, 2.75, 3.00, 3.25, 3.50, and 5.00 units. These numbers were chosen to focus on data collection around the edge cases for the 1 to 3 unit specification (Figure 7). Data were taken at 0 and 5 units as extreme cases outside the specification bounds. Data was taken at 2 units as the nominal setting.

Figure 7. Markers showing the powder layer thicknesses that were tested for the Powder Layer Thickness Test. The minimum and maximum specifications, 1 and 3 units, are highlighted in red. The nominal value, 2 units, is highlighted in green.

Where applicable, the camera was placed in the build chamber with its removable mount at each layer reading. All readings were taken from the same part studied in previous tests. The camera was positioned over each part and an image was captured. The recoater was swept left to right then right to left between each layer set, pushing a set amount of powder with every pass. For documentation purposes, the powder layer thickness sampling test was referred to as T3. Images were saved with the following naming convention: "Test#_Camera acronym_Layer height_Replicatet #." Here, the replicate number represents the repeat number. For example, the measurement which was taken for the first setup with the iPhone 12 camera with no powder on it was named: T3_PC_0_R1.

5.5.5. Comparing First vs Second Configuration

Variability in image intensity results between first and second configurations was compared for all cameras with the goal of determining if the setup configuration used yielded different results for the same setup. The hypothesis was that the mean intensity values for a second configuration and first configuration would be the same for each individual camera. Data for both the first configuration and second configuration was analyzed for the Camera Repeatability Test (T0 and T1) as well as the Area Sampling Test (T0.2 and T1.2).

The compiled results of these tests will inform the timing for testing. If results show that a first configuration and second configuration are all equivalent then there is more flexibility in where the final testing can take place during the machine setup. Allowing the analysis to be done with a first configuration or second configuration means that adjustments can easily be made since the machine door can still be opened.

5.5.6. Variability from the On-Machine 4K Video and Captured Images
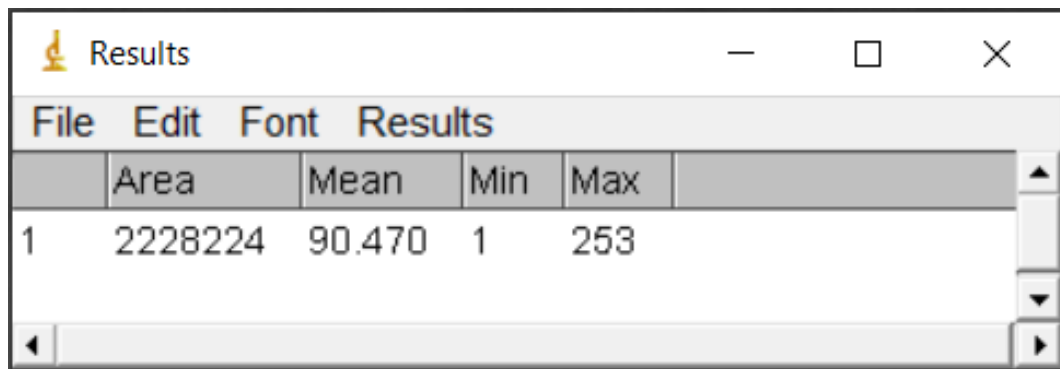
Data from the on-machine camera was collected in two ways as described previously. A nested analysis of variance was performed to detect how much of the overall image intensity variability came from the different cameras. The hypothesis is that these images will yield the same image intensity results.

5.6. Image Analysis with ImageJ

5.6.1. Introduction
All images were analyzed in the Image Analysis Software. Images from all cameras were analyzed as PNG images. The area analyzed, mean intensity value of the image, minimum intensity value of a pixel on the image, and maximum intensity value of a pixel on the image

were recorded. Image intensity values could range from 0 to 255. For the purpose of the tests described here, only the mean intensity value was used for analysis. An example of the the Image Analysis Software results as they are reported is shown in Figure 8 below. The results for each image were copied from the Image Analysis Software and pasted into a spreadsheet denoting which image the results were for with the naming conventions described in Section 5.5. The data in the spreadsheet was reformatted for ease of use before being analyzed in MiniTab.

Figure 8. Example results for average intensity as seen in the Image Analysis Software for all image analyses

5.6.2. Area Selection

the Image Analysis Software has several area selection tools which allow you to select a portion of an image to be analyzed. The polygon tool was used as the image selection tool. The freehand selection tool was also considered, but proved to be more difficult to use since a single line had to be drawn around the entire part border. The polygon area selection tool in the Image Analysis Software tool is highlighted below in Figure 9. Once the polygon has been created, points can be added and the shape can be moved or deleted [73]. The shape was moved to the next image when it could be to keep results as consistent as possible. Many individual images required new polygon selection areas to be drawn since the alignment and orientation of each image was not exactly the same for all setups.
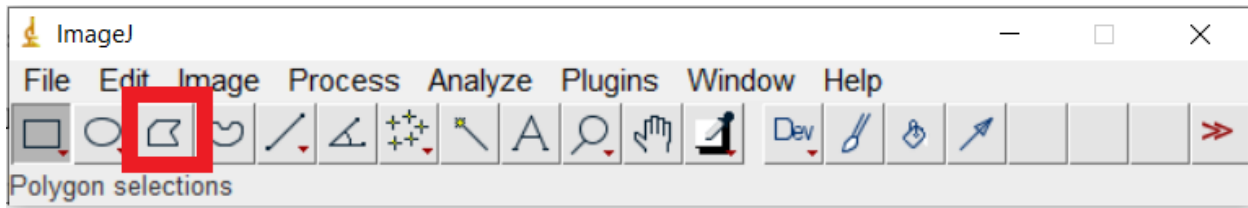
Figure 9. Area selection tools in the Image Analysis Software. The polygon selection tool is boxed in red.

Image selection was not needed for the images captured with the Spectral Instruments RVT100 camera for most tests, since the images did not capture a border of the part. Some images from the Spectral Instruments RVT100 for the Area Sampling Test did require image selection where the border of the part was showing. These images were cropped using the polygon selection tool as described above.

5.6.3. Macros

the Image Analysis Software allows for the creation of macros as a .JIM file. A macro allows for an input sequence to be automated by recording keystrokes or mouse actions [74]. They are typically used to replace repetitive actions for data analysis in spreadsheets, word processing, or in this case image analysis. the Image Analysis Software has a built-in macro generator which uses a command recorder [74]. The macro recorder could be used in combination with the polygon area selection tool to record where line segments were drawn on an image. Where the alignment and orientation of images were consistent, the macro could be used to remove some variation in the analysis process.

Macros were used for analyzing all the images from the on-machine camera. Setup 1 for the first configuration used one macro while all other setups used a different macro since the camera position was adjusted slightly after the data was collected for the Setup 1 first

configuration. Separate macros were required for images captured from the 4K videos and captured images since the perspective of each image was different.

5.6.3. Image Analysis Procedure

A standardized procedure was followed for analyzing each image recorded in the Image Analysis Software. In total, 885 images were analyzed. The analyses were grouped by test, camera, and other variables described in Section 5.5. The details for each analysis are outlined in Section 5.5. The results of each analysis are outlined in Chapter 6.

Chapter 6: Results and Discussion

6.1.   Introduction

The analyses for each test were performed one after the other since all data to be analyzed for all tests had already been collected. Ideally, data would be collected for one test then immediately analyzed so that cameras which did not perform well could be eliminated before moving on to the next test. Due to time constraints, this approach was not taken. Images were analyzed in the Image Analysis Software. The results were compiled in Microsoft Excel then analyzed in MiniTab 20.1.3.

6.2.   Camera Repeatability Test

The camera repeatability test aimed to establish which camera gave the most repeatable results. The hypothesis was that the GoPro would be the most repeatable. To determine the repeatability of each camera, a variability chart was created in Minitab 20.1.3. The variability chart is a graphical representation of the average image intensity for three setups with five repeats each for each camera. The graph includes standard deviation bars on each average and shows the variation for both layer thicknesses analyzed (0 and 3 units). A standard deviation graph was also created to show how the standard deviation of the intensity for a given part varies across the five repeats for each camera, layer thickness, and setup. Data analysis was performed to determine the variability overall with data from all setups and between repeats for a single setup.

6.2.1. Overall Variability for All Setups

Ideally, the three setups will have little variation between the mean intensity at each layer thickness setup. It is also ideal to have the largest difference between the mean intensity at a layer thickness of 0 units and the mean intensity at a layer thickness of 3 units. A larger gap between layer thicknesses would indicate that it should be easier to distinguish among all layer thicknesses with greater granularity.

The results show that the largest distinction in image intensity can be made for the on-machine camera captured images for both first and second configurations. Screenshots from the 4K videos and captured camera images show very similar results. Conclusions were drawn by analyzing the Coefficient of Variation (the ratio of the standard deviation to the average) shown in Tables 2 and 3. A Coefficient of Variation (CV) below 10% was considered good for this test. For the first configuration, the CV was greater than 10% for the on-machine camera and the Spectral Instruments RVT100 camera at 3 unit layer thickness. For the second configuration, the CV was greater than 10% for the on-machine camera and Spectral Instruments RVT100 camera at 3 unit layer thickness and the GoPro HERO7 Black at both 0 and 3 unit layer thickness. The variability charts are shown in Figures 10 and 12. The standard deviation charts are shown in Figures 11 and 13.

Table 2. Mean intensity value, standard deviation, and coefficient of variation for each camera found from the data from all setups for the Camera Repeatability Test for the first configuration (T0).

First Configuration (T0)	Layer height (units)	Mean Intensity	Standard Deviation	Coefficient of Variation
3DP vid	0	26.5	0.71	3%
	3	145.21	28.31	19%
3DP cam	0	24.55	0.47	2%
	3	145.37	27.14	19%
SI	0	55.91	2.07	4%
	3	106.44	16.51	16%
GP	0	72.08	4.55	6%
	3	111.82	8.76	8%
UM	0	99.97	7.16	7%
	3	136.43	6.98	5%
PC	0	121.31	3.44	3%
	3	132.83	6.03	5%

Table 3. Mean intensity value, standard deviation, and coefficient of variation for each camera found from the data from all setups for the Camera Repeatability Test for the second configuration (T1).

Second Configuration (T1)	Layer height (units)	Mean Intensity	Standard Deviation	Coefficient of Variation
3DP vid	0	31.317	0.562	2%
	3	181.056	30.421	17%
3DP cam	0	28.525	0.301	1%
	3	179.881	29.851	17%
SI	0	62.476	3.88	6%
	3	123.527	27.032	22%
GP	0	61.448	7.303	12%
	3	93.716	11.087	12%
UM	0	111.294	8.523	8%
	3	136.045	4.026	3%
PC	0	92.494	8.214	9%
	3	122.366	8.455	7%
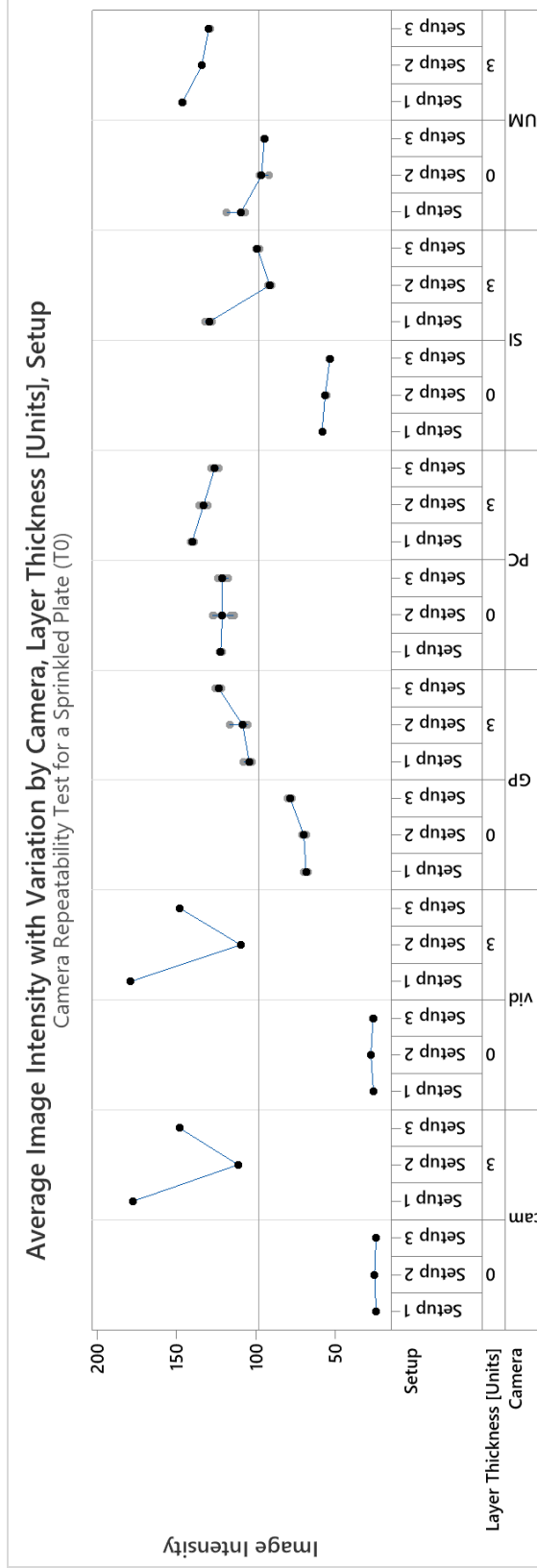
Figure 10. Variability chart for the Camera Repeatability Test for the First Configuration (T0). The largest differential in image intensity from 0 to 3 unit layer thickness can be seen for the on-machine camera. The on-machine camera also shows a large variance from setup to setup at 3 unit layer thickness.
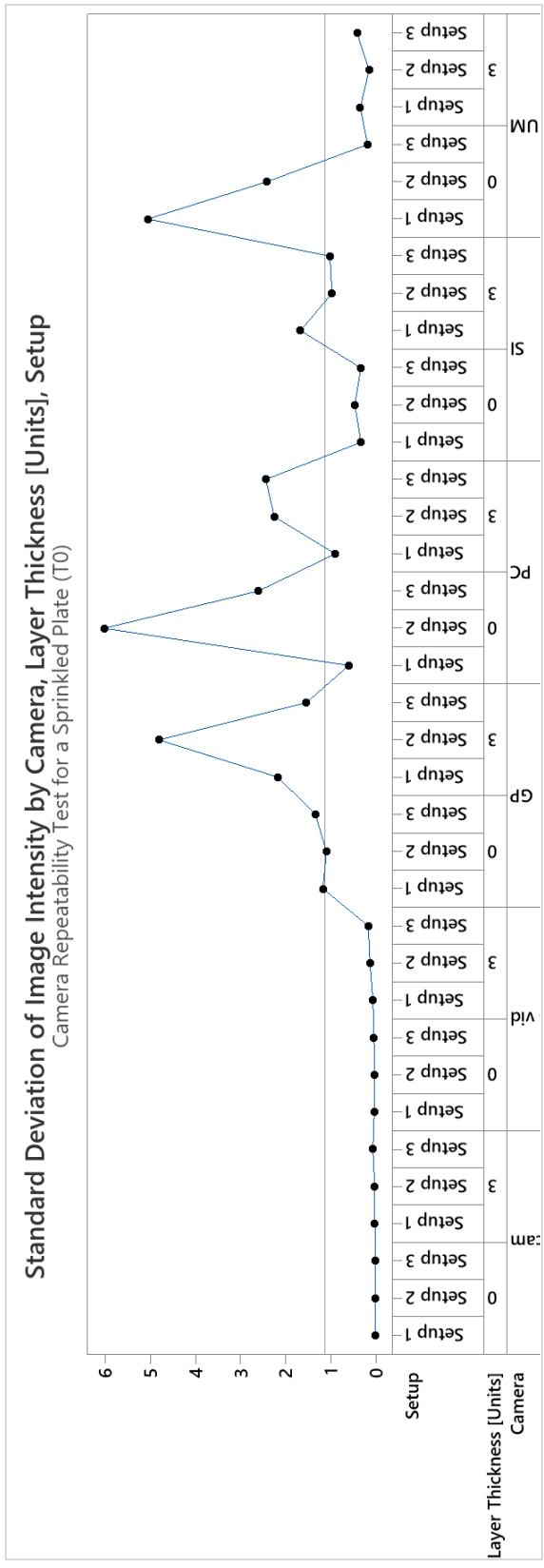
Figure 11. Standard deviation chart for the Camera Repeatability Test for the First Configuration (T0). The largest standard deviation can be seen for the GoPro HERO7 Black and iPhone 12 at 3 units layer thickness for setup 2 and the STPCTOU Wireless Digital Microscope at 0 units layer thickness for setup 1.
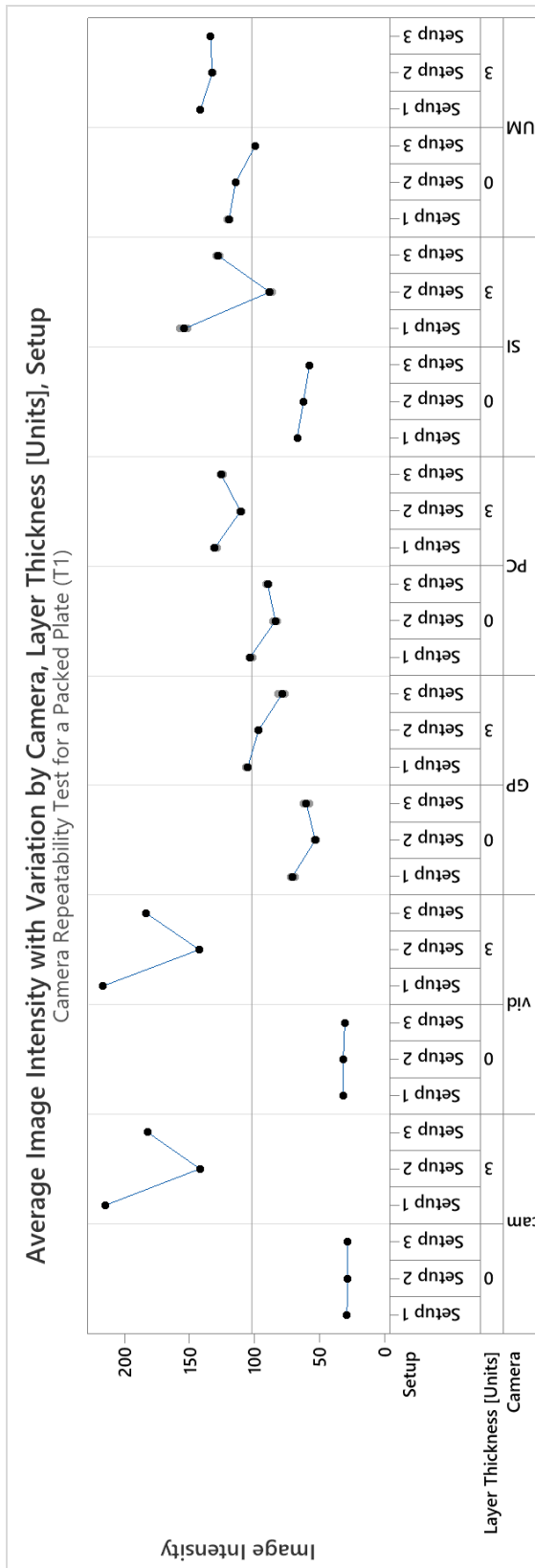
Figure 12. Variability chart for the Camera Repeatability Test for the Second Configuration (T1). The largest differential in image intensity from 0 to 3 unit layer thickness can be seen for the on-machine camera. The 3 on-machine camera also shows a large variance from setup to setup at 3 unit layer thickness.
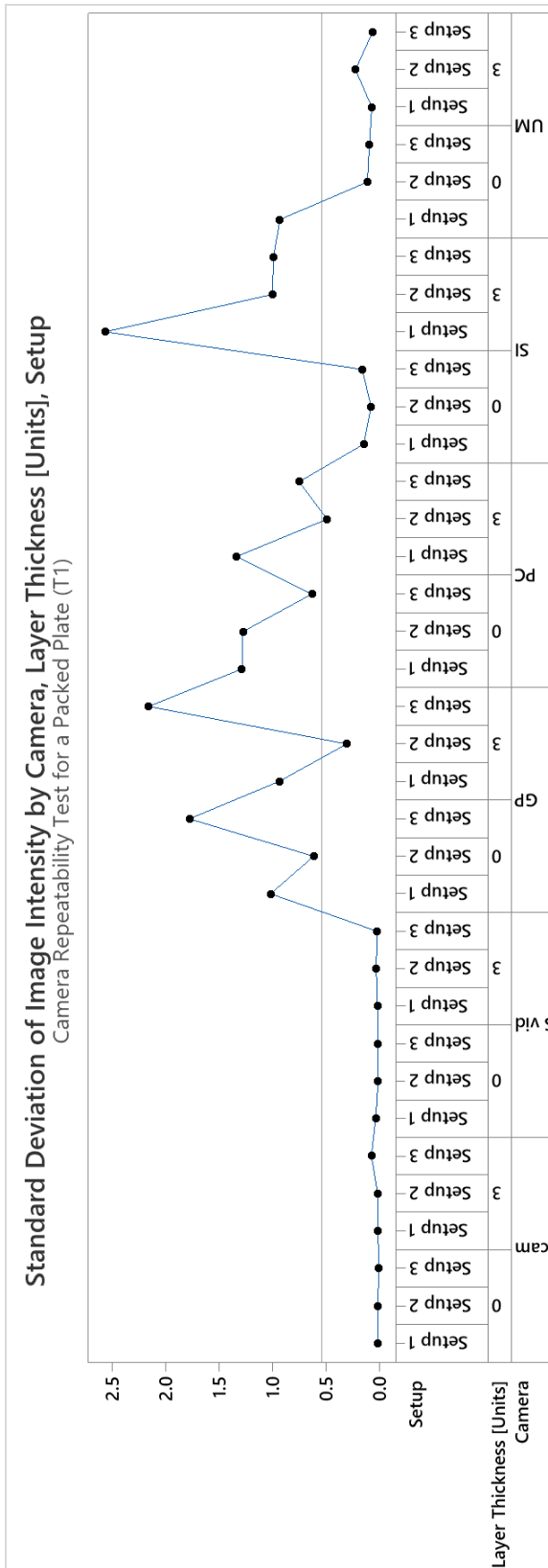
Figure 13. Standard deviation chart for the Camera Repeatability Test for the Second Configuration (T1). The largest standard deviation can be seen for the GoPro HERO7 Black and iPhone 12 at 3 units layer thickness for setup 2 and the STPCTOU Wireless Digital Microscope at 0 units layer thickness for setup 1.

6.2.2. Variability Within a Setup

The variability within a setup was analyzed by comparing Repeats 1 to 5 to each other for each camera, layer thickness, and setup combination. The averaged values for the on-machine camera as discussed above were used for this study. Conclusions were drawn by looking at the coefficient of variation (CV). The CV was below 5% for all camera, layer thickness, and setup combinations for both the first and second configurations. The conclusion from this analysis is that all cameras can yield repeatable results. Since this is the case, single images were captured for each data point for all following tests performed

Table 4. Mean intensity value, standard deviation, and coefficient of variation for each camera for each setup found from the data from the Camera Repeatability Test for the first configuration (T0).

T0	Layer height (units)	Mean Intensity			Standard Deviation			Coefficient of Variation		
		Setup 1	Setup 2	Setup 3	Setup 1	Setup 2	Setup 3	Setup 1	Setup 2	Setup 3
3DP vid	**0**	25.88	27.49	26.13	0.03	0.02	0.04	0%	0%	0%
	3	178.53	109.33	147.76	0.06	0.12	0.15	0%	0%	0%
3DP cam	**0**	24.21	25.21	24.23	0.01	0.01	0.01	0%	0%	0%
	3	177.31	110.96	147.85	0.02	0.03	0.06	0%	0%	0%
SI	**0**	58.21	56.27	53.25	0.30	0.42	0.30	1%	1%	1%
	3	129.29	91.12	98.90	1.50	0.87	0.91	1%	1%	1%
GP	**0**	68.26	69.69	78.28	1.05	0.98	1.20	2%	1%	2%
	3	104.05	108.11	123.30	1.95	4.31	1.38	2%	4%	1%
UM	**0**	109.18	96.22	94.51	4.53	2.16	0.17	4%	2%	0%
	3	145.96	133.85	129.48	0.31	0.14	0.38	0%	0%	0%
PC	**0**	121.97	120.91	121.04	0.54	5.39	2.33	0%	4%	2%
	3	139.94	132.74	125.83	0.81	2.02	2.18	1%	2%	2%

Table 5. Mean intensity value, standard deviation, and coefficient of variation for each camera for each setup found from the data from the Camera Repeatability Test for the second configuration (T1).

T1	Layer height (units)	Mean Intensity			Standard Deviation			Coefficient of Variation		
		Setup 1	Setup 2	Setup 3	Setup 1	Setup 2	Setup 3	Setup 1	Setup 2	Setup 3
3DP vid	0	29.196	33.222	31.115	0.032	0.016	0.004	0%	0%	0%
	3	163.702	158.183	185.507	0.019	0.024	0.015	0%	0%	0%
3DP cam	0	27.358	32.255	29.91	0.009	0.014	0.001	0%	0%	0%
	3	162.248	157.143	183.598	0.012	0.011	0.02	0%	0%	0%
SI	0	67.276	62.375	57.777	0.131	0.068	0.143	0%	0%	0%
	3	154.045	88.415	128.123	2.298	0.895	0.886	1%	1%	1%
GP	0	70.845	53.294	60.206	0.911	0.549	1.591	1%	1%	3%
	3	105.292	96.962	78.894	0.839	0.271	1.934	1%	0%	2%
UM	0	119.592	114.692	99.597	0.832	0.099	0.083	1%	0%	0%
	3	141.683	132.554	133.898	0.062	0.199	0.057	0%	0%	0%
PC	0	103.507	84.025	89.95	1.151	1.142	0.565	1%	1%	1%
	3	130.658	110.828	125.611	1.196	0.437	0.672	1%	0%	1%

6.3.   Area Sampling Test within a Part

The Area Sampling Test was performed to determine if sampling from one area of the part gave consistent results across the part for sensors which could not capture images of the entire part. The hypothesis was that the results would be consistent across the part. This test was performed for the Spectral Instruments RVT100 camera (SI) and the STPCTOU Wireless Digital Microscope (UM). An ANOVA was performed for each of the cameras. The ANOVA was split

up by camera and by layer thickness. In total, four ANOVA were performed originally. An additional test was added after analyzing the second test's results:
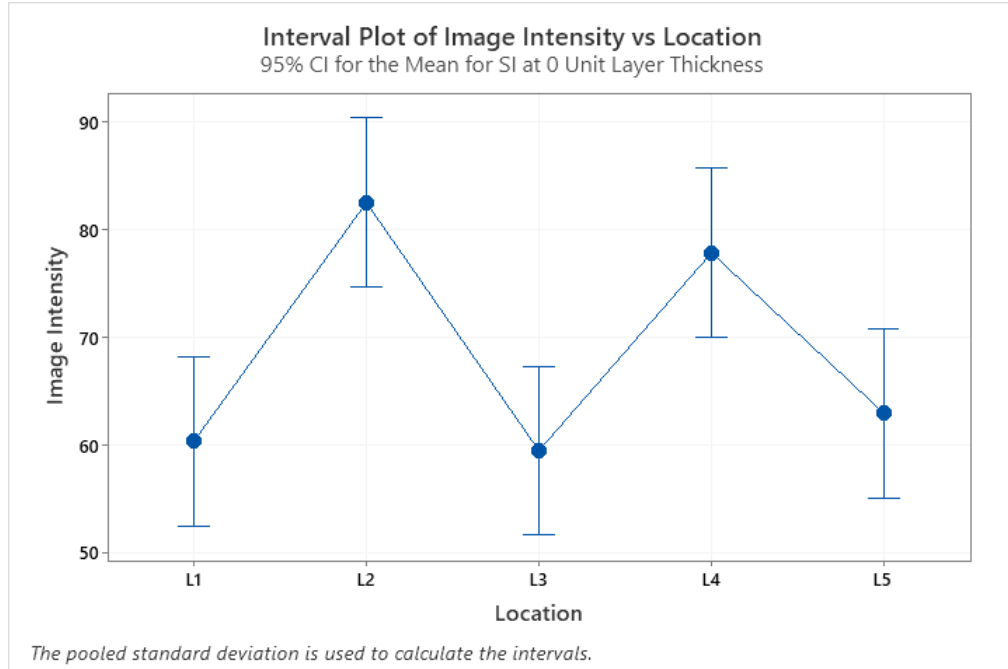
1. SI at 0 unit layer thickness

2. SI at 3 unit layer thickness

3. SI at 3 unit layer thickness with L3 excluded

4. UM at 0 unit layer thickness

5. UM at 3 unit layer thickness

The null hypothesis for each ANOVA was that all means are equal. The significance level, alpha, was set to 0.05. The resulting p-values are shown in Table 6. The resulting Interval Plots are also shown below in Figures 14 -- 18. Full results from the ANOVA are shown in the Appendix.

Table 6. The resulting p-values for an ANOVA comparing the image intensity values taken from different locations on the part for the Spectral Instruments RVT100 (SI) camera and the STPCTOU Wireless Digital Microscope (UM). Five locations were used for the SI camera and 3 locations were used for the UM camera. P-values show that both cameras did not give consistent results across all locations.

Camera	Layer Thickness [Units]	P-Value
SI	0	0.000
SI	3	0.029
UM	0	0.011
UM	3	0.033
SI (L3 excluded)	3	0.942

The resulting p-values from the ANOVA for the Spectral Instruments RVT100 camera at 0 units and 3 units layer thickness were 0.000 and 0.029, respectively. The p-values indicate that the null hypothesis should be rejected at the significance level of 5% for both tests for the SI camera. This means that the Spectral Instruments RVT100 camera did not give consistent results across different sampling locations on the part.
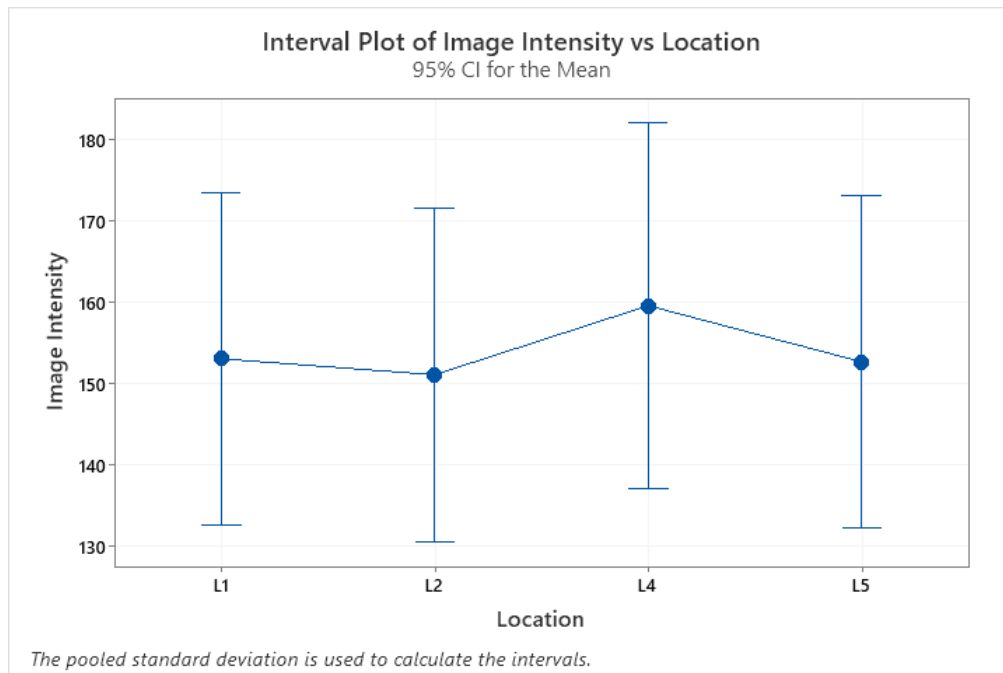
76

Figure 14. Interval plot for the ANOVA comparing the image intensity for five different locations on the part with images captured from the Spectral Instruments RVT100 camera for 0 unit layer thickness on a second configuration. Results show that results show significant variation from location to location.
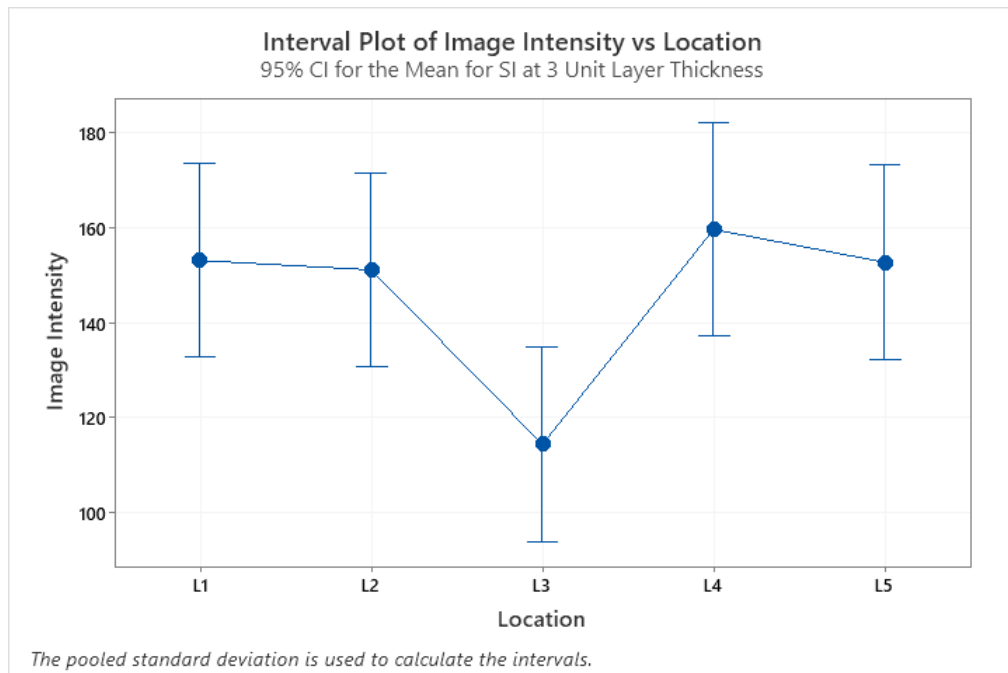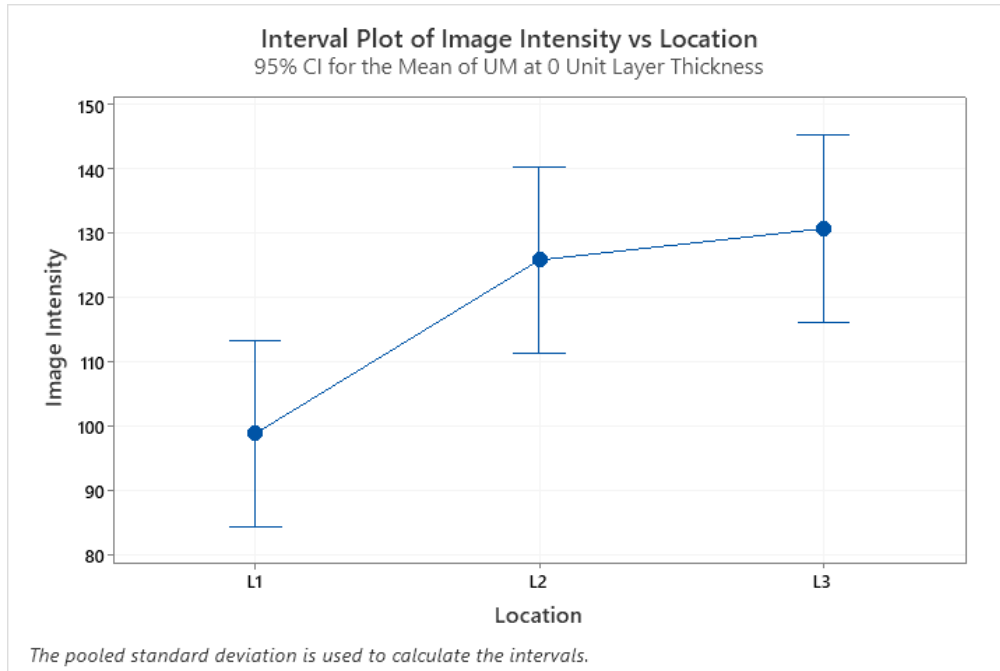

Figure 15. Interval plot for the ANOVA comparing the image intensity for five different locations on the part with images captured from the Spectral Instruments RVT100 camera for 3 unit layer thickness on a second configuration. Results show that results show significant variation from location to location.

The resulting Interval Plot shows that location L3 seems to be lower than the resulting image intensities from the rest of the sampling locations. Another ANOVA was performed leaving out the results from location L3. The results from this ANOVA show give a p-value of 0.942, which indicates that the null hypothesis cannot be rejected. This is an indication that results across the part are similar for all locations aside from L3. An investigation as to why this result occurred should be performed as future work.
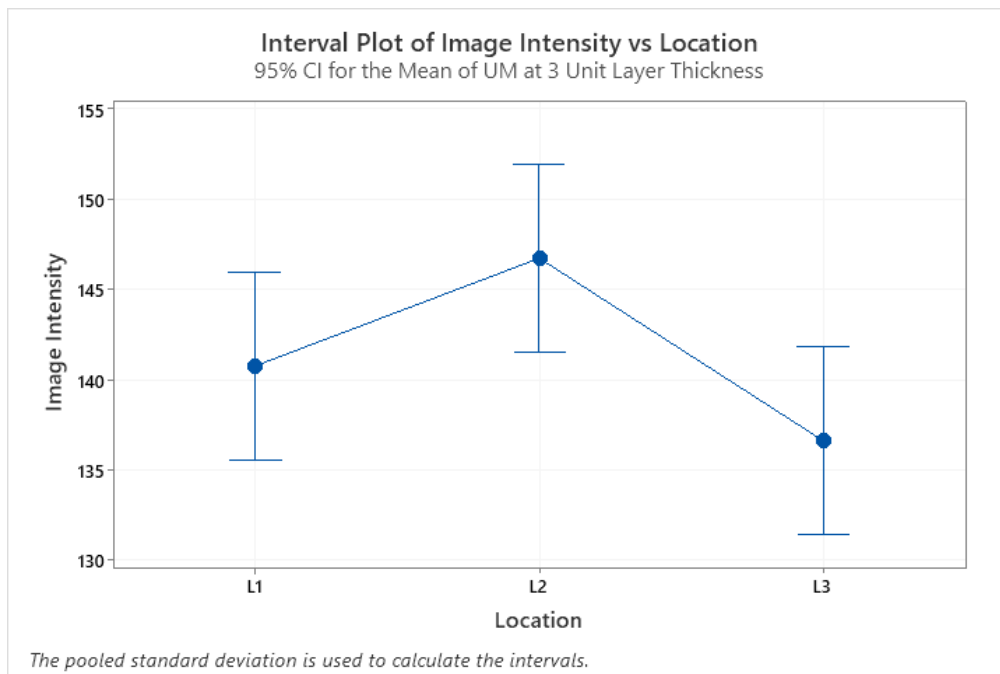

Figure 16. Interval plot for the ANOVA comparing the image intensity for five different locations on the part with images captured from the Spectral Instruments RVT100 camera for 3 unit layer thickness on a second configuration with the third location, L3, excluded. Results show that there is not statistically significant variation from location to location.

The resulting p-values from the ANOVA for the STPCTOU Wireless Digital Microscope at 0 units and 3 units layer thickness were 0.011 and 0.033, respectively. The p-values indicate that the null hypothesis should be rejected for both tests for the UM camera. This means that the STPCTOU Wireless Digital Microscope did not give consistent results across different sampling locations on the part.

Figure 17. Interval plot for the ANOVA comparing the image intensity for three different locations on the part with images captured from the STPCTOU Wireless Digital Microscope for 0 unit layer thickness on a second configuration. Results show that results show variation from location to location.

Figure 18. Interval plot for the ANOVA comparing the image intensity for three different locations on the part with images captured from the STPCTOU Wireless Digital Microscope for 3 unit layer thickness on a second configuration. Results show that results show variation from location to location.

6.4. Powder Layer Thickness Test

The goal of the Powder Layer Thickness Test was to determine if a clear relationship could be formed between the thickness of the powder across a part in units and the image intensity. The data was first plotted on scatter plots with connected lines showing the layer thickness vs image intensity for each camera and each setup. The resulting scatter plots are shown below in the Appendix. As shown in the plots, the on-machine camera seems to have the most linear plot at first glance. The Spectral Instruments RVT100 seems to have some outliers for layers thinner than 1 unit layer thickness.

The hypothesis was that the relationship between layer thickness and image intensity would be linear until it reached an asymptote for very thick layers (about 5 units and up). To test this hypothesis, a linear regression was performed for the data from each setup on each camera. Then, a linear regression was performed for each camera for all data points, regardless of setup. This analysis aimed to determine if a single linear equation could be used to describe the expected relationship between layer thickness in units and image intensity.

The R-squared value, which is an indicator of how well the linear correlation fits the model, is shown in Table 7 below. For the purpose of this test, R-squared values above 70% were viewed as having a strong correlation and R-squared values above 90% show a very strong correlation. Linear regression models resulting in a strong correlation are highlighted in green in Table 7. The resulting charts from the linear regressions for individual setups are shown in Figures 20 -- 24. The resulting charts from the linear regressions for combined setups are shown in Figure 25.

The strongest correlation was seen for the on-machine cameras. The phone camera images for each setup had a strong linear correlation when analyzed individually, but not when

all the data was analyzed together. The linear correlation for the STPCTOU Wireless Digital Microscope was strong for setup 2 and 3 but not for setup 1 or the combined data. The GoPro HERO7 Black only showed a strong linear correlation for data from Setup 2. The Spectral Instruments RVT100 did not show a strong correlation for any setup or the combined data.

Table 7. Results from a linear correlation study for all cameras. An R-squared value was analyzed and is reported below for each setup and for all three setups combined for each camera. Layer thickness was varied from 0 to 5 units with the most data taken around the minimum and maximum values at 1 and 3 units.

	Image Intensity for 3DP vid	Image Intensity for 3DP cam	Image Intensity for SI	Image Intensity for GP	Image Intensity for UM	Image Intensity for PC
Setup 1	89.5%	88.8%	56.3%	41.6%	52.8%	71.3%
Setup 2	96.1%	96.1%	3.7%	78.6%	77.5%	87.8%
Setup 3	97.0%	96.8%	47.0%	57.5%	81.3%	90.9%
All	84.7%	84.0%	28.8%	45.8%	55.0%	70.0%
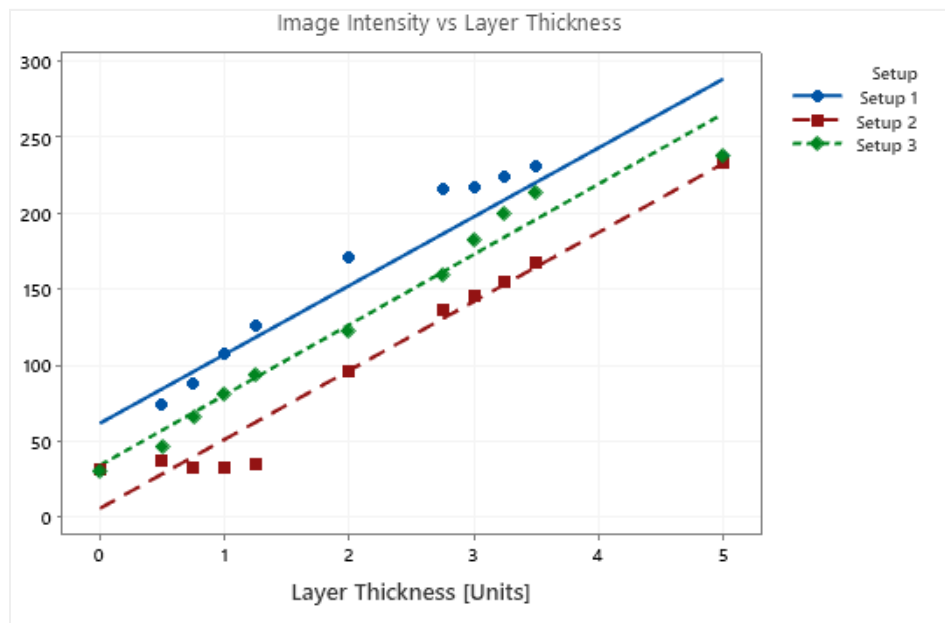
Figure 19. Scatter plot showing the layer thickness vs image intensity with the linear correlation for the on-machine camera for images captured from a 4K video. Results show a strong linear correlation for all setups.
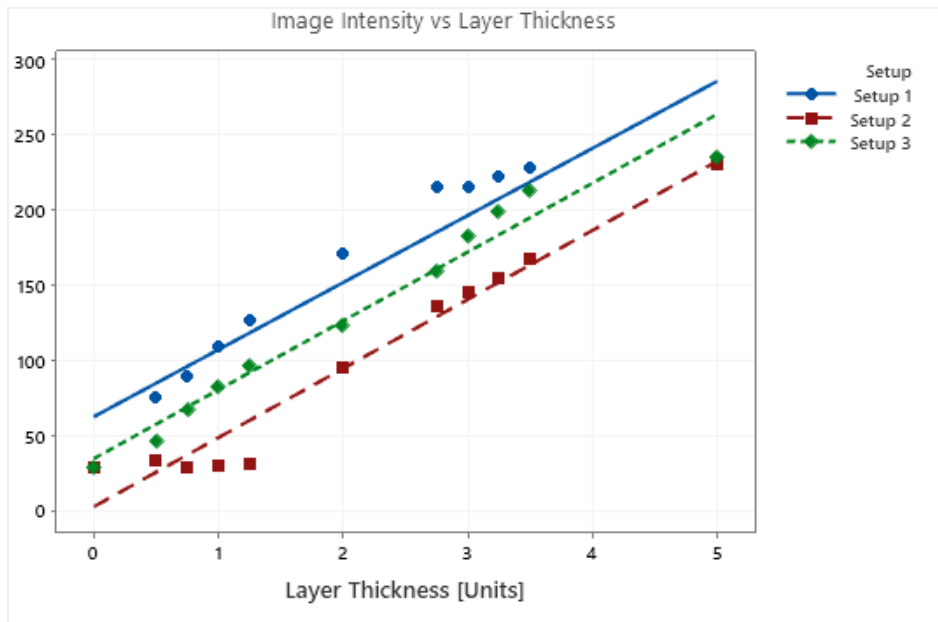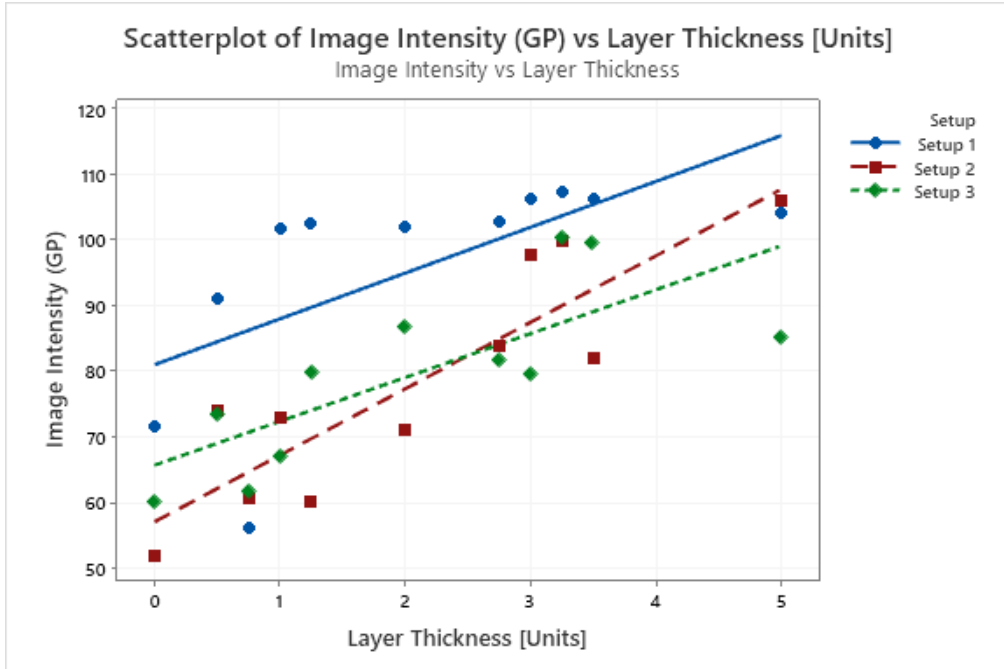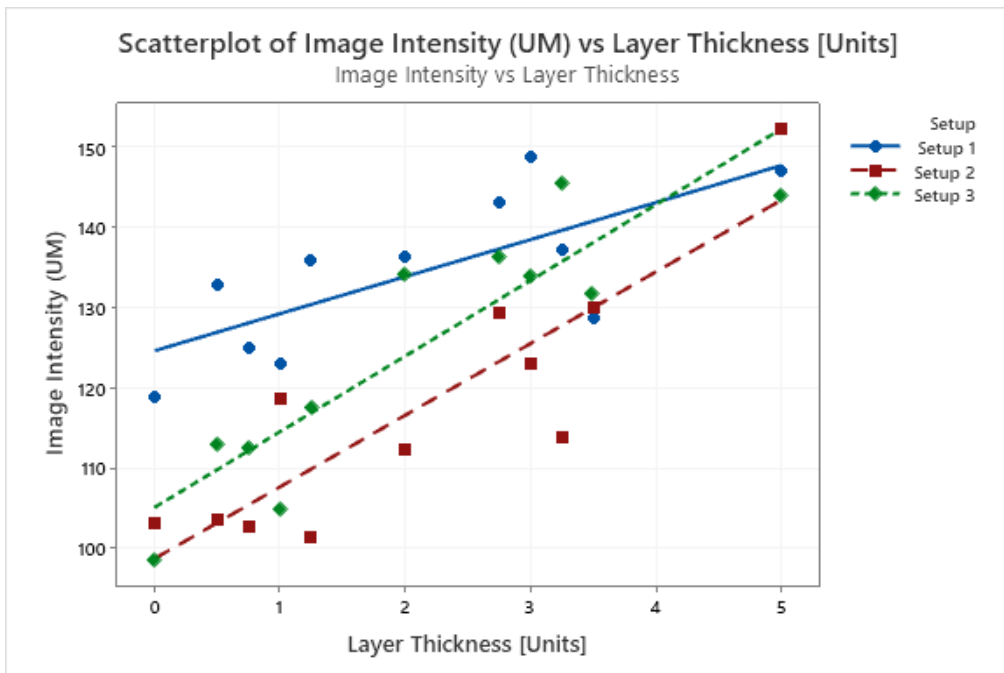
Figure 20. Scatter plot showing the layer thickness vs image intensity with the linear correlation for the on-machine camera for images captured from the image capture tool. Results show a strong linear correlation for all setups.
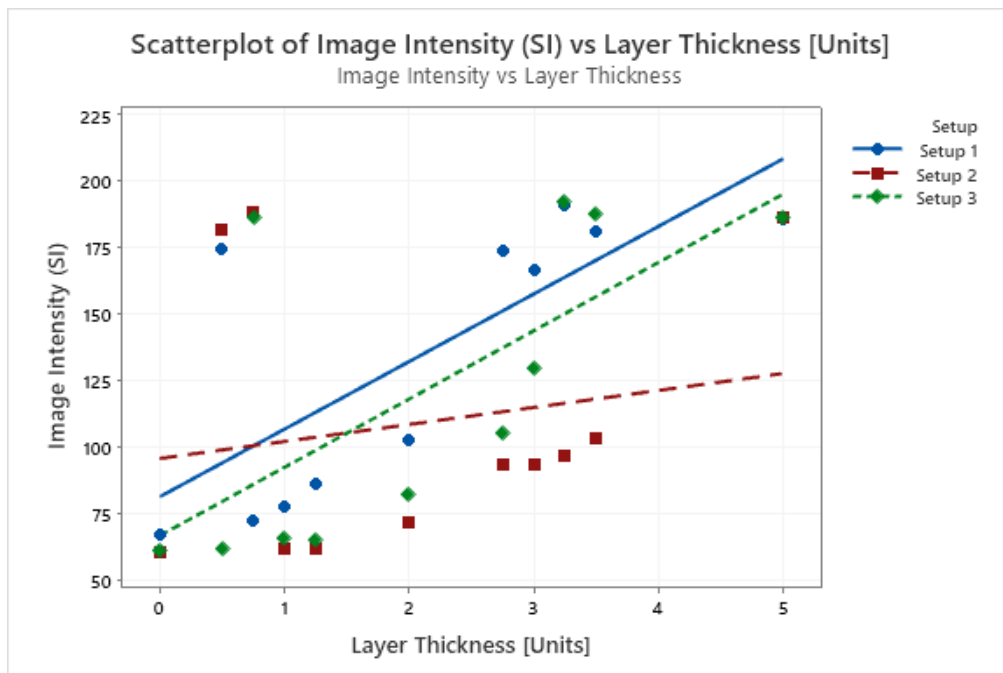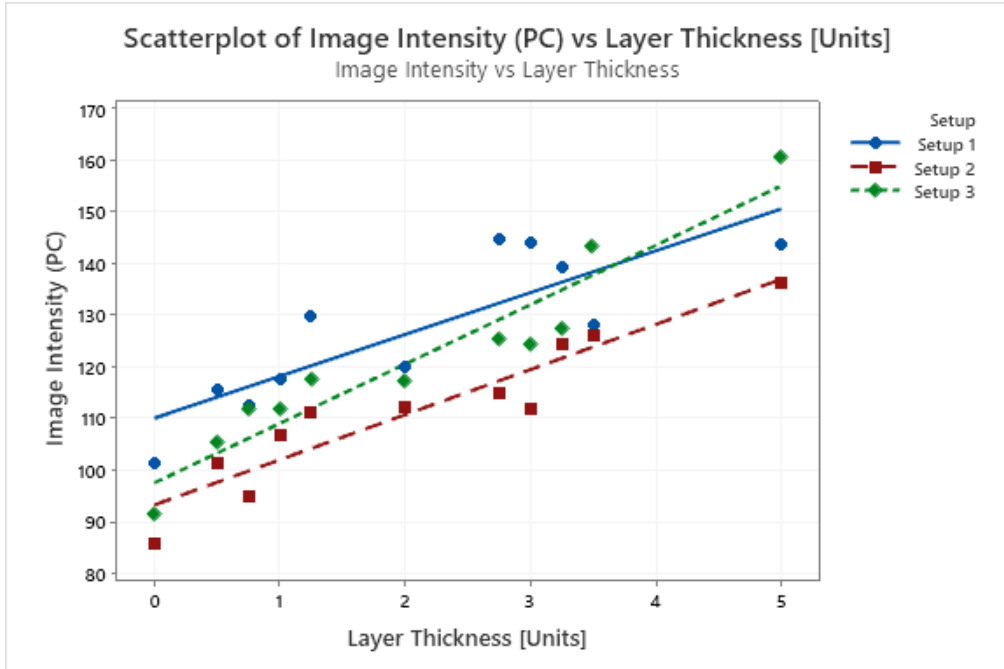

Figure 21. Scatter plot showing the layer thickness vs image intensity with the linear correlation for the Spectral Instruments RVT100 camera. Results do not show a strong linear correlation for any setup.

Figure 22. Scatter plot showing the layer thickness vs image intensity with the linear correlation for the GoPro HERO7 Black camera. Results do not show a strong linear correlation for any setup aside from Setup 2 with a R-squared value of 78.6%.

Figure 23. Scatter plot showing the layer thickness vs image intensity with the linear correlation for the STPCTOU Wireless Digital Microscope. Results show a strong linear correlation for Setup 2 and 3 with a R-squared value of 77.5% and 81.3%, respectively.
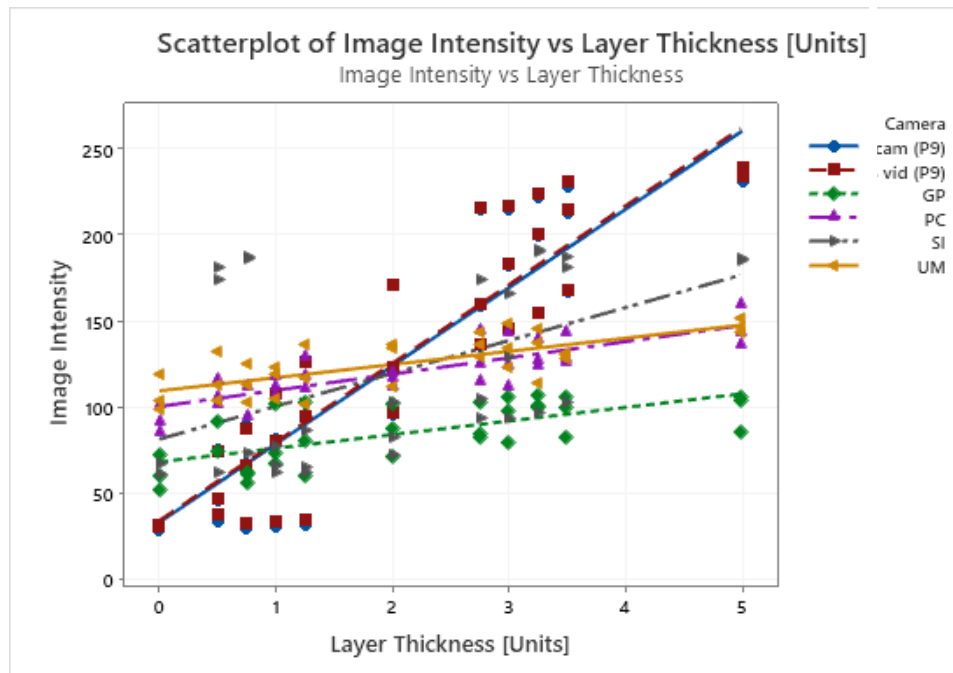
Figure 24. Scatter plot showing the layer thickness vs image intensity with the linear correlation for the iPhone 12 camera. Results show a strong linear correlation for Setups 1, 2, and 3, but not for the combined setup data.


Figure 25. Scatter plot showing the layer thickness vs image intensity with the linear correlation for the combined data from all setups for each camera. Results show a strong linear correlation (greater than 70% R-squared value) only for the on-machine camera images (both 4K video and captured images).

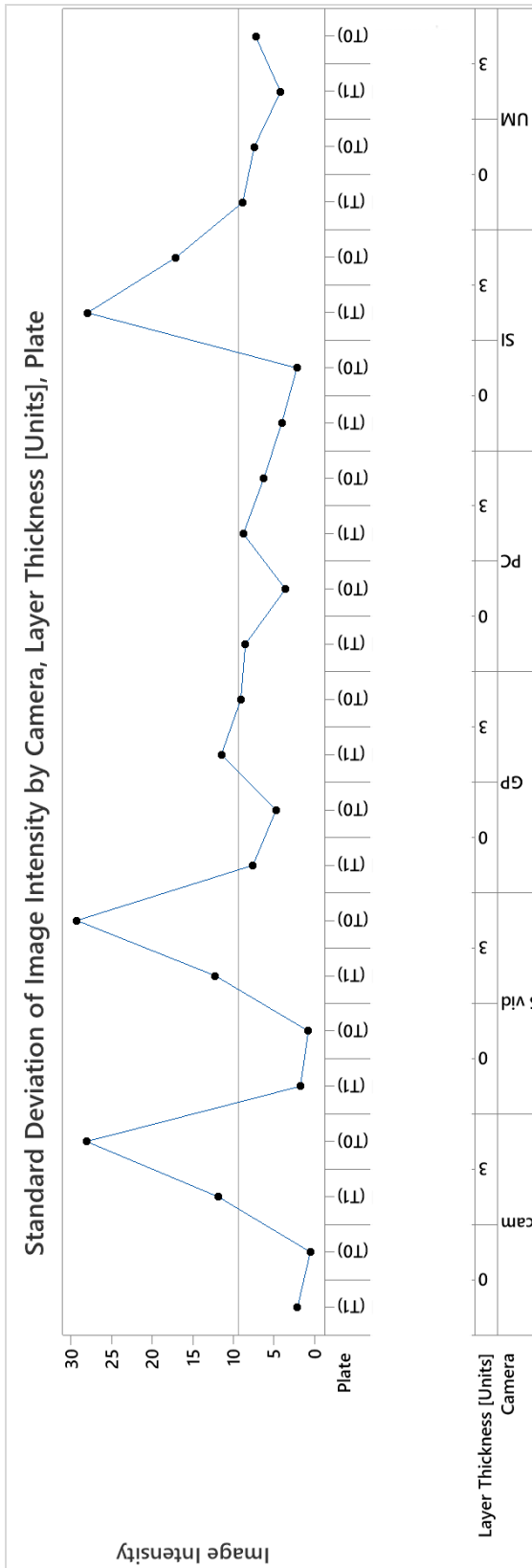## 6.5.   Comparing First vs Second Configuration

The goal of comparing the configuration results was to determine if the image intensity analysis results are the same regardless of configuration. The hypothesis was that the mean intensity values for a second configuration and the mean intensity value for a first configuration would be the same for each individual camera. Data for both the first configuration and second configuration was analyzed for the Camera Repeatability Test as well as the Area Sampling Test. The results are outlined below.

6.5.1.   From Camera Repeatability Test

The data from the Camera Repeatability Test was first organized into a variability chart to show the variation in readings for each camera, layer thickness, and test setup. The mean, standard deviation, and coefficient of variation for the image intensity for each camera, setup, and layer thickness combination is shown below in Table 8. The resulting variability chart, shown in Figure 26, shows that the readings for second configurations and first configurations appear to be fairly close for all cameras. The variability appears to be highest for the on-machine cameras for the first configurations at 3 units layer thickness and the second configuration for the Spectral Instruments RVT100 camera at 3 units layer thickness. This is reflected in the standard deviation plot shown in Figure 27.
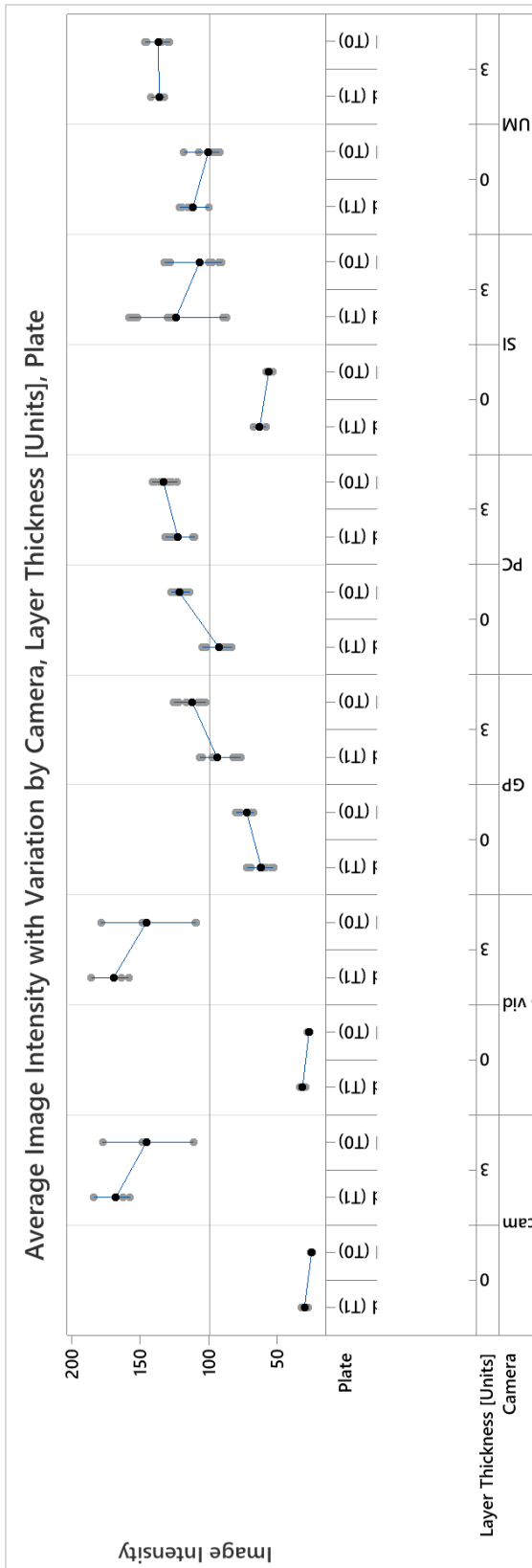
Figure 26. Variability chart to compare results from the First Configuration (T0) to the Second Configuration (T1).

Figure 27. Standard deviation chart to compare results from the First Configuration (T0) to the Second Configuration (T1).

Table 8. Mean image intensity, standard deviation, and coefficient of variation for each camera, each setup configuration, and each layer thickness.

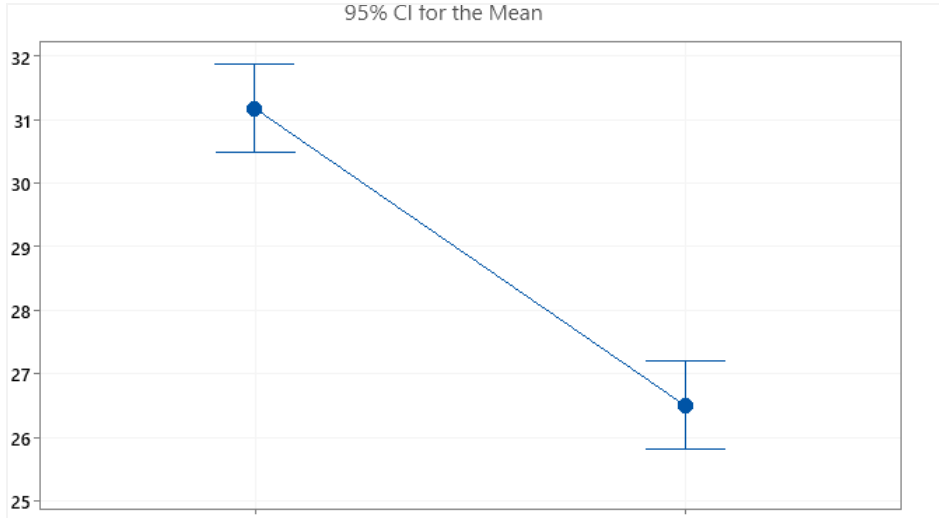| Camera	Layer Thickness	First Configuration			Second Configuration		
		Mean Image Intensity	Standard Deviation	Coefficient of Variation	Mean Image Intensity	Standard Deviation	Coefficient of Variation
3DP vid	0 units	26.498	0.711	2.7%	31.177	1.644	5.3%
3DP cam		24.549	0.466	1.9%	29.841	2.000	6.7%
SI		55.912	2.070	3.7%	62.476	3.880	6.2%
GP		72.076	4.554	6.3%	61.448	7.303	11.9%
UM		99.970	7.161	7.2%	111.294	8.523	7.7%
PC		121.307	3.440	2.8%	92.494	8.214	8.9%
3DP vid	3 units	145.207	28.312	19.5%	169.131	11.797	7.0%
3DP cam		145.371	27.144	18.7%	167.663	11.459	6.8%
SI		106.436	16.507	15.5%	123.527	27.032	21.9%
GP		111.819	8.758	7.8%	93.716	11.087	11.8%
UM		136.430	6.976	5.1%	136.045	4.026	3.0%
PC		132.834	6.029	4.5%	122.366	8.455	6.9%

An ANOVA was performed to compare the first and second configuration for each camera to determine if there was a significant difference in the means. There were twelve ANOVA tests performed: one at each layer thickness (0 and 3 units) for each of the six cameras. The null hypothesis for each ANOVA was that all means are equal. The significance level, alpha, was set to 0.05. The resulting p-values are shown in Table 9 below. The values used for the second configuration for the on-machine camera were the average values from all parts as described in the Camera Repeatability Test.

Table 9. P-value results from an ANOVA to determine if there is a difference between the first and second configurations for all cameras for each layer thickness. A statistically significant difference was found between the first and second configuration for the Spectral Instruments RVT100 and the STPCTOU Wireless Digital Microscope.

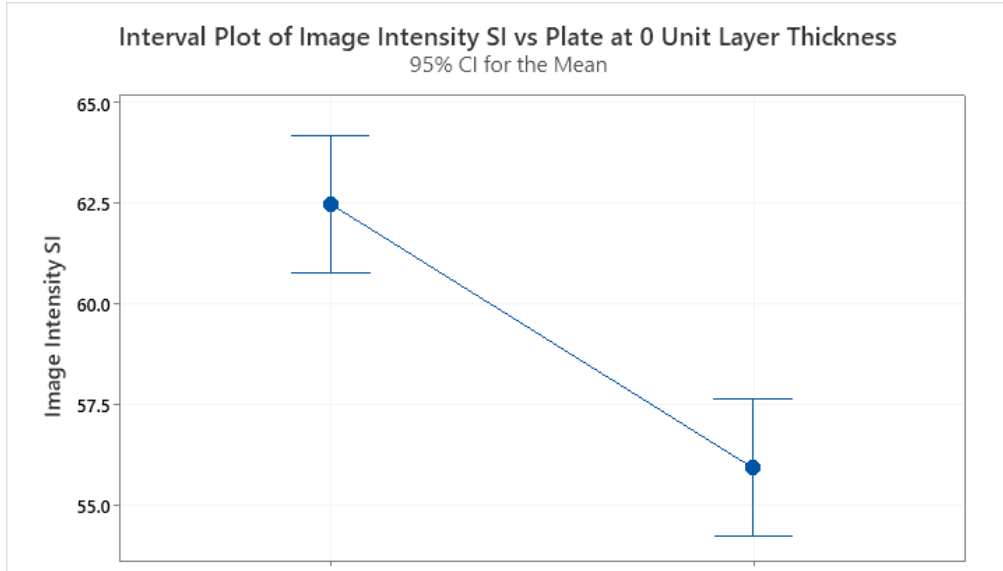| Camera	Layer Thickness	P-Value
3DP vid		0.000
3DP cam		0.000
SI		0.000
GP	0 units	0.000
UM		0.001
PC		0.000
3DP vid		0.007
3DP cam		0.008
SI		**0.053**
GP	3 units	0.000
UM		**0.859**
PC		0.001

The p-values indicate that there is a significant difference in the mean intensity values from first configurations and second configurations for all cameras at 0 unit layer thickness. At 3 unit layer thickness, the Spectral Instruments RVT100 and the STPCTOU Wireless Digital Microscope do not show a significant difference between the mean intensity values. The on-machine camera (both 4K video screenshots and captured images), GoPro HERO7 Black, and iPhone 12 camera show a significant difference in the mean intensity values for first and second configurations at 3 unit layer thickness. The resulting Interval Plots are also shown below in Figures 28 -- 39.
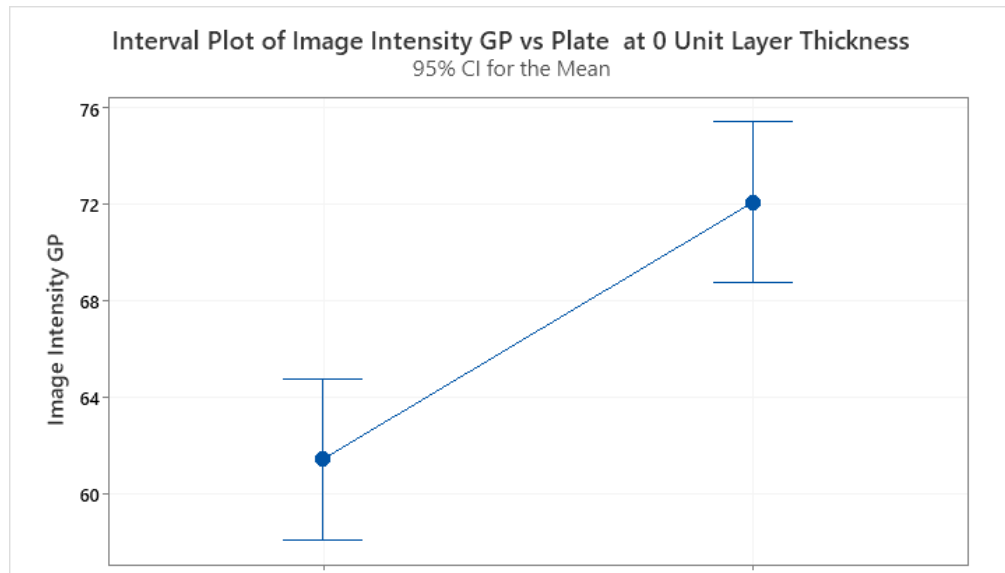
Figure 28. Interval plot for the ANOVA comparing the image intensity for the first and second configurations for the on-machine camera for images captured from a 4K video at 0 unit layer thickness. Results show that there is a statistically significant variation from the first to second configuration. T1 is shown on the left while T0 is shown on the right.
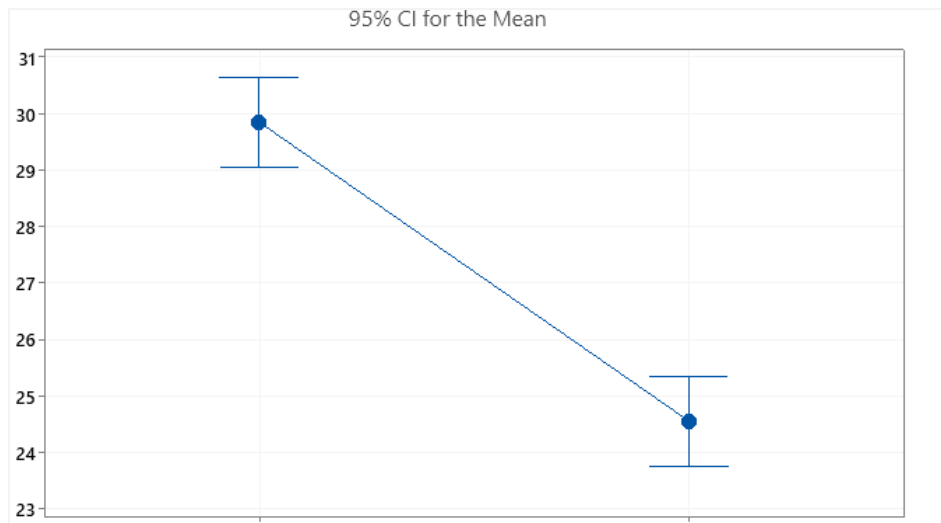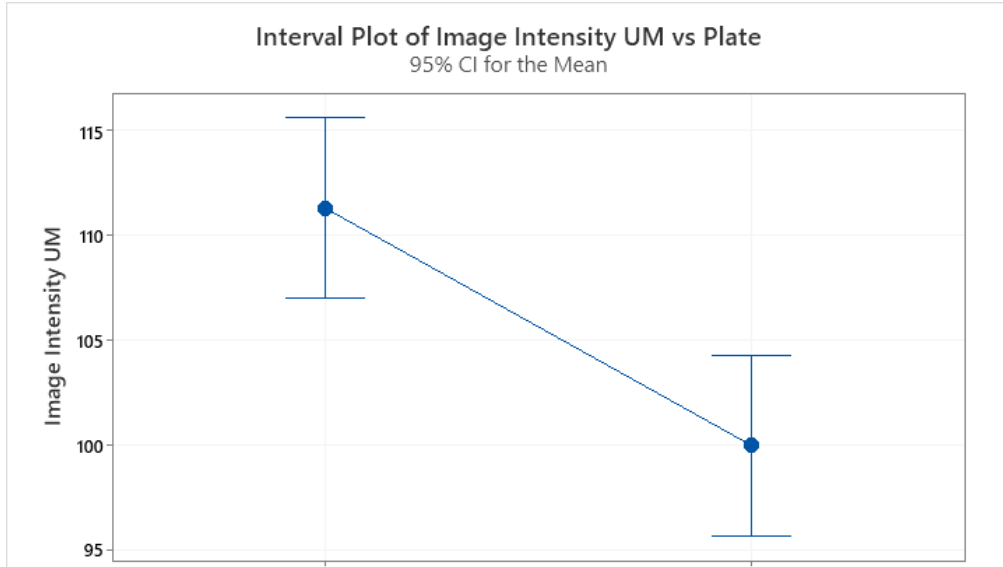

Figure 29. Interval plot for the ANOVA comparing the image intensity for the first and second configurations for the on-machine camera for images captured from a captured image at 0 unit layer thickness. Results show that there is a statistically significant variation from the first to second configuration. T1 is shown on the left while T0 is shown on the right.

Figure 30. Interval plot for the ANOVA comparing the image intensity for the first and second configurations for the Spectral Instruments RVT100 camera at 0 unit layer thickness. Results show that there is a statistically significant variation from the first to second configuration. T1 is shown on the left while T0 is shown on the right.

Figure 31. Interval plot for the ANOVA comparing the image intensity for the first and second configurations for the GoPro HERO7 Black camera at 0 unit layer thickness. Results show that there is a statistically significant variation from the first to second configuration. T1 is shown on the left while T0 is shown on the right.

Figure 32. Interval plot for the ANOVA comparing the image intensity for the first and second configurations for the STPCTOU Wireless Digital Microscope at 0 unit layer thickness. Results show that there is a statistically significant variation from the first to second configuration. T1 is shown on the left while T0 is shown on the right.
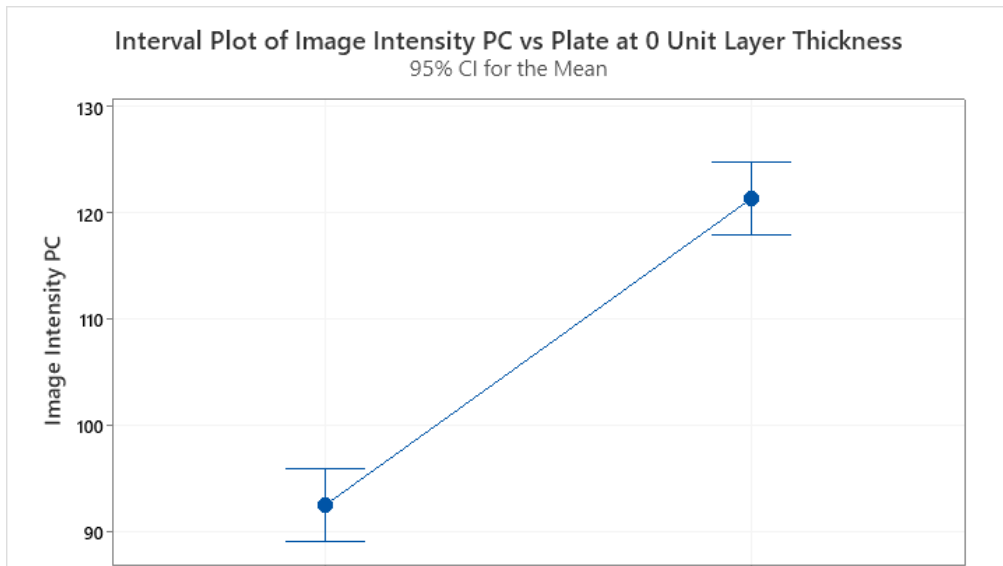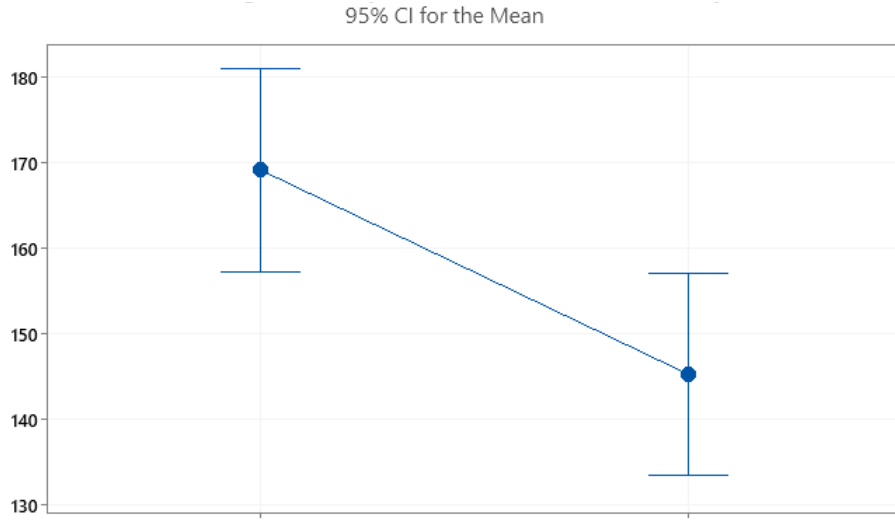

Figure 33. Interval plot for the ANOVA comparing the image intensity for the first and second configurations for the iPhone 12 camera at 0 unit layer thickness. Results show that there is a statistically significant variation from the first to second configuration. T1 is shown on the left while T0 is shown on the right.

Figure 34. Interval plot for the ANOVA comparing the image intensity for the first and second configurations for the on-machine camera for images captured from a 4K video at 3 unit layer thickness. Results show that there is a statistically significant variation from the first to second configuration. T1 is shown on the left while T0 is shown on the right.

Figure 35. Interval plot for the ANOVA comparing the image intensity for the first and second configurations for the on-machine camera for images captured from a captured image at 3 unit layer thickness. Results show that there is a statistically significant variation from the first to second configuration. T1 is shown on the left while T0 is shown on the right.
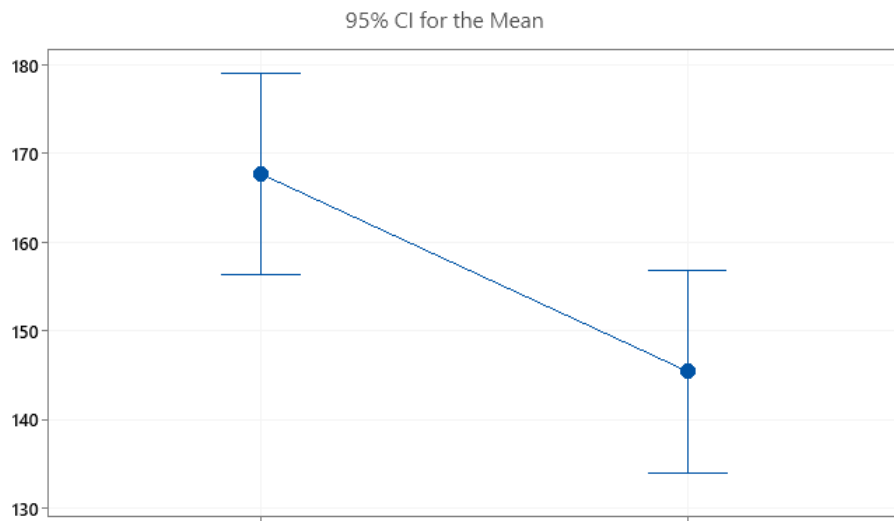
Figure 36. Interval plot for the ANOVA comparing the image intensity for the first and second configurations for the Spectral Instruments RVT100 camera at 3 unit layer thickness. Results show that there is a statistically significant variation from the first to second configuration. T1 is shown on the left while T0 is shown on the right.
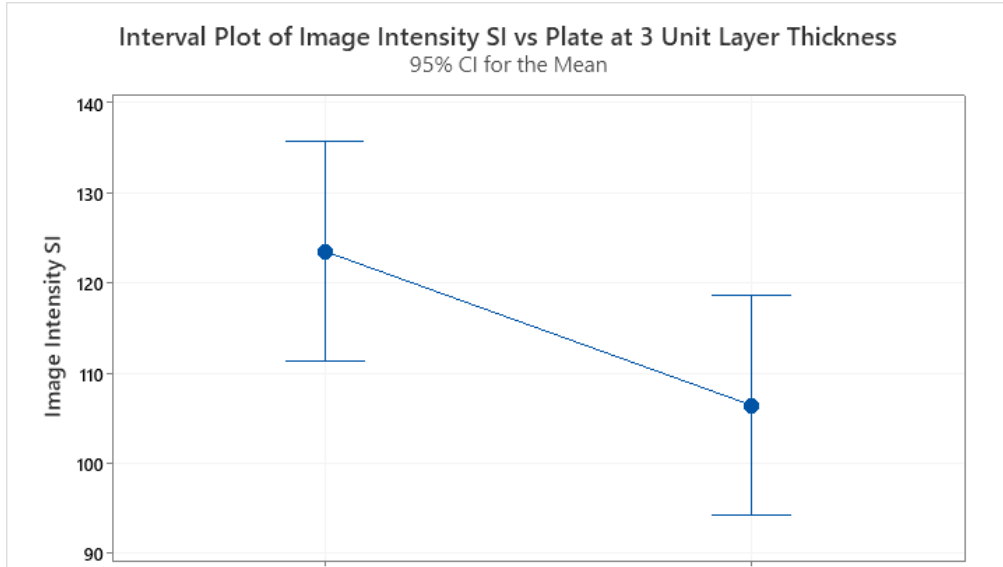

Figure 37. Interval plot for the ANOVA comparing the image intensity for the first and second configurations for the GoPro HERO7 Black camera at 3 unit layer thickness. Results show that there is a statistically significant variation from the first to second configuration. T1 is shown on the left while T0 is shown on the right.
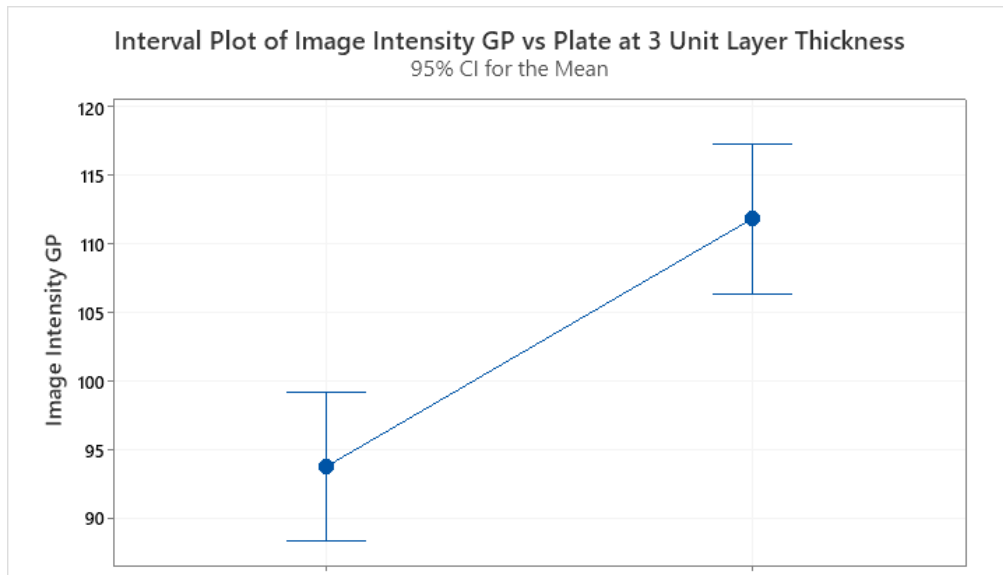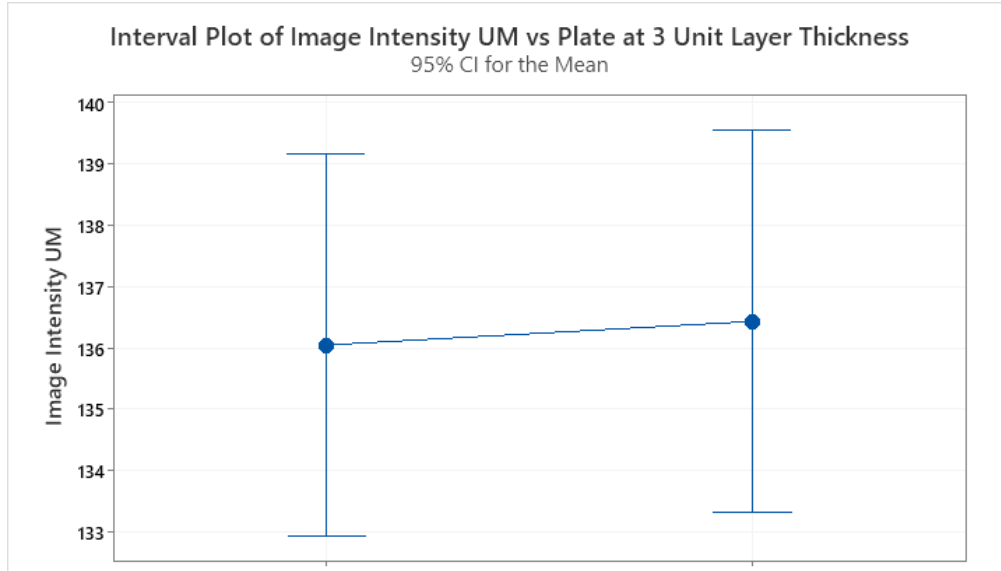
Figure 38. Interval plot for the ANOVA comparing the image intensity for the first and second configurations for the STPCTOU Wireless Digital Microscope at 3 unit layer thickness. Results show that there is a statistically significant variation from the first to second configuration. T1 is shown on the left while T0 is shown on the right.

Figure 39. Interval plot for the ANOVA comparing the image intensity for the first and second configurations for the iPhone 12 camera at 3 unit layer thickness. Results show that there is a statistically significant variation from the first to second configuration. T1 is shown on the left while T0 is shown on the right.
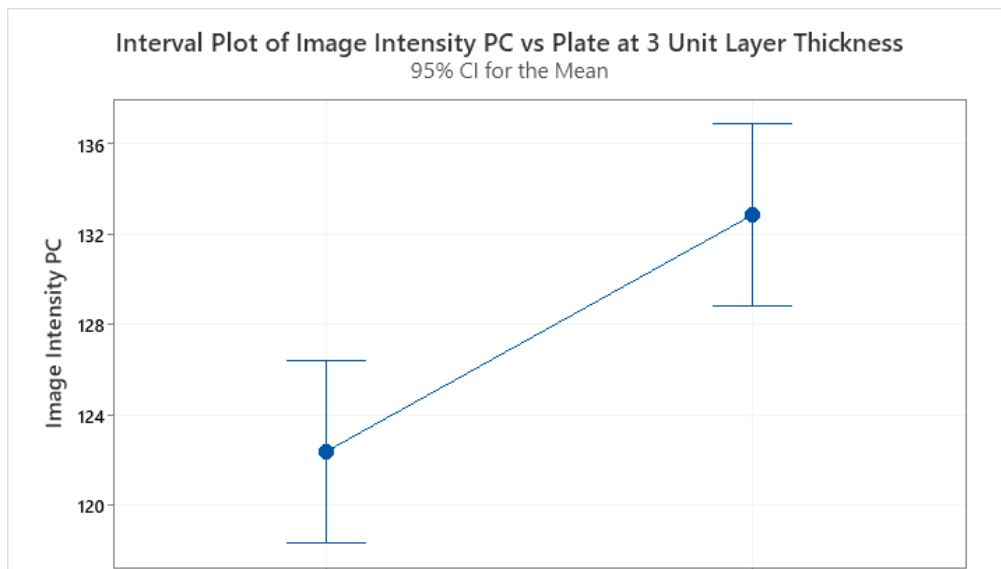
6.5.2. From Area Sampling Test

The data from the Area Sampling Test was first organized into a variability chart to show the variation in readings for each camera, layer thickness, and setup configuration. Data from all locations was averaged into a single mean. The mean, standard deviation, and coefficient of variation for the image intensity for each camera, setup, and layer thickness combination is shown below in Table 10. The resulting variability chart, shown in Figure 40, shows that the readings for second configurations and first configurations appear to be fairly close for all cameras aside from the on-machine camera at 3 units layer thickness. This is reflected in the standard deviation plot shown in Figure 41.
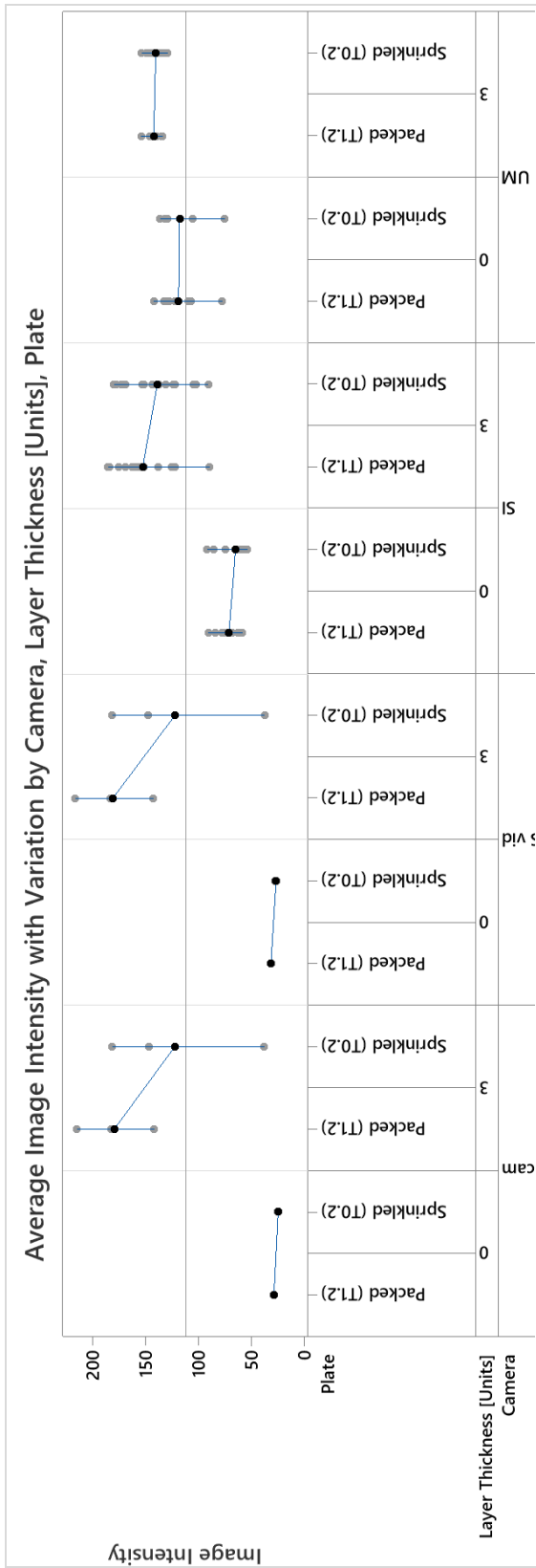
Figure 40. Variability chart for the Area Sampling Test for the First Configuration (T0) vs the Second Configuration (T1).
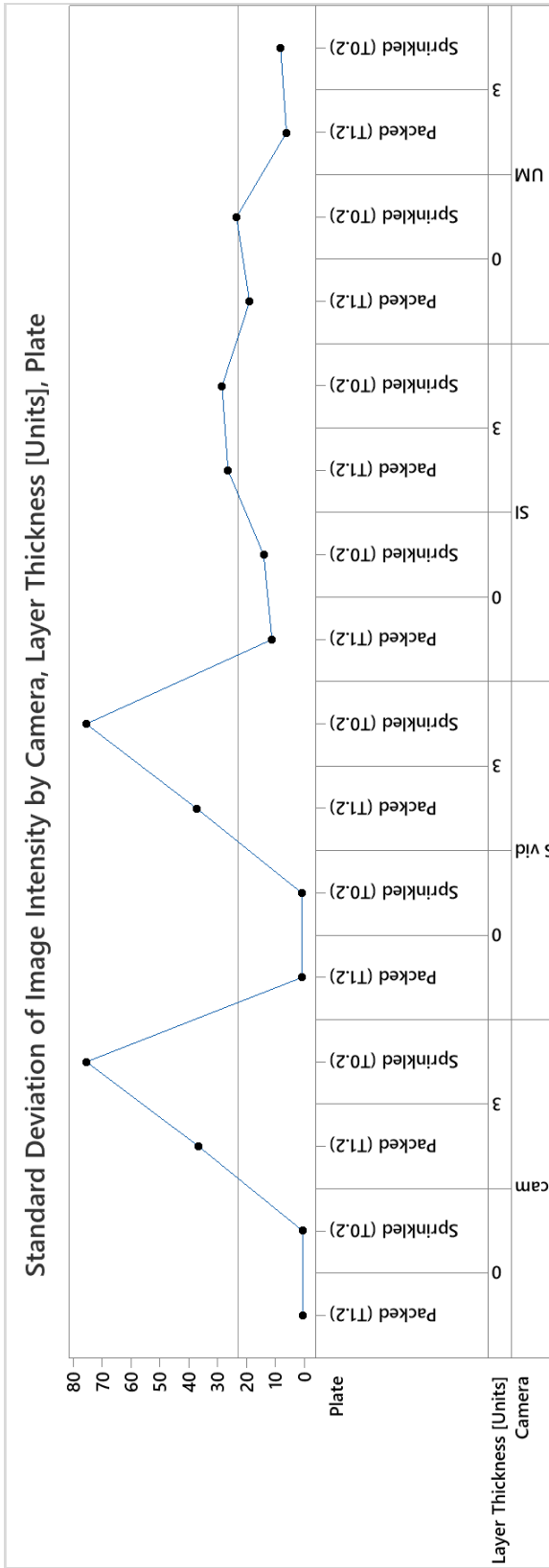
Figure 41. Standard deviation chart for the Area Sampling Test for the First Configuration (T0) vs the Second Configuration (T1).

Table 10. Mean image intensity, standard deviation, and coefficient of variation for each camera, each setup configuration, and layer thicknesses 0 and 3 units. The data for these tables was taken from the Area Sampling Test to compare the first configuration to the second configuration.

Camera	Layer Thickness	First Configuration			Second Configuration		
		Mean Image Intensity	Standard Deviation	Coefficient of Variation	Mean Image Intensity	Standard Deviation	Coefficient of Variation
3DP vid	0 units	31.349	0.581	1.9%	26.465	0.693	2.6%
3DP cam		28.507	0.304	1.1%	24.484	0.435	1.8%
SI		71.033	10.752	15.1%	64.892	13.305	20.5%
UM		118.814	17.816	15.0%	117.857	21.397	18.2%
3DP vid	3 units	181.010	30.404	16.8%	122.234	61.592	50.4%
3DP cam		179.773	29.845	16.6%	122.227	61.548	50.4%
SI		152.731	25.386	16.6%	139.010	27.467	19.8%
UM		142.268	5.788	4.1%	140.475	7.694	5.5%

An ANOVA was performed to compare the first and second configurations for each camera to determine if there was a significant difference in the means. There were eight ANOVA tests performed. An ANOVA was performed at each layer thickness (0 and 3 units) for the on-machine camera for 4K video screenshots and captured images, the Spectral Instruments RVT100 camera, and the STPCTOU Wireless Digital Microscope. The null hypothesis for each ANOVA was that all means are equal. The significance level, alpha, was set to 0.05. The resulting p-values are shown in Table 11 below. There were five locations for each setup for the Spectral Instruments RVT100 camera, three locations for the STPCTOU Wireless Digital Microscope, and one location for each of the image types for the on-machine camera which was taken as a reference.

Table 11. P-value results from an ANOVA to determine if there is a difference between the first and second configurations for all cameras for each layer thickness with data from the Area Sampling Test. A statistically significant difference was found between the first and second configuration for all cameras aside from the cameras at 0 unit layer thickness.

Camera	Layer Thickness	P-Value
3DP vid	0 units	0.002
3DP cam		0.000
SI		**0.235**
UM		**0.932**
3DP vid	3 units	**0.239**
3DP cam		**0.300**
SI		**0.190**
UM		**0.605**

The p-values indicate that there is not a significant difference in the mean intensity values from first configurations and second configurations for the Spectral Instruments RVT100 or the STPCTOU Wireless Digital Microscope at 0 unit layer thickness. There is a significant difference between the first and second configurations for both types of the images captured with the on-machine camera at 0 unit layer thickness. There is not a significant difference in mean intensity value for any of the cameras at 3 unit layer thickness. The resulting Interval Plots are also shown below in Figures 42 -- 49. Full results from the ANOVA are shown in the Appendix.
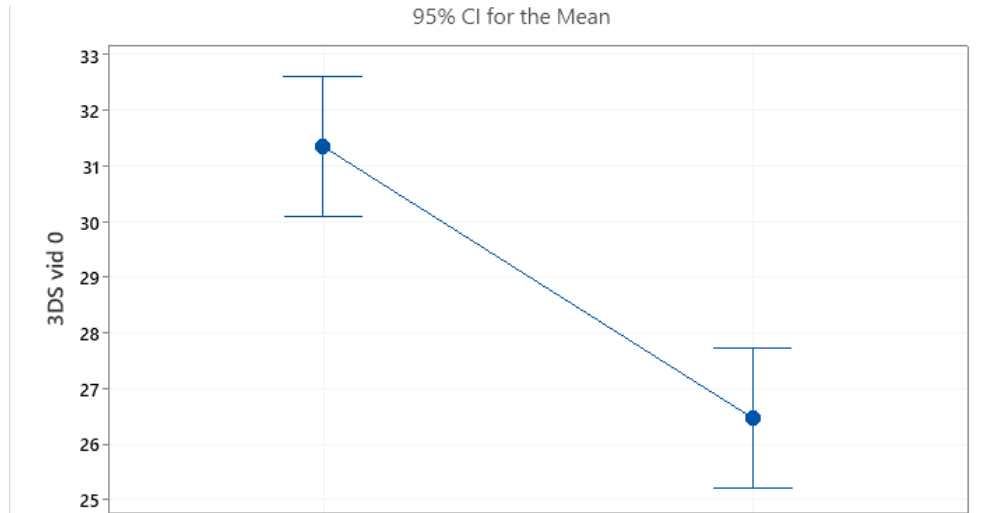
Figure 42. Interval plot for the ANOVA comparing the image intensity for the first and second configurations for the on-machine camera for images captured from a 4K video at 0 unit layer thickness with data captured for the Area Sampling Test. Results show that there is a statistically significant variation from the first to the second configuration. T1 is shown on the left while T0 is shown on the right.
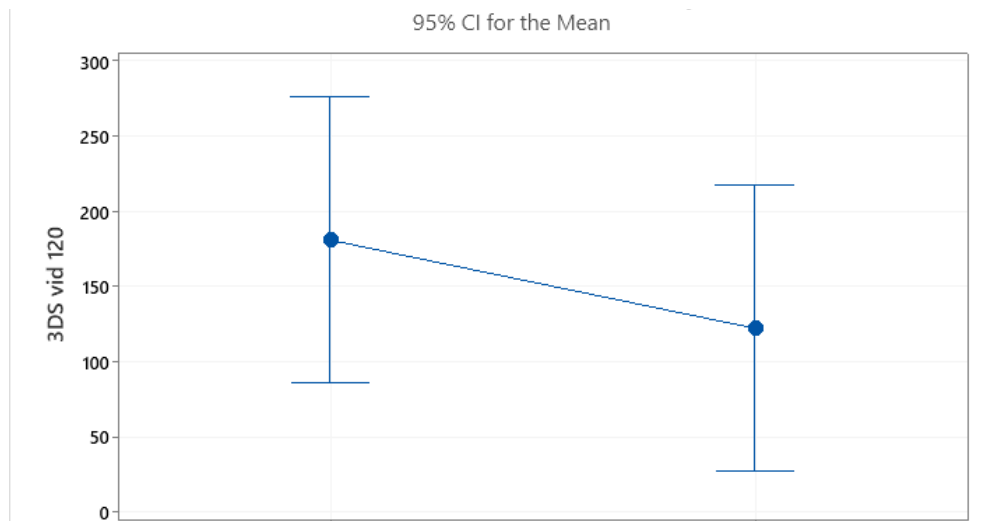
Figure 43. Interval plot for the ANOVA comparing the image intensity for the first and second configurations for the on-machine camera for images captured from a 4K video at 3 unit layer thickness with data captured for the Area Sampling Test. Results show that there is not a statistically significant variation from the first to the second configuration. T1 is shown on the left while T0 is shown on the right.
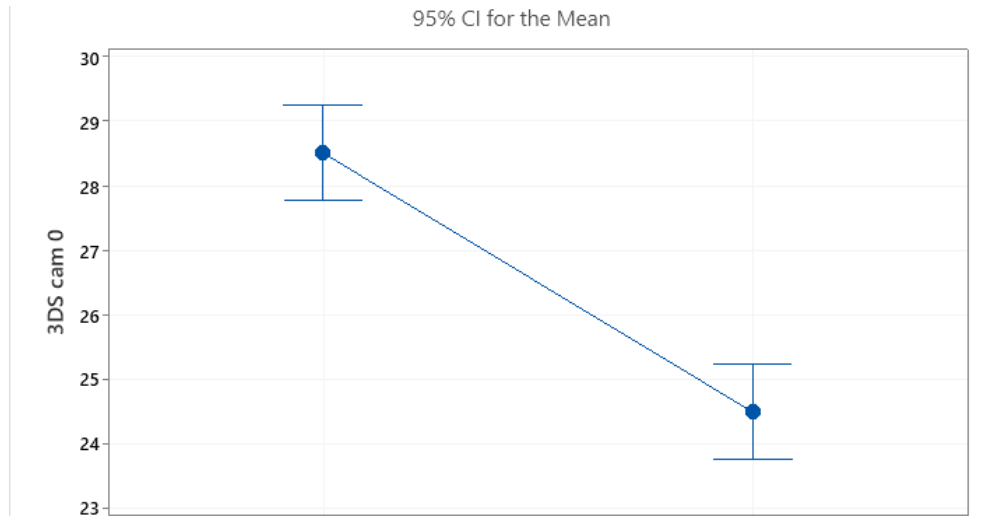
Figure 44. Interval plot for the ANOVA comparing the image intensity for the first and second configurations for the on-machine camera for images captured from the image capture tool at 0 unit layer thickness with data captured for the Area Sampling Test. Results show that there is a statistically significant variation from the first to the second configuration. T1 is shown on the left while T0 is shown on the right.
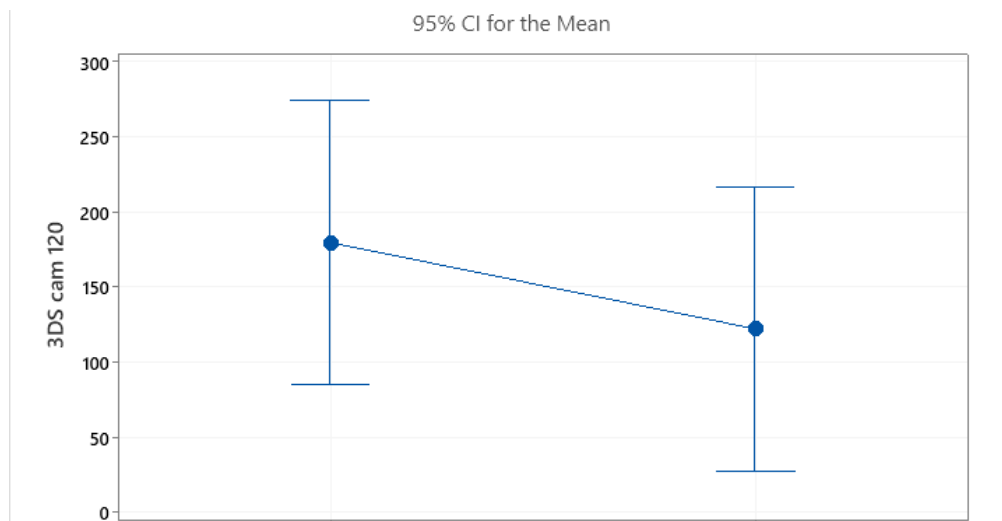

Figure 45. Interval plot for the ANOVA comparing the image intensity for the first and second configurations for the on-machine camera for images captured from the image capture tool at 3 unit layer thickness with data captured for the Area Sampling Test. Results show that there is a statistically significant variation from the first to the second configuration. T1 is shown on the left while T0 is shown on the right.

Figure 46. Interval plot for the ANOVA comparing the image intensity for the first and second configurations for the Spectral Instruments RVT100 at 0 unit layer thickness with data captured for the Area Sampling Test. Results show that there is not a statistically significant variation from the first to the second configuration. T1 is shown on the left while T0 is shown on the right.

Figure 47. Interval plot for the ANOVA comparing the image intensity for the first and second configurations for the Spectral Instruments RVT100 camera at 3 unit layer thickness with data captured for the Area Sampling Test. Results show that there is not a statistically significant variation from the first to the second configuration. T1 is shown on the left while T0 is shown on the right.
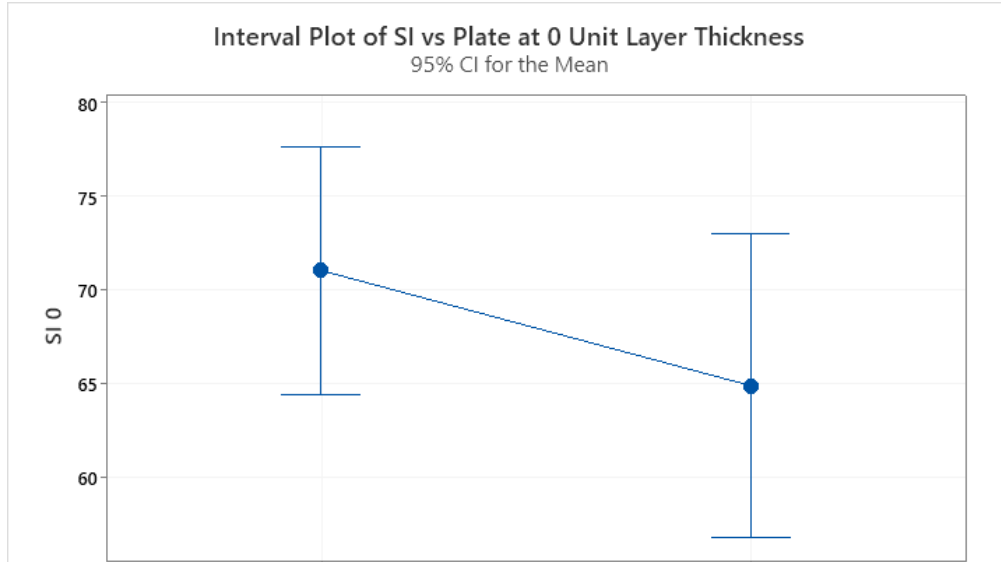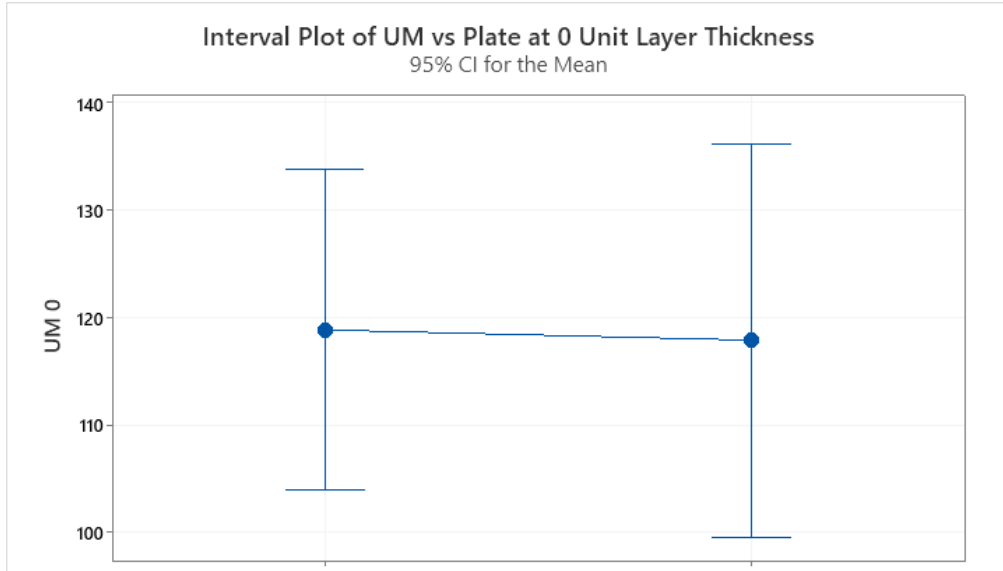
Figure 48. Interval plot for the ANOVA comparing the image intensity for the first and second configurations for the STPCTOU Wireless Digital Microscope at 0 unit layer thickness with data captured for the Area Sampling Test. Results show that there is not a statistically significant variation from the first to the second configuration. T1 is shown on the left while T0 is shown on the right.
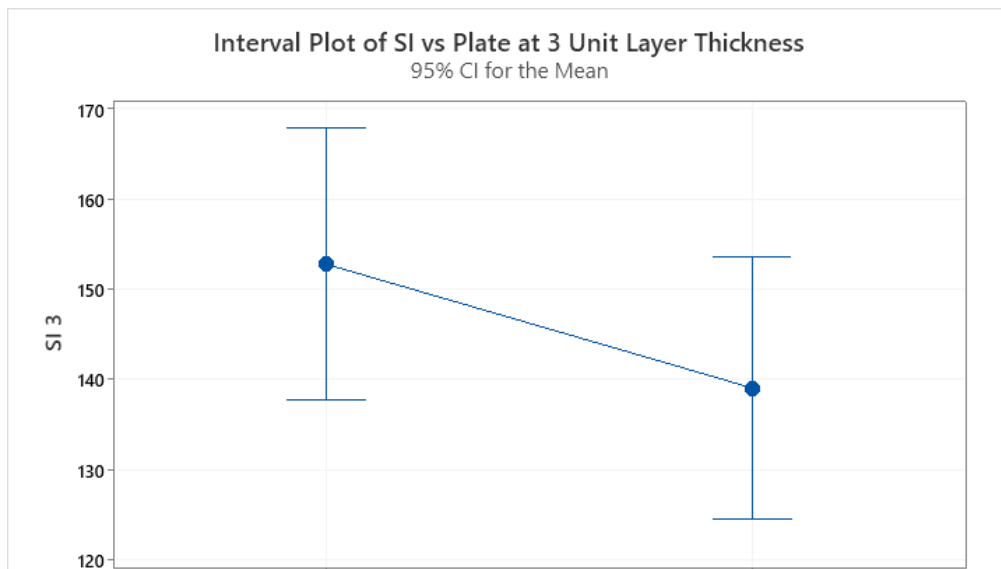

Figure 49. Interval plot for the ANOVA comparing the image intensity for the first and second configurations for the STPCTOU Wireless Digital Microscope at 0 unit layer thickness with data captured for the Area Sampling Test. Results show that there is not a statistically significant variation from the first to the second configuration. T1 is shown on the left while T0 is shown on the right.
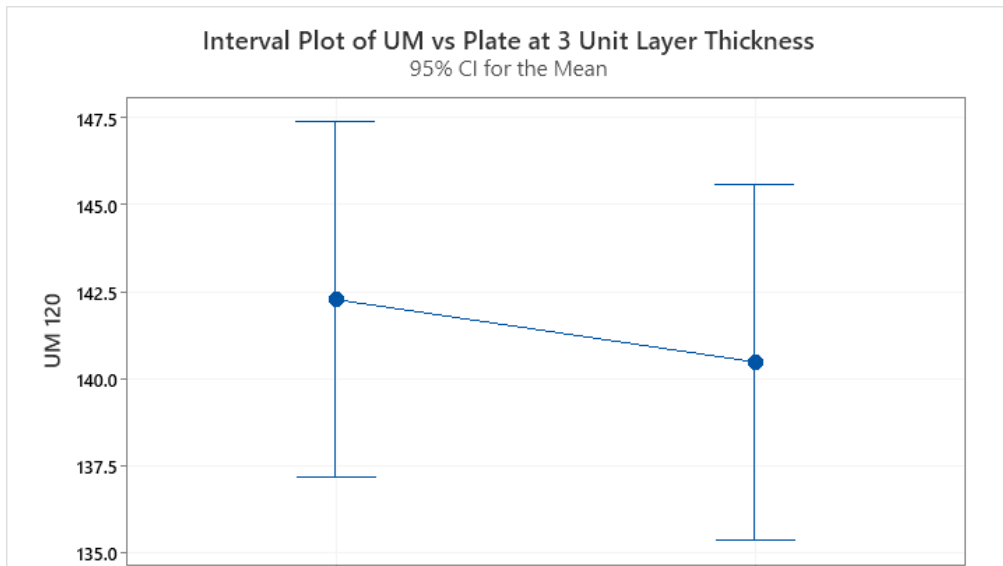
6.5.3. Conclusions of the Setup Configuration Comparison

Both tests show that the first and second configurations do not yield the same results for the on-machine camera from video screenshots or captured images at 0 unit layer thickness. Both tests also show that the Spectral Instruments RVT100 and STPCTOU Wireless Digital Microscope do yield the same results for first and second configurations at 3 unit layer thickness. The test results show conflicting results for the Spectral Instruments RVT100 and STPCTOU Wireless Digital Microscope at 0 unit layer thickness which shows equal means for the area sampling test data but not the camera repeatability test. The on-machine camera from both video screenshots and captured images at 3 unit layer thickness also show conflicting results with the null hypothesis (means equal) rejected only for the area sampling test. There is no area sampling data to compare to for the GoPro HERO7 Black or iPhone 12 cameras since they were not tested as parts of the Area Sampling Test.

6.6.   Variability from 4K Video and Captured Images

A Nested ANOVA for the data from each test was performed to analyze the variation in image intensity results for the two types of on-machine camera images: 4K video screenshots and captured images. The Nested ANOVA from all tests shows that the variation between the 4K video and captured image contributes little to no variation to the results compared to the other factors. Consequently, it can be concluded that the 4K video and captured images result in the same image intensity values for each part. The adjusted perspective of the 4K video does not seem to affect the results of the image intensity analysis in the Image Analysis Software. This is also reflected in each of the variability charts (Figures 50 -- 53) as the lines between the camera

and video data is flat and has little variability reflected by the standard deviation lines. Moving

forward, captured images could be used as they take less time to capture and post-process.

Table 12. The camera's contribution to variance percentage for a nested ANOVA to determine if there is a difference between images captured with the on-machine camera via the 4K video and camera image capture tool with data captured from all tests. Results show that the camera was not the major contributing factor to variation for any of the tests.

Test	Camera Contribution to Variance
Camera Repeatability (T0 & T1)	2.00%
Area Sampling (T0.2 & T1.2)	0.00%
Powder Layer Thickness (T3)	3.00%
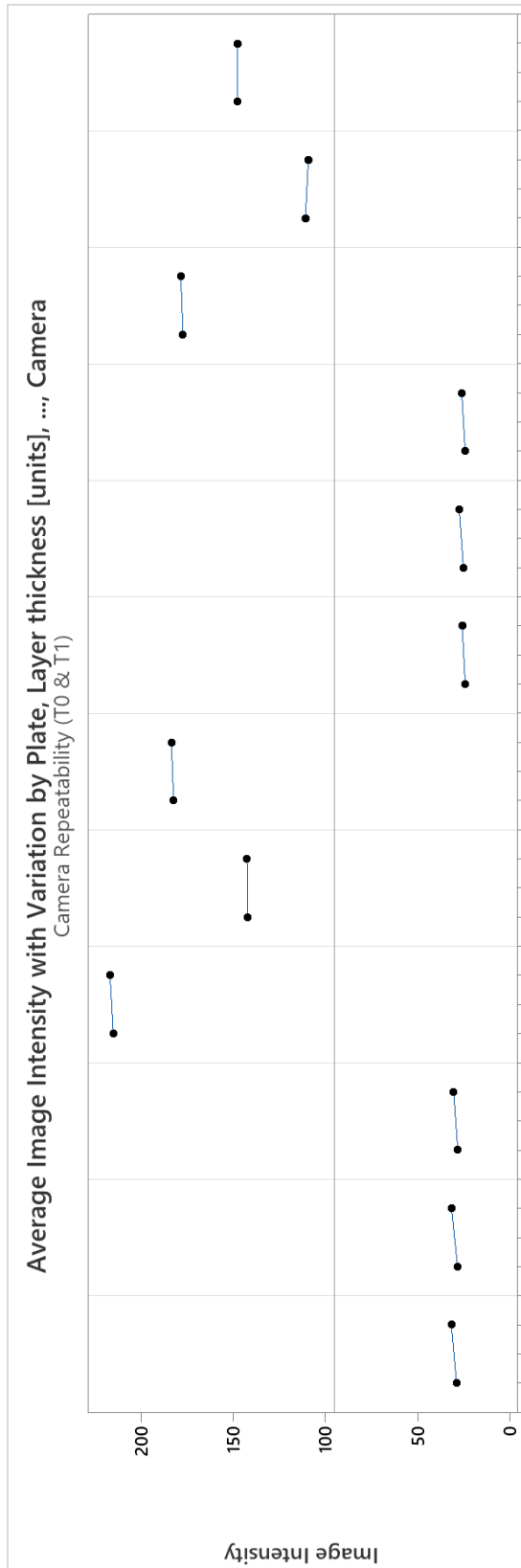
Figure 50. Variability chart to compare results from the on-machine camera images captured via a 4K video screenshot and the image capture tool on the machine organized by the plate, setup, and camera for the Camera Repeatability Test (T0 & T1).
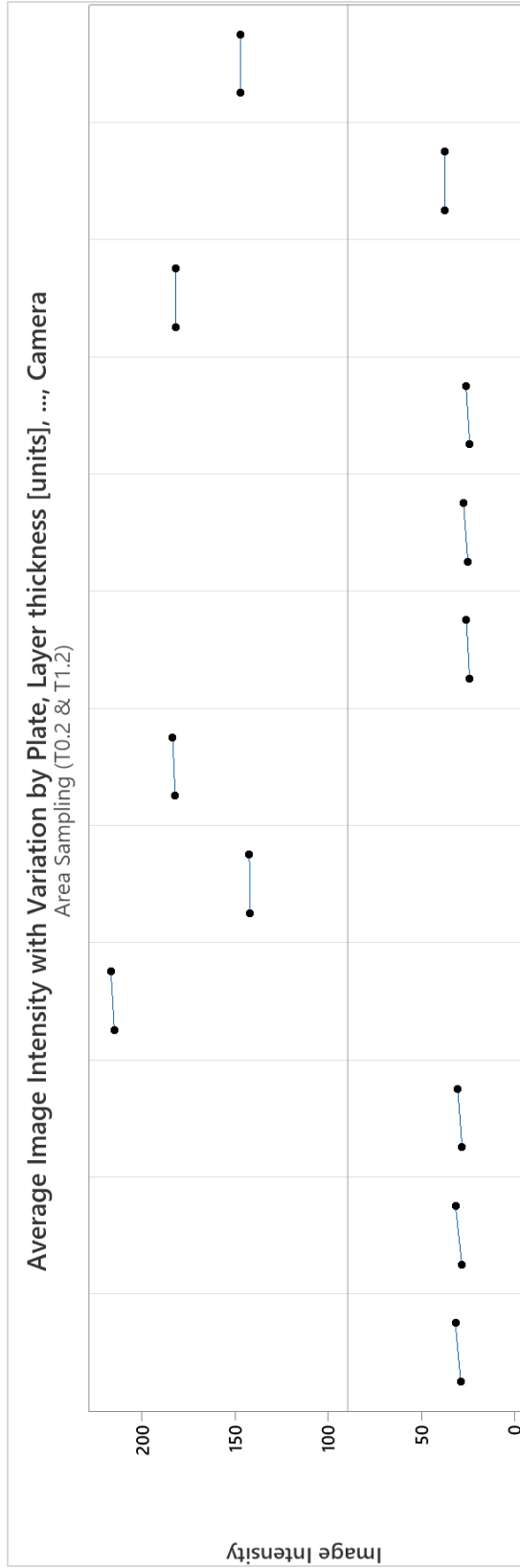
Figure 51. Variability chart to compare results from the on machine camera images captured via a 4K video screenshot and the image capture tool on the machine organized by the plate, setup, and camera for the Area Sampling Test (T0.2 and T1.2).
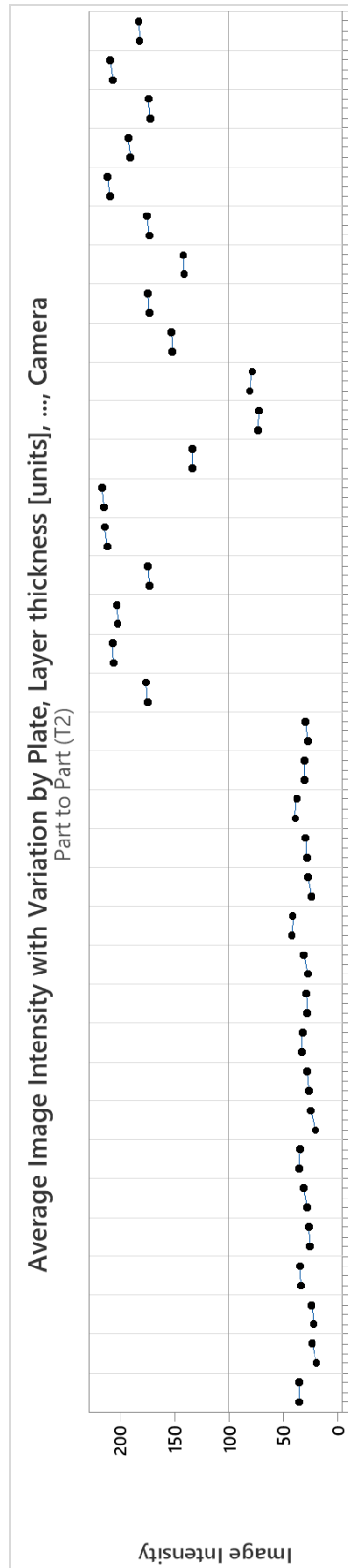
Figure 52. Variability chart to compare results from the on machine camera images captured via a 4K video screenshot and the image capture tool on the machine organized by the layer thickness, setup, part number, and camera for the Part to Part Sampling Test (T2).
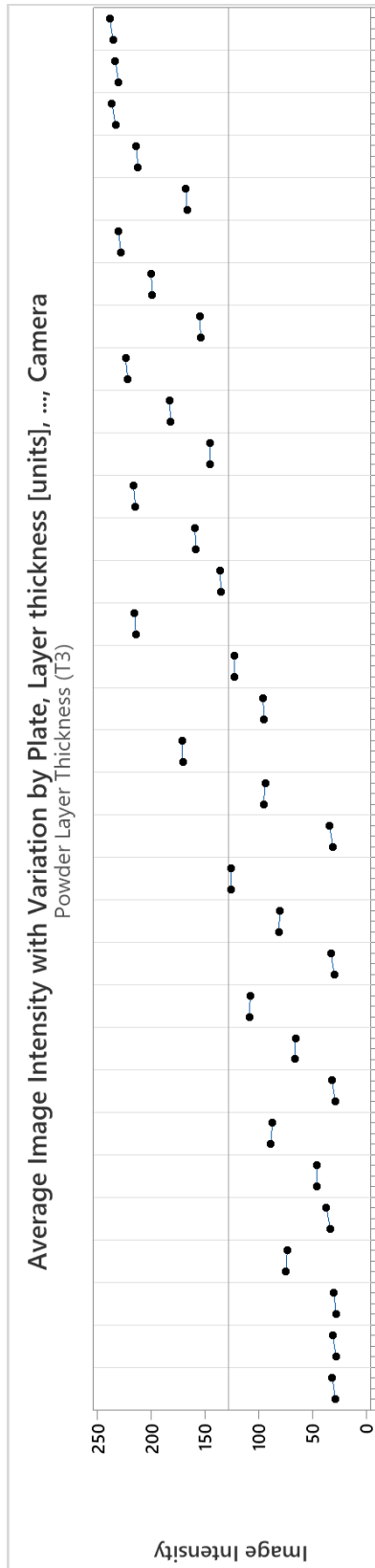
Figure 53. Variability chart to compare results from the on machine camera images captured via a 4K video screenshot and the image capture tool on the machine organized by the layer thickness, setup, part number, and camera for the Powder Layer Thickness Test (T3).

Chapter 7: Conclusion

7.1.   Conclusion

The results from all tests are captured in Table 13 below. A result was noted as "good" if the results seem to give results that would lead to a promising tool that could be used to characterize a pertinent layer setup with repeatable and reproducible results. The result was noted as "OK" if results were somewhat promising, but not the best option or if it gave a mix of good and bad results for a multifaceted test. Results were noted as "bad" where not promising and "N/A" where the test was not run for that camera.

The results of the Camera Repeatability Test show that all cameras tested yield repeatable results. Setup to setup variability contributes greatly to the overall process variability and should be further characterized but gives variable results for the Spectral Instruments RVT100 and GoPro HERO7 Black. The Area Sampling test yielded repeatable results for the Spectral Instruments RVT100 but not the STPCTOU Wireless Digital Microscope. The Powder Layer Thickness Test showed that the best linear correlation can be found for the on-machine camera and the iPhone 12.

Altogether, the on-machine produced the most promising results overall. The performance of the on-machine camera was further characterized by studies conducted in Kota[13] and Sabarad's[14] theses. Images captured from the 4K videos and captured images do not produce results that are significantly different, so the image capture methods can be used interchangeably.

---

[13] M. Kota, "Using Optical Imaging and Image Processing to Verify Initial Layer Setup in a Laser Powder Bed Fusion Process," thesis, 2022.

[14] S. Sabarad, "Comparing Various Methods for Validation of the Initial Layer in an LPBF process using Optical and Displacement Sensors," thesis, 2022.

Table 13. Overall conclusions from all tests conducted. The on-machine camera was determined to yield the best results according to all testing. The images captured from screenshots from a 4K video and the image capture tool were determined not to yield significantly different results.

Test	3DP vid	3DP cam	SI	GP	UM	PC
Camera repeatability: overall	OK	OK	Good	Good	Good	Good
Camera repeatability: within a setup	Good	Good	Bad	Bad	OK	OK
Area sampling	N/A	N/A	Good *	N/A	Bad	N/A
Powder layer thickness	Good	Good	Bad	Bad	Bad	Good
1st vs 2nd Configuration	OK	OK	Good	Bad	Good	Bad

*Only good when excluding location L3

7.2. Future Work and Recommendations

Additional studies should be conducted to fully characterize the on-machine camera. These can be done with captured images since they require less time to process and yield the same results as the 4K video screenshots. All testing for this project was performed on a single machine with one batch of powder and one build platform. Further tests should be performed to characterize the process across several machines, powder lots, and build platforms. These variables should be organized into a Design of Experiments to characterize the process. More data should be collected and integrated into a robust verification tool. the Image Analysis Software results analysis could expand from only looking at image intensity to standard deviation to further characterize the image results across a part.

7.3.   Full Project Conclusion

The overall goal of the project was to create a verification tool that could be used during a build setup process to check the quality of a layer. The project aimed to use the existing sensors and cameras available on the machine to perform this check. The performance of other available cameras was studied in this thesis. The results show that the on-machine camera yielded the most repeatable and reproducible results. In addition, results from the Powder Layer Thickness study showed the strongest linear correlation between layer thickness and image intensity for the on-machine camera. This thesis found that results from the on-machine camera as captured images and 4K video screenshots yield the same results, so captured images can be used moving forward.

The Micro-Epsilon laser line scanner showed promise over the Keyence confocal chromatic sensor in providing measurements for correlation. The correlation is not possible with the setup and data alignment methods used in Wittenbrink's thesis. Improvements to the testing equipment including the development of a micron-scale repeatable mount and precision stage will improve the results. This is detailed in Wittenbrink's thesis[15].

From our analysis of the on-machine camera, we were also able to establish a broad range of intensity limits that were detailed in the results sections of Kota's thesis[16]. If there were more replicates from the camera repeatability test,the variance would have been refined and would have provided more credibility to the analysis. Also, we could have possibly increased the confidence level of the significance test.

---

[15] J. Wittenbrink, "Using Displacement Sensors to Characterize Critical Powder Layers in Laser Powder Bed Fusion" thesis, 2022.

[16] M. Kota, "Using Optical Imaging and Image Processing to Verify Initial Layer Setup in a Laser Powder Bed Fusion Process," thesis, 2022.

Exploring the in-machine camera gave promising results in distinguishing between pertinent layers. Gauge Repeatability and Reproducibility (GR&R) proved that the results were repeatable across different setups. The second method, (Convolutional Neural Network (CNN) based machine learning model), classified the images with 94% accuracy. All of these results have been discussed in detail in Satvik Sabarad's thesis[17].

---

[17] S. Sabarad, "Comparing Various Methods for Validation of the Initial Layer in an LPBF process using Optical and Displacement Sensors," thesis, 2022.

References

[1] *Optimising Performance and Manufacturability for Additive Manufacturing | ManufacturingTomorrow*. https://manufacturingtomorrow.com/article/2020/03/optimising-performance-and-manufacturability-for-additive-manufacturing/15026. Accessed 1 Aug. 2022.

[2] S. S. Babu, L. Love, R. Dehoff, W. Peter, T. R. Watkins, and S. Pannala, "Additive Manufacturing of materials: Opportunities and challenges," *MRS Bulletin*, vol. 40, no. 12, pp. 1154–1161, 2015.

[3] R. McCann *et al.*, "In-situ sensing, process monitoring and machine control in Laser Powder Bed Fusion: A review," *Additive Manufacturing*, vol. 45, p. 102058, Sep. 2021, doi: 10.1016/j.addma.2021.102058.

[4] M. S. Hossain and H. Taheri, "In situ process monitoring for additive manufacturing through acoustic techniques," *Journal of Materials Engineering and Performance*, vol. 29, no. 10, pp. 6249–6262, 2020.

[5] M. Saleem and G. Krammer, "Optical in-situ measurement of filter cake height during bag filter plant operation - ScienceDirect," *Science Direct*. https://www.sciencedirect.com/science/article/pii/S0032591006005468 (accessed Jun. 28, 2022).

[6] D. Pal, N. Patil, K. Zeng, and B. Stucker, "An Integrated Approach to Additive Manufacturing Simulations Using Physics Based, Coupled Multiscale Process Modeling," *Journal of Manufacturing Science and Engineering*, vol. 136, no. 6, Oct. 2014, doi: 10.1115/1.4028580.

[7] "Machine Learning: A Game Changer for Additive Manufacturing Quality," *Sigma Additive Solutions*. https://sigmaadditive.com/machine-learning-a-game-changer-for-additive-manufacturing-quality-assurance/ (accessed Jun. 15, 2022).

[8] R. Frye, C. Xuan Yu, S. Betts, and L. Jacquemetton, "Data Registration and Machine Learning for Anomaly Detection," *Sigma Labs Technical Paper*, pp. 1–8,Oct. 2019.

[9] L. Jacquemetton and S. Betts, "PrintRite3D Alerts for Anomaly Detection," *Sigma Labs Technical Paper*, pp. 1–10, Oct. 2019.

[10] "QM Coating - Concentration monitoring system by Concept Laser | DirectIndustry." https://www.directindustry.com/prod/concept-laser/product-15662-1827567.html (accessed Jun. 29, 2022).

[11]   C. Burgess, "OPTICAL SPECTROSCOPY | Radiation Sources," in *Encyclopedia of Analytical Science (Second Edition)*, P. Worsfold, A. Townshend, and C. Poole, Eds. Oxford: Elsevier, 2005, pp. 427–431. doi: 10.1016/B0-12-369397-7/00429-5.

[12]   A. Cosentino, "Practical notes on ultraviolet technical photography for art examination," *Cultural Heritage Science Open Source*. Online: https://chsopensource.org/download-practical-notes-on-ultraviolet-technical-photography-for-art-examination/ (accessed Jun. 14, 2022)

[13]   "Lidar - A measurement technique that uses light emitted from a sensor to measure the range to a target object. · VectorNav." https://www.vectornav.com/applications/lidar-mapping (accessed Jun. 15, 2022).

[14]   A. Thompson, I. Maskery, and R. K. Leach, "X-ray computed tomography for additive manufacturing: a review," *Meas. Sci. Technol.*, vol. 27, no. 7, p. 072001, Jun. 2016, doi: 10.1088/0957-0233/27/7/072001.

[15]   M. S. Xavier, S. Yang, C. Comte, A. Bab-Hadiashar, N. Wilson, and I. Cole, "Nondestructive quantitative characterisation of material phases in metal additive manufacturing using multi-energy synchrotron X-rays microtomography," *Int J Adv Manuf Technol*, vol. 106, no. 5, pp. 1601–1615, Jan. 2020, doi: 10.1007/s00170-019-04597-y.

[16]   J.R. Fowler and A. M. Ilyas, "The Accuracy of Digital Radiography in Orthopaedic Applications," *Clin Orthop Relat Res*, vol. 469, no. 6, pp. 1781–1784, Jun. 2011, doi: 10.1007/s11999-010-1628-6.

[17]   "X-ray - NHS." https://www.nhs.uk/conditions/x-ray/ (accessed Jul. 09, 2022).

[18]   "What is lidar? Learn How Lidar Works," *Velodyne Lidar*. https://velodynelidar.com/what-is-lidar/ (accessed Jun. 15, 2022).

[19]   "Lidar - A measurement technique that uses light emitted from a sensor to measure the range to a target object. VectorNav." https://www.vectornav.com/applications/lidar-mapping (accessed Jun. 15, 2022).

[20]   "NIR Technology. ThermoFisher Scientific." https://www.thermofisher.com/us/en/home/industrial/spectroscopy-elemental-isotope-analysis/spectroscopy-elemental-isotope-analysis-learning-center/molecular-spectroscopy-information/nir-technology.html (accessed Jun. 10, 2022).

[21]   M.-E. M.- info@micro-epsilon.de, "Laser triangulation | Micro-Epsilon," *Micro-Epsilon Messtechnik*. https://www.micro-epsilon.com (accessed Jun. 30, 2022).

[22]   "Laser scanners for 2D/3D profile measurement | Micro-Epsilon Optronic GmbH."
        https://www.micro-optronic.com/technology/Laser-Profil-Scanner/ (accessed Jun. 30,
        2022).

[23]   B. Smith, "A Comparison of Optical Methods Used for Topography," AZoM.com,
        Feb. 01, 2019. https://www.azom.com/article.aspx?ArticleID=17573 (accessed Jul. 07,
        2022).

[24]   A. Townsend, L. Pagani, P. Scott, and L. Blunt, "Areal surface texture data extraction
        from X-ray computed tomography reconstructions of metal additively manufactured
        substrates," *Precision Engineering*, vol. 48, pp. 254–264, Apr. 2017, doi:
        10.1016/j.precisioneng.2016.12.008.

[25]   "CCS Prima Confocal Displacement Sensor," Acuity Laser.
        https://www.acuitylaser.com/product/laser-sensors/confocal-sensors/ccs-prima-confocal-
        displacement-sensor/ (accessed Jun. 19, 2022).

[26]   Z. Li *et al.*, "In Situ 3D Monitoring of Geometric Signatures in the
        Powder-Bed-Fusion Additive Manufacturing Process via Vision Sensing Methods,"
        Sensors, vol. 18, no. 4, Art. no. 4, Apr. 2018, doi: 10.3390/s18041180.

[27]   J. C. A. Read, "Stereo vision and strabismus," Eye, vol. 29, no. 2, pp. 214–224, Feb.
        2015, doi: 10.1038/eye.2014.279.

[28]   Z. Yaqoob, J. Wu, and C. Yang, "Spectral domain optical coherence tomography: a
        better OCT imaging strategy," *BioTechniques*, vol. 39, no. 6S, pp. S6–S13, Dec. 2005,
        doi: 10.2144/000112090.

[29]   A. Neef, V. Seyda, D. Herzog, C. Emmelmann, M. Schönleber, and M.
        Kogel-Hollacher, "Low Coherence Interferometry in Selective Laser Melting," *Physics
        Procedia*, vol. 56, pp. 82–89, Jan. 2014, doi: 10.1016/j.phpro.2014.08.100.

[30]   J. A. Kanko, A. P. Sibley, and J. M. Fraser, "In situ morphology-based defect
        detection of selective laser melting through inline coherent imaging," *Journal of
        Materials Processing Technology*, vol. 231, pp. 488–500, May 2016, doi:
        10.1016/j.jmatprotec.2015.12.024.

[31]   P. J. DePond *et al.*, "In situ measurements of layer roughness during laser powder
        bed fusion additive manufacturing using low coherence scanning interferometry,"
        Materials & Design, vol. 154, pp. 347–359, Sep. 2018, doi:
        10.1016/j.matdes.2018.05.050.

[32]   "Thermal sensors: Characteristics and applications," *Lynred.com*. [Online]. Available:
        https://lynred.com/blog/thermal-sensors-characteristics-and-applications. [Accessed:
        15-Jun-2022].

[33]   "Hints for Selecting the Correct Temperature Sensor for Your Application,"
        www.agilent.com, 16-Apr-2008. [Online]. Available:
        https://www.newark.com/wcsstore/ExtendedSitesCatalogAssetStore/cms/asset/images/a
        mericas/common/mro/on_demand/nov2013/Hints-for-Selecting-the-Correct-Temperatur
        e-Sensor-for-Your-Application.pdf. [Accessed: 11-Jun-2022].

[34]   How to Get Great Results with an Infrared Thermometer.
        https://www.fluke.com/en-us/learn/blog/temperature/how-to-get-great-results-with-an-in
        frared-thermometer. Accessed 15 June 2022.

[35]   MoviTHERM, "What is flash thermography?," MoviTHERM, 08-Jul-2022. [Online].
        Available: https://movitherm.com/knowledgebase/what-is-flash-thermography/.
        [Accessed: 15-Jun-2022].

[36]   H. Rieder, M. Spies, J. Bamberg, and B. Henkel, "On- and offline ultrasonic
        characterization of components built by SLM additive manufacturing," Minneapolis,
        Minnesota, 2016, p. 130002. doi: 10.1063/1.4940605.

[37]   W. Nan, M. Pasha, T. Bonakdar, A. Lopez, and U. Zafar, "Jamming during particle
        spreading in additive manufacturing," Powder Technology, vol. 338, pp. 253–362, Oct.
        2018, doi: https://doi.org/10.1016/j.powtec.2018.07.030.

[38]   A. Phua, P. S. Cook, C. H. J. Davies, and G. W. Delaney, "Powder spreading over
        realistic laser melted surfaces in metal additive manufacturing," Additive Manufacturing
        Letters, vol. 3, p. 100039, Dec. 2022, doi: 10.1016/j.addlet.2022.100039.

[39]   F. Rosala, Improvement and Development of Powder Spreadability Testing. 2021.
        Accessed: Jul. 27, 2022. [Online]. Available:
        http://urn.kb.se/resolve?urn=urn:nbn:se:kth:diva-301259

[40]   "Standard terminology of Powder Metallurgy," ASTM International - Standards
        Worldwide. [Online]. Available: https://www.astm.org/b0243-22.html. [Accessed:
        31-Jul-2022].

[41]   M. Mitterlehner, H. Gschiel, H. Danninger, and C. Gierl-Mayer, "Investigation of the
        Impact of Powder Shape on Spreading Dense Layers Using the Spreading Tester," Berg
        Huettenmaenn Monatsh, vol. 167, no. 7, pp. 300–307, Jul. 2022, doi:
        10.1007/s00501-022-01243-1.

[42]   R. Behringer (whose?) R. P. Behringer, "Jamming in granular materials," Comptes
        Rendus Physique, vol. 16, no. 1, pp. 10–25, 2015.

[43]   F. Hunter, S. Biver, P. Fuqua, and R. Reid, Light - science and magic an introduction
        to photographic lighting. New York: Routledge, 2021.

[44]   T. Craeghs, S. Clijsters, and E. Yasa, "Online Quality Control of Selective Laser Melting," University of Texas Libraries, Jun. 2011, [Online]. Available: https://repositories.lib.utexas.edu/handle/2152/88350

[45]   L. Scime, D. Siddel, S. Baird, and V. Paquit, "Layer-wise anomaly detection and classification for Powder Bed Additive Manufacturing Processes: A machine-agnostic algorithm for real-time pixel-wise semantic segmentation," *Additive Manufacturing*, vol. 36, p. 101453, 2020.

[46]   F. Caltanissetta, M. Grasso, S. Petrò, and B. M. Colosimo, "Characterization of in-situ measurements based on layerwise imaging in Laser Powder Bed Fusion," *Additive Manufacturing*, vol. 24, pp. 183–199, 2018.

[47]   T. Furumoto, "Experimental investigation of melt pool behaviour during selective laser melting by high speed imaging," *CRP Annals - Manufacturing Technology*," May 2018. [Online]. Available: https://www.researchgate.net/publication/324915801_Experimental_investigation_of_melt_pool_behaviour_during_selective_laser_melting_by_high_speed_imaging (accessed June 15, 2022).

[48]   M. Abdelrehman, E. Edward, and N. Abdalla, "Flaw detection in powder bed fusion using optical imaging," *Additive Manufacturing*, vol. 15, May 2017, doi: https://www.sciencedirect.com/science/article/pii/S2214860416301026.

[49]   F. G. Fischer, N. Birk, L. Rooney, L. Jauer, and J. H. Schleifenbaum, "Optical process monitoring in laser powder bed fusion using a recoater-based line camera," *Additive Manufacturing*, vol. 47, p. 102218, 2021.

[50]   W. Lin, D. A. Gonçalves, A. de Pereira, M. Pereira, and W. L. Weingaertner, "Quality Analysis Method for powder deposited layers applicable to selective laser sintering and selective laser melting processes," *Journal of Laser Applications*, vol. 31, no. 2, p. 022306, 2019.

[51]   T. Kumar and K. Verma, "A theory based on conversion of RGB image to Gray Image," *International Journal of Computer Applications*, vol. 7, no. 2, pp. 5–12, 2010.

[52]   "How are images stored on a computer: Grayscale & RGB image formats," *Analytics Vidhya*, 18-Mar-2021. [Online]. Available:

https://www.analyticsvidhya.com/blog/2021/03/grayscale-and-rgb-format-for-storing-images/. [Accessed: 31-Jul-2022].

[53]   bjorn@acuitylaser.com, "Laser Triangulation Sensors - Non-Contact Measurement," *Acuity Laser*. https://www.acuitylaser.com/sensor-resources/laser-triangulation-sensors/ (accessed Jul. 08, 2022).

[54]   F. Froment, "An Introduction to Laser Triangulation Sensors," *Third Dimension*, Apr. 08, 2021. https://www.third.com/an-introduction-to-laser-triangulation-sensors/ (accessed Jul. 08, 2022).

[55]   S. Donadello, M. Motta, A. G. Demir, and B. Previtali, "Monitoring of laser metal deposition height by means of coaxial laser triangulation," *Optics and Lasers in Engineering*, vol. 112, pp. 136–144, Jan. 2019, doi: 10.1016/j.optlaseng.2018.09.012.

[56]   M. Erler, A. Streek, C. Schulze, and H. Exner, "Novel Machine and Measurement Concept for Micro Machining by Selective Laser Sintering," 2014. doi: 10.26153/tsw/15660.

[57]   "What is Laser Triangulation," *MoviMed*. https://www.movimed.com/knowledgebase/what-is-laser-triangulation/ (accessed Jul. 08, 2022).

[58]   F. Aquino, W. M. Jadwisienczak, and F. Rahman, "Effect of laser speckle on light from laser diode-pumped phosphor-converted light sources," *Appl. Opt., AO*, vol. 56, no. 2, pp. 278–283, Jan. 2017, doi: 10.1364/AO.56.000278.

[59]   "What is Structured Light Imaging? | RoboticsTomorrow." https://roboticstomorrow.com/article/2018/04/what-is-structured-light-imaging/11821 (accessed Jul. 07, 2022).

[60]   B. Zhang, J. Ziegert, F. Farahi, and A. Davies, "In situ surface topography of laser powder bed fusion using fringe projection," *Additive Manufacturing*, vol. 12, pp. 100–107, Oct. 2016, doi: 10.1016/j.addma.2016.08.001.

[61]   A. D. Elliott, "Confocal Microscopy: Principles and Modern Practices," Curr Protoc Cytom, vol. 92, no. 1, p. e68, Mar. 2020, doi: 10.1002/cpcy.68.

[62]   J. Elambasseril, J. Rogers, C. Wallbrink, D. Munk, M. Leary, and M. Qian, "Laser powder bed fusion additive manufacturing (LPBF-AM): the influence of design features and LPBF variables on surface topography and effect on fatigue properties," Critical Reviews in Solid State and Materials Sciences, vol. 0, no. 0, pp. 1–37, Mar. 2022, doi: 10.1080/10408436.2022.2041396.

[63]   "Technical Explanation for Displacement Sensors and Measurement Sensors,"
        OMRON. https://www.ia.omron.com/support/guide/56/introduction.html (accessed Jun.
        21, 2022).

[64]   C. Jones, "Factors to consider when selecting confocal displacement sensors,"
        Eureka, Jun. 05, 2018.
        https://www.eurekamagazine.co.uk/content/technology/factors-to-consider-when-selecti
        ng-confocal-displacement-sensors/ (accessed Jun. 20, 2022).

[65]   Keyence, Confocal Displacement Sensor CL-3000 Series.

[66]   Y. Yang, "CONFOCAL SCANNING IMAGING SYSTEM FOR SURFACE
        CHARACTERIZATION IN ADDITIVE MANUFACTURING SYSTEM," p. 79, Dec.
        2019, [Online]. Available:
        https://etd.ohiolink.edu/apexprod/rws_etd/send_file/send?accession=dayton1576066631
        705912&disposition=inline

[67]   "Large Field of View 3D Snapshot Sensor | Gocator 3210 3D Smart Sensors | LMI
        Technologies," Feb. 21, 2017. https://lmi3d.com/series/gocator-3210/ (accessed Jun. 06,
        2022).

[68]   "Extreme Environments - Spectral Instruments," Mar. 16, 2021.
        https://specinstcameras.com/cameras/extreme/ (accessed Jul. 06, 2022).

[69]   "What is CMOS sensor? - Definition from WhatIs.com," WhatIs.com.
        https://www.techtarget.com/whatis/definition/CMOS-sensor (accessed May 16, 2022).

[70]   Proto G Engineering, Vacuum Chamber VS GoPro HERO4 Black, (Nov. 05, 2015).
        Accessed: Jul. 06, 2022. [Online Video]. Available:
        https://www.youtube.com/watch?v=U9FjMFajTWI

[71]   "Amazon.com : STPCTOU Wireless Digital Microscope 50X-1000X 1080P
        Handheld Portable Mini WiFi USB Microscope Camera with 8 LED Lights for
        iPhone/iPad/Smartphone/Tablet/PC : Electronics."
        https://www.amazon.com/Microscope-PFC-Optics-50X-1000X-Smartphone/dp/B07M97
        SRFN/ref=sr_1_1_sspa?keywords=bluetooth+microscope&qid=1653578799&sr=8-1-sp
        ons&psc=1&smid=A1BIG265MJBW5C&spLa=ZW5jcnlwdGVkUXVhbGlmaWVyPUF
        SVDJNREo0WEc1RkkmZW5jcnlwdGVkSWQ9QTA0NTk4NTkySFVZSEFYRDFHM
        TQ4JmVuY3J5cHRlZEFkSWQ9QTAxMDE2NTRaSlY0MkVSRDdPQlkmd2lkZ2V0T
        mFtZT1zcF9hdGYmYWN0aW9uPWNsaWNrUmVkaXJlY3QmZG9Ob3RMb2dDbGlja
        z10cnVl (accessed Jun. 12, 2022).

[72]   "iPhone 12 and iPhone 12 mini - Technical Specifications," Apple.
        https://www.apple.com/iphone-12/specs/ (accessed Jul. 20, 2022).

[73]   "Tools." https://imagej.nih.gov/ij/docs/tools.html (accessed Jul. 26, 2022).

[74]   "What is a Macro? - Definition from Techopedia," Techopedia.com.
     http://www.techopedia.com/definition/3833/macro (accessed Jul. 26, 2022).

Appendix

A. 1. Full ANOVA Results for the Area Sampling Test

One-way ANOVA: Image Intensity versus Location for SI at 0 Unit Layer Thickness

Method

Null hypothesis	All means are equal
Alternative hypothesis	Not all means are equal
Significance level	α = 0.05
Rows unused	5

Equal variances were assumed for the analysis.

Factor Information

Factor	Levels	Values
Location	5	L1, L2, L3, L4, L5

Analysis of Variance

Source	DF	Adj SS	Adj MS	F-Value	P-Value
Location	4	2311	577.86	8.14	0.000
Error	20	1419	70.96		
Total	24	3731			

Model Summary

S	R-sq	R-sq(adj)	R-sq(pred)
8.42353	61.96%	54.35%	40.56%

Means

Location	N	Mean	StDev	95% CI
L1	5	60.30	6.99	(52.44, 68.16)
L2	5	82.46	6.34	(74.60, 90.32)
L3	5	59.43	5.73	(51.58, 67.29)
L4	5	77.80	13.63	(69.94, 85.66)
L5	5	62.89	6.87	(55.03, 70.75)

Pooled StDev = 8.42353

The pooled standard deviation is used to calculate the intervals.

One-way ANOVA: Image Intensity versus Location for SI at 3 Unit Layer Thickness

Method

Null hypothesis	All means are equal
Alternative hypothesis	Not all means are equal
Significance level	$\alpha = 0.05$
Rows unused	1

Equal variances were assumed for the analysis.

Factor Information

Factor	Levels	Values
Location	5	L1, L2, L3, L4, L5

Analysis of Variance

Source	DF	Adj SS	Adj MS	F-Value	P-Value
Location	4	7636	1908.9	3.26	0.029
Error	24	14067	586.1		
Total	28	21702			

Model Summary

S	R-sq	R-sq(adj)	R-sq(pred)
24.2097	35.18%	24.38%	5.46%

Means

Location	N	Mean	StDev	95% CI
L1	6	152.99	23.40	(132.59, 173.39)
L2	6	151.03	22.55	(130.63, 171.42)
L3	6	114.3	25.1	(93.9, 134.7)
L4	5	159.5	23.1	(137.2, 181.9)
L5	6	152.6	26.5	(132.2, 173.0)

Pooled StDev = 24.2097

Interval Plot of Image Intensity vs Location
95% CI for the Mean for SI at 3 Unit Layer Thickness

The pooled standard deviation is used to calculate the intervals.
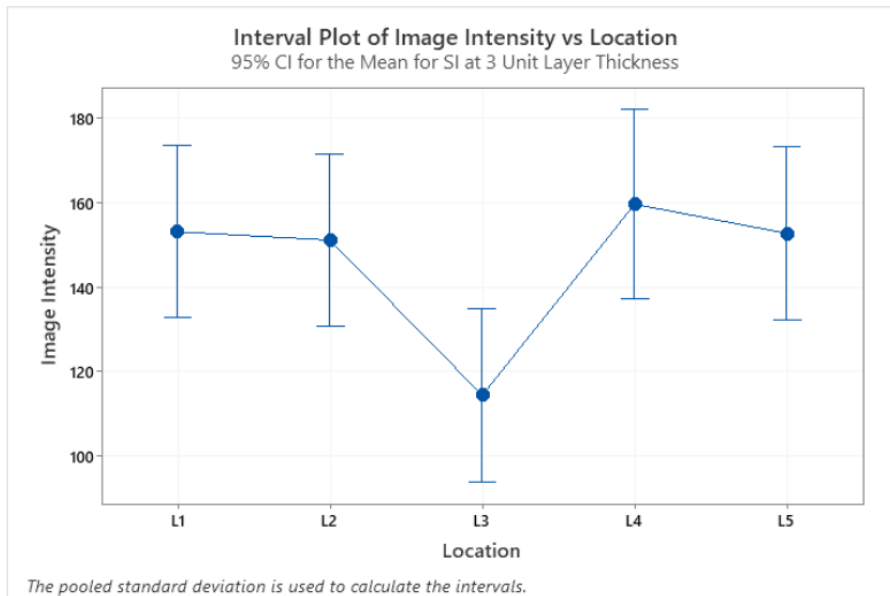
One-way ANOVA: Image Intensity versus Location for SI at 3 Units with L3 Removed

Method

Null hypothesis	All means are equal
Alternative hypothesis	Not all means are equal
Significance level	$\alpha = 0.05$
Rows unused	1

Equal variances were assumed for the analysis.

Factor Information

Factor	Levels	Values
Location	4	L1, L2, L4, L5

Analysis of Variance

Source	DF	Adj SS	Adj MS	F-Value	P-Value
Location	3	222.3	74.10	0.13	0.942
Error	19	10917.6	574.61		
Total	22	11139.9			

Model Summary

S	R-sq	R-sq(adj)	R-sq(pred)
23.9711	2.00%	0.00%	0.00%

Means

Location	N	Mean	StDev	95% CI
L1	6	152.99	23.40	(132.51, 173.47)
L2	6	151.03	22.55	(130.54, 171.51)
L4	5	159.5	23.1	(137.1, 182.0)
L5	6	152.6	26.5	(132.1, 173.1)

Pooled StDev = 23.9711
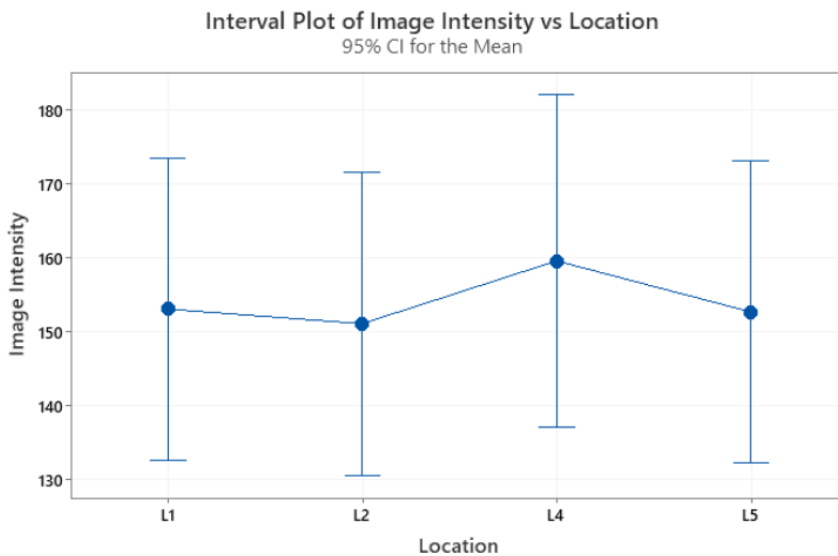
The pooled standard deviation is used to calculate the intervals.

One-way ANOVA: Image Intensity versus Location

Method

Null hypothesis	All means are equal
Alternative hypothesis	Not all means are equal
Significance level	$\alpha = 0.05$
Rows unused	3

Equal variances were assumed for the analysis.

Factor Information

Factor	Levels	Values
Location	3	L1, L2, L3

Analysis of Variance

Source	DF	Adj SS	Adj MS	F-Value	P-Value
Location	2	2944	1471.8	6.63	0.011
Error	12	2664	222.0		
Total	14	5607			

Model Summary

S	R-sq	R-sq(adj)	R-sq(pred)
14.8984	52.50%	44.58%	25.78%

Means

Location	N	Mean	StDev	95% CI
L1	5	98.8	22.4	(84.3, 113.3)
L2	5	125.79	10.60	(111.27, 140.31)
L3	5	130.68	7.31	(116.16, 145.20)

Pooled StDev = 14.8984

Interval Plot of Image Intensity vs Location
95% CI for the Mean of UM at 0 Unit Layer Thickness

The pooled standard deviation is used to calculate the intervals.
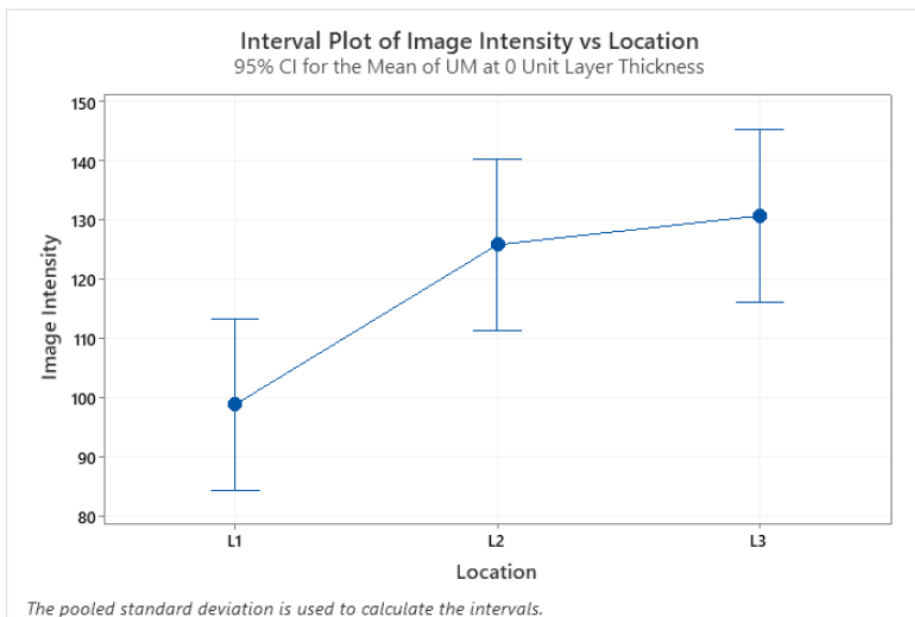
One-way ANOVA: Image Intensity versus Location for UM at 3 Unit Layer Thickness

Method

Null hypothesis   All means are equal
Alternative hypothesis   Not all means are equal
Significance level   α = 0.05

Equal variances were assumed for the analysis.

Factor Information

Factor	Levels	Values
Location	3	L1, L2, L3

Analysis of Variance

Source	DF	Adj SS	Adj MS	F-Value	P-Value
Location	2	311.2	155.61	4.34	0.033
Error	15	537.5	35.84		
Total	17	848.8			

Model Summary

S	R-sq	R-sq(adj)	R-sq(pred)
5.98632	36.67%	28.22%	8.80%

Means

Location	N	Mean	StDev	95% CI
L1	6	140.77	8.19	(135.56, 145.98)
L2	6	146.74	4.32	(141.53, 151.95)
L3	6	136.61	4.66	(131.40, 141.82)

Pooled StDev = 5.98632

Interval Plot of Image Intensity vs Location
95% CI for the Mean of UM at 3 Unit Layer Thickness
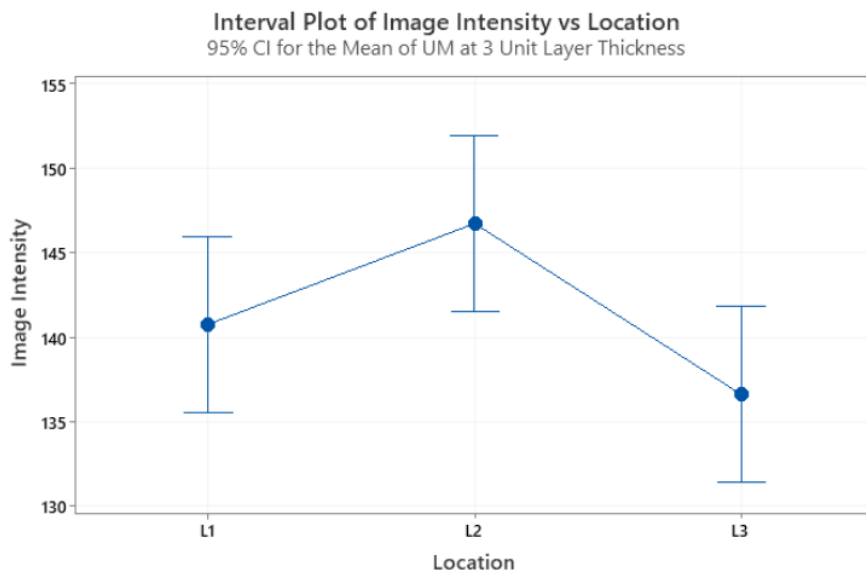
The pooled standard deviation is used to calculate the intervals.

A. 2. Powder Layer Thickness Test

A.2.1. Scatter Plots for all Cameras

Results were studied to find the linear correlation in further studies. Layer thickness varied from 0 to 5 units with the most data taken around 1 and 3 units.
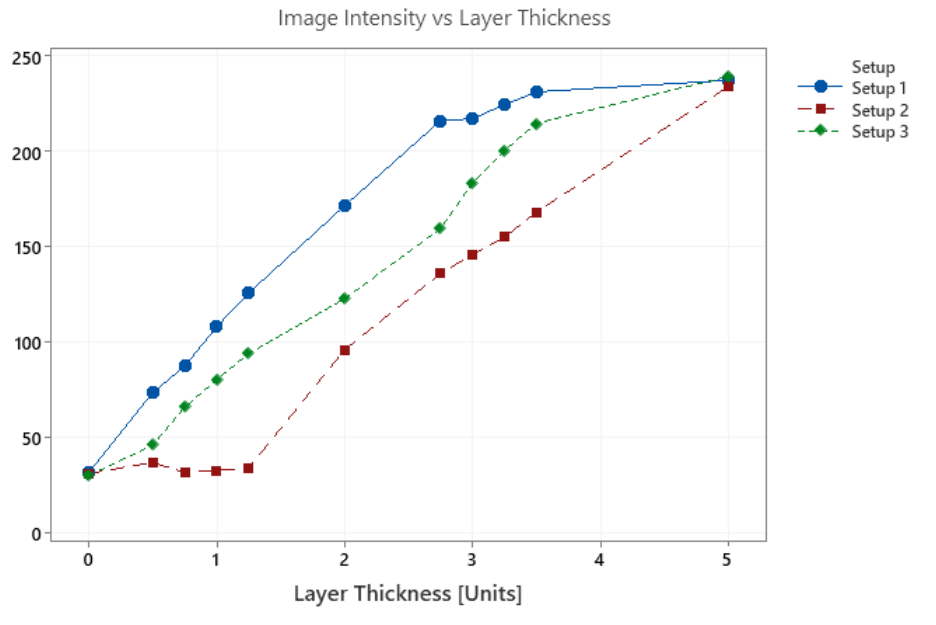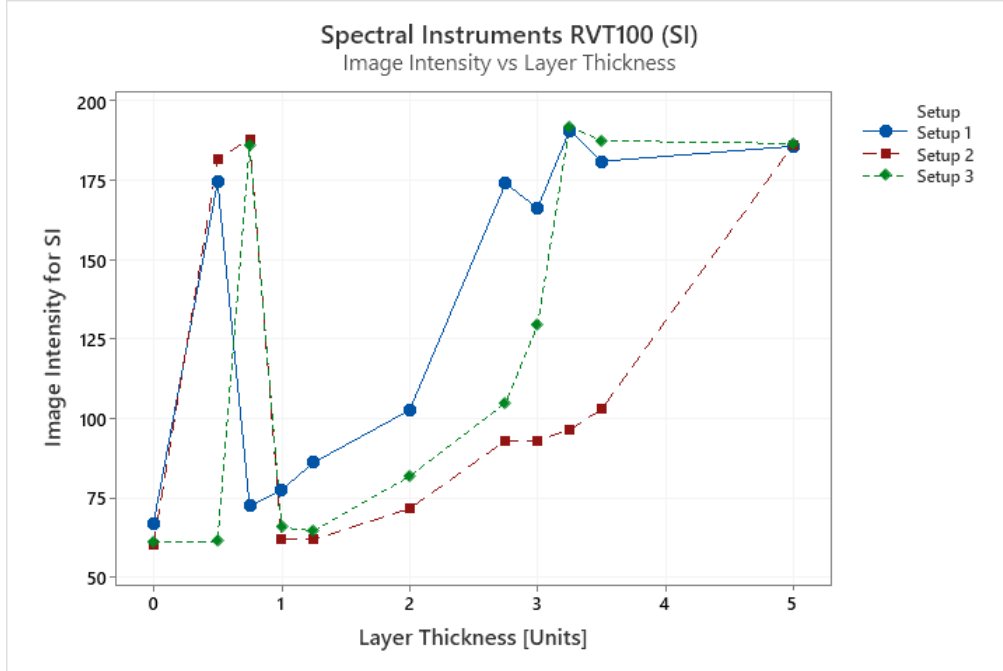

Scatter plot showing the layer thickness vs image intensity for the on-machine camera for images captured from a 4K video.
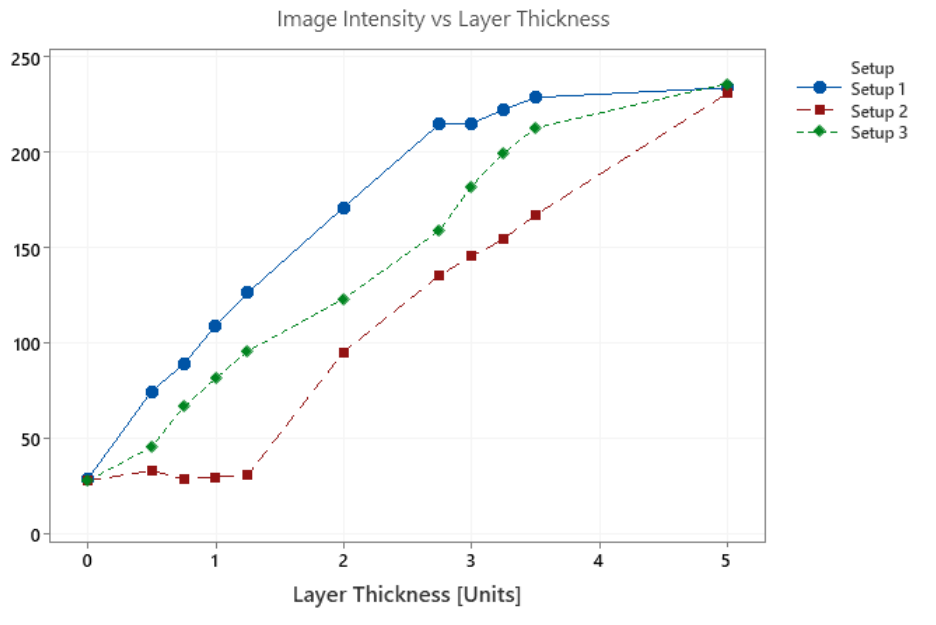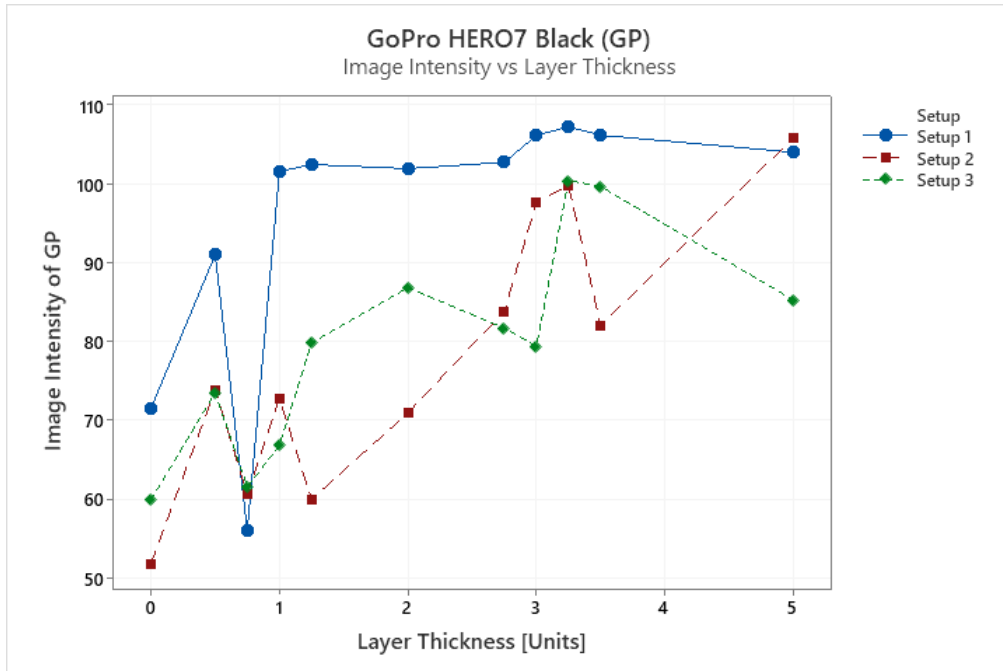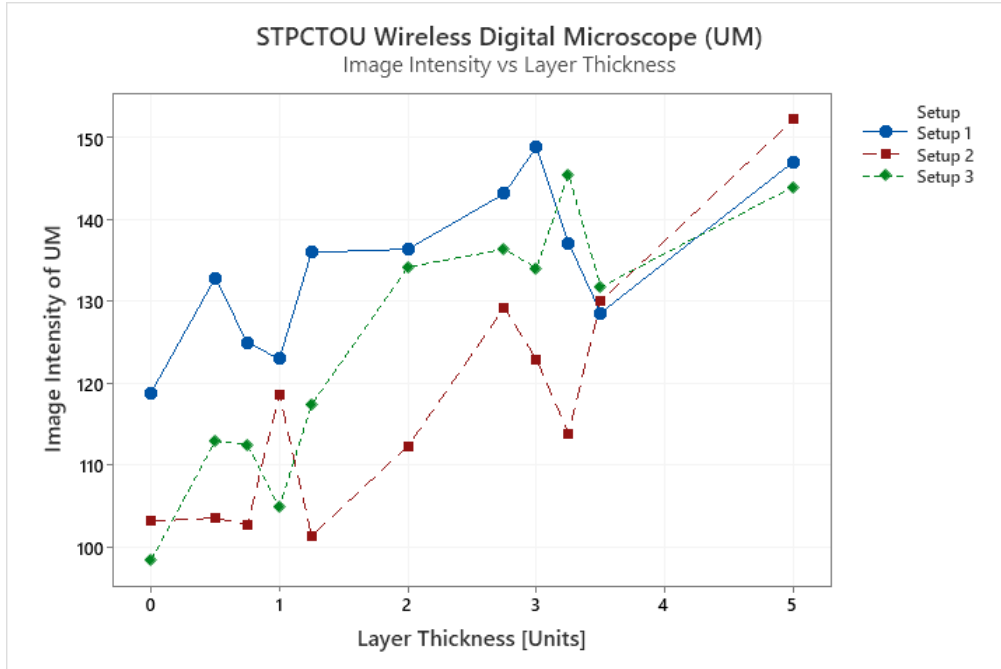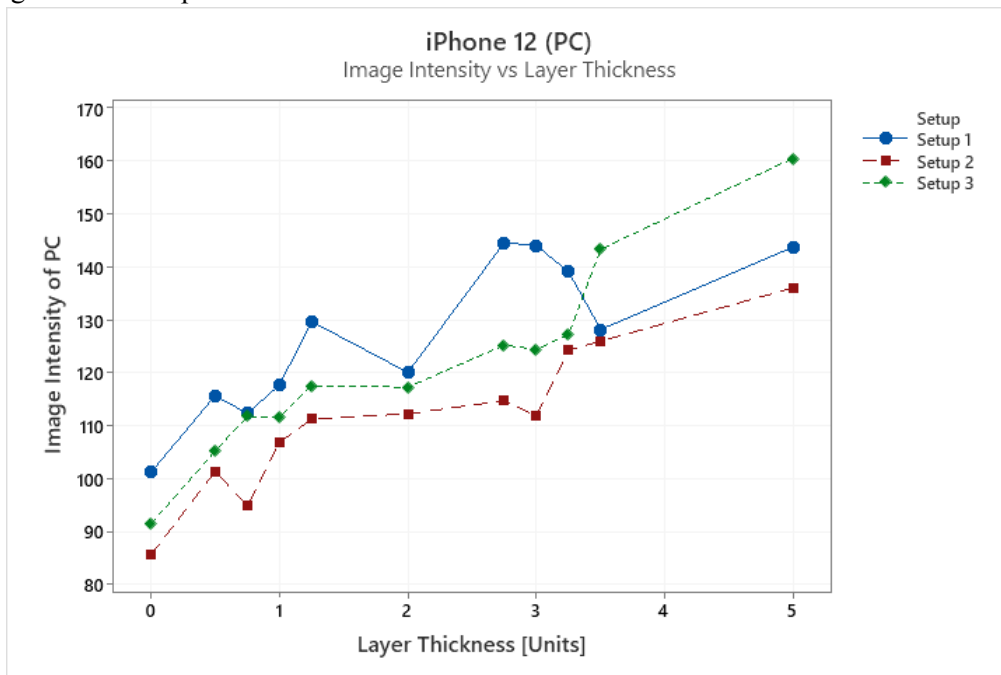

Scatter plot showing the layer thickness vs image intensity for the on-machine camera for images captured from the image capture.

Scatter plot showing the layer thickness vs image intensity for the Spectral Instruments RVT100 camera.

Scatter plot showing the layer thickness vs image intensity for the GoPro HERO7 Black camera for images captured from the image capture.
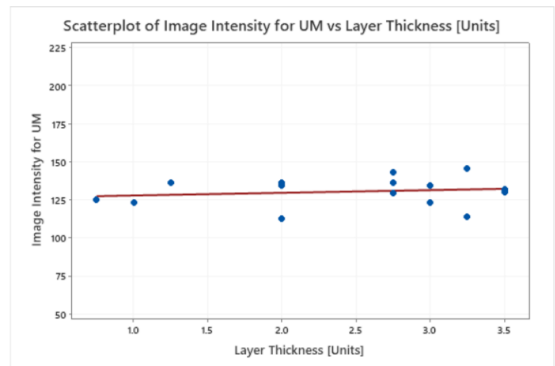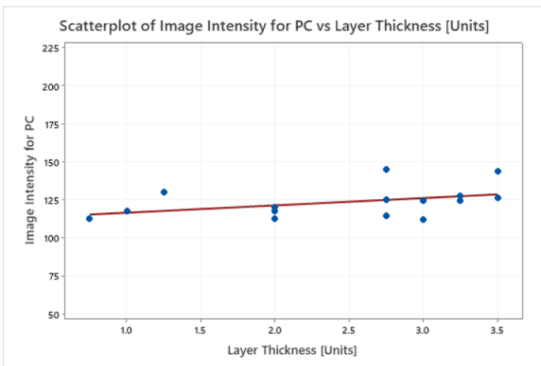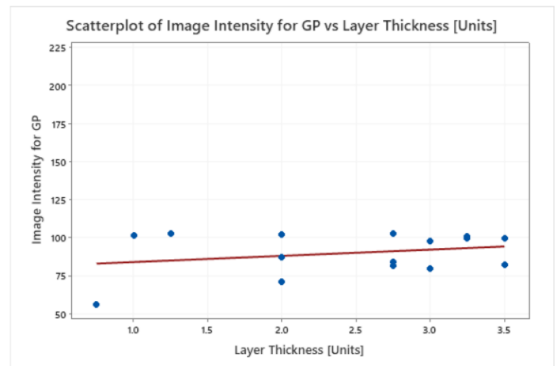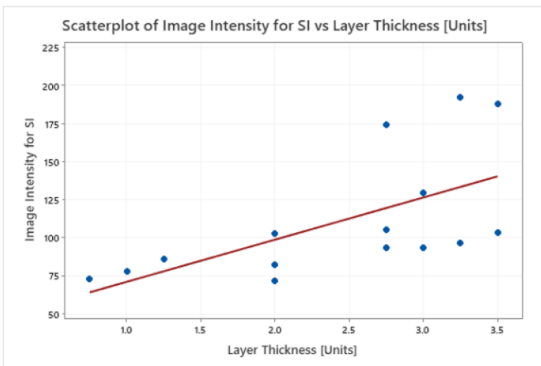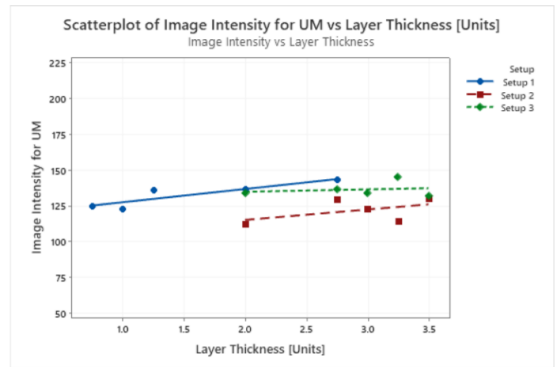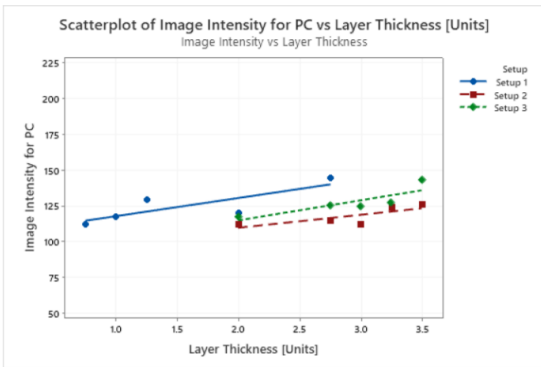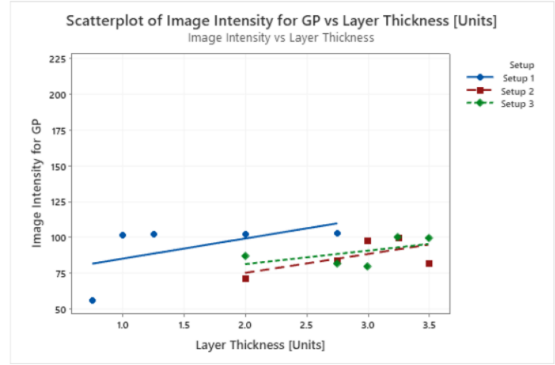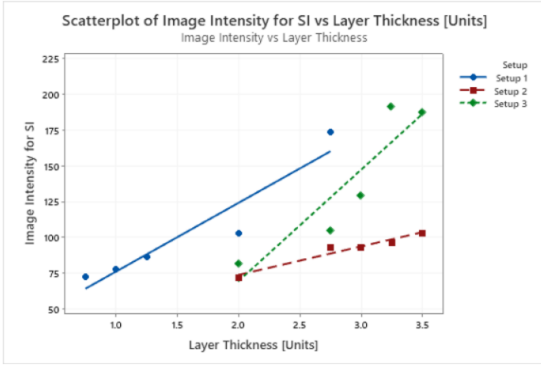
Scatter plot showing the layer thickness vs image intensity for the STPCTOU Wireless Digital Microscope.

Scatter plot showing the layer thickness vs image intensity for theiPhone 12 camera.

A.2.2. Scatterplots for Only Good Setups

A. 3. Full Nested ANOVA Results for 3DP vid vs 3DP cam

Nested ANOVA: Camera Repeatability (T0 & T1)

Analysis of Variance for Image Intensity

Source	DF	SS	MS	F	P
Plate	1	11747.4628	11747.4628	1.894	0.241
Setup	4	24808.5079	6202.1270	0.064	0.990
Layer thickness [units]	6	580641.8073	96773.6346	10371.741	0.000
Camera	12	111.9661	9.3305	3115.614	0.000
Error	96	0.2875	0.0030		
Total	119	617310.0317			

Variance Components

Source	Var Comp.	% of Total	StDev
Plate	92.422	0.95	9.614
Setup	-4528.575*	0.00	0.000
Layer thickness [units]	9676.430	99.03	98.369
Camera	1.866	0.02	1.366
Error	0.003	0.00	0.055
Total	9770.721		98.847

Value is negative, and is estimated by zero.

Expected Mean Squares

1 Plate	1.00 (5) + 5.00 (4) + 10.00 (3) + 20.00 (2) + 60.00 (1)
2 Setup	1.00 (5) + 5.00 (4) + 10.00 (3) + 20.00 (2)
3 Layer thickness [units]	1.00 (5) + 5.00 (4) + 10.00 (3)
4 Camera	1.00 (5) + 5.00 (4)
5 Error	1.00 (5)

Nested ANOVA: Area Sampling (T0.2 & T1.2)

Analysis of Variance for Image Intensity

Source	DF	SS	MS	F	P
Plate	1	5880.9573	5880.9573	0.123	0.760
Layer thickness [units]	2	96002.8146	48001.4073	9460.411	0.000
Camera	4	20.2957	5.0739	0.003	1.000
Error	16	28193.8543	1762.1159		
Total	23	130097.9220			

Variance Components

Source	Var Comp.	% of Total	StDev
Plate	-3510.037*	0.00	0.000
Layer thickness [units]	7999.389	81.95	89.439
Camera	-585.681*	0.00	0.000
Error	1762.116	18.05	41.978
Total	9761.505		98.800

Value is negative, and is estimated by zero.

Expected Mean Squares

1 Plate	1.00 (4) + 3.00 (3) + 6.00 (2) + 12.00 (1)
2 Layer thickness [units]	1.00 (4) + 3.00 (3) + 6.00 (2)
3 Camera	1.00 (4) + 3.00 (3)
4 Error	1.00 (4)